Expansion Microscopy combined with Super-Resolution Fluorescence Microscopy

DISSERTATION ZUR ERLANGUNG DES
NATURWISSENSCHAFTLICHEN DOKTORGRADES DER
JULIUS-MAXIMILIANS-UNIVERSITÄT WÜRZBURG

vorgelegt von

Fabian Ulrich Zwettler

geboren in Waldkirch

Würzburg, September 2020

Eingereicht am: .....

Mitglieder der Promotionskommission:

Vorsitzender: .....
Gutachter: Prof. Dr. Markus Sauer
Gutachter: Prof. Dr. Ricardo Benavente
Gutachter: .....

Tag des Promotionskolloquiums: .....

Doktorurkunde ausgehändigt am: .....

Zusammenfassung

Die Fluoreszenzmikroskopie ist eine Form der Lichtmikroskopie, die sich im Laufe des 20. Jahrhunderts entwickelt hat und heutzutage standardmäßig in der Molekular- und Zellbiologie zur Erforschung von Aufbau und Funktion biologischer Moleküle eingesetzt wird. Hochauflösende Verfahren der Fluoreszenzmikroskopie, wie die *d*STORM (*direct* Stochastic Optical Reconstruction Microscopy) Technik, ermöglichen die Visualisierung zellulärer Strukturen im Nanometer-Größenbereich (10^{-9} m). Dadurch konnte bereits die Zusammensetzung und Funktion unterschiedlicher Biopolymere, wie die von Proteinen, Lipiden und Nukleinsäuren, bis hin zum dreidimensionalen (3D) Aufbau ganzer Organellen entschlüsselt werden.

In der Praxis zeigt sich jedoch, dass diese Bildgebungsverfahren und ihre Weiterentwicklungen immer noch vor großen Herausforderungen stehen, bevor eine effektive Auflösung von unter $\sim$ 10 nm erreicht werden kann. Die größte Hürde stellt die Art und Weise der Markierung von Biomolekülen dar. Bei dieser wird zum Nachweis molekularer Strukturen häufig die sogenannte Immunfärbung als Standardmethode eingesetzt. Antikörper, welche mit Fluoreszenzmolekülen gekoppelt werden, erkennen und binden hierbei spezifisch und mit hoher Affinität den Molekülabschnitt der Zielstruktur, auch Epitop oder Antigen genannt. Die Fluoreszenzmoleküle dienen als Reportermoleküle, welche mit Hilfe eines Fluoreszenzmikroskops abgebildet werden. Die Größe der Antikörper, mit einer Länge von etwa 10-15 nm im Falle von Immunglobulin G (IgG) Antikörpern, bewirkt jedoch eine Detektion der fluoreszierenden Moleküle verschoben zur eigentlichen Lage des untersuchten Antigens. In Regionen mit räumlich dicht nebeneinander liegenden Epitopen kann es zusätzlich zur sterischen Hinderung zwischen den Antikörpern kommen. Dies führt zu einer unzureichenden Markierungsdichte und stellt - zusammen mit der verschobenen Detektion der Fluoreszenzmoleküle - eine Limitierung der zu erreichenden Auflösung dar.

Die Expansionsmikroskopie (ExM) ist ein neu entwickeltes Verfahren, welches eine Auflösungsverbesserung durch die physikalische Expansion eines untersuchten Objekts erreicht. Hierbei werden biologische Proben, wie beispielsweise kultivierte Zellen, Gewebeschnitte,

ganze Organe oder isolierte Organellen, chemisch in ein quellbares Polymer verankert. Durch Absorption von Wasser vergrößert dieser sogenannte Superabsorber sein eigenes Volumen und zieht während der räumlichen Expansion die kovalent gebundenen Biomoleküle isotrop auseinander. Standardmäßig wird durch dieses Verfahren eine Vergrößerung der Proben um etwa das vierfache Volumen erreicht, wobei bereits Protokollvarianten entwickelt wurden, die eine bis zu 50-fache Expansion erzielt haben.

Da die ExM-Technik zunächst nur die Probenbehandlung zur Verankerung und Vergrößerung der Probe selbst beinhaltet, kann sie mit unterschiedlichen Standardmethoden der Fluoreszenzmikroskopie kombiniert werden. Dadurch verbessert sich die Auflösung des verwendeten Bildgebungsverfahrens theoretisch linear um den Faktor der Volumenvergrößerung der ExM behandelten Probe. Eine unzureichende Markierungsdichte und die Größe der verwendeten Antikörper können auch hier die effektiv erreichbare Auflösung beeinträchtigen. Die Kombination der ExM mit hochauflösenden Verfahren der Fluoreszenzmikroskopie stellt eine vielversprechende Strategie zur Erhöhung der bisher erreichbaren Auflösung in der Lichtmikroskopie dar.

In dieser Arbeit werde ich mehrere von mir entwickelte ExM Varianten vorstellen, welche die Kombination von ExM mit konfokaler Mikroskopie, SIM (Structured Illumination Microscopy), STED (STimulated Emission Depletion) und *d*STORM zeigen. Um die Verbindung mit dem jeweiligen Bildgebungsverfahren zu ermöglichen, optimierte ich bestehende ExM-Protokolle und entwickelte unterschiedliche Expansionsstrategien. Dadurch konnte ich neue strukturelle Erkenntnisse von isolierten Zentriolen aus der Grünalge *Chlamydomonas reinhardtii* durch die Verbindung von ExM mit STED und konfokaler Mikroskopie gewinnen. In einem weiteren Projekt kombinierte ich 3D-SIM mit ExM und untersuchte den molekularen Aufbau des sogenannten synaptonemalen Komplexes. Diese Struktur bildet sich in eukaryotischen Zellen während der Reifeteilung (Meiose) aus und trägt zum Austausch des genetischen Materials zwischen homologen Chromosomen bei.

Vor allem in Verbindung mit *d*STORM zeigte sich das hohe Potential der ExM-Methode, die bisherigen Limitierungen moderner Techniken der Fluoreszenzmikroskopie zu überwinden. In diesem Projekt expandierte ich Mikrotubuli in Säugetierzellen, ein Polymer des Zytoskeletts, sowie isolierte Zentriolen aus *C. reinhardtii*. Dadurch, dass die Markierung erst nach dem Expandieren der Proben erfolgte, gelang es, den Abstandsfehler der Markierung deutlich zu verringern und eine verbesserte Markierungsdichte zu erreichen. Diese Vorteile

könnten in Verbindung mit der Einzelmolekülsensititvität und hohen Auflösung der *d*STORM Methode Wegbereiter zur Erreichung einer molekularen Auflösung sein.

Abstract

Fluorescence microscopy is a form of light microscopy that has developed during the 20th century and is nowadays a standard tool in Molecular and Cell biology for studying the structure and function of biological molecules. High-resolution fluorescence microscopy techniques, such as *d*STORM (*direct* Stochastic Optical Reconstruction Microscopy) allow the visualization of cellular structures at the nanometre scale (10^{-9} m). This has already made it possible to decipher the composition and function of various biopolymers, such as proteins, lipids and nucleic acids, up to the three-dimensional (3D) structure of entire organelles.

In practice, however, it has been shown that these imaging methods and their further developments still face great challenges in order to achieve an effective resolution below ~ 10 nm. This is mainly due to the nature of labelling biomolecules. For the detection of molecular structures, immunostaining is often performed as a standard method. Antibodies to which fluorescent molecules are coupled, recognize and bind specifically and with high affinity to the molecular section of the target structure, also called epitope or antigen. The fluorescent molecules serve as reporter molecules which are imaged with the use of a fluorescence microscope. However, the size of these labels with a length of about 10-15 nm in the case of immunoglobulin G (IgG) antibodies, cause a detection of the fluorescent molecules shifted to the real position of the studied antigen. In dense regions where epitopes are located close to each other, steric hindrance between antibodies can also occur and leads to an insufficient label density. Together with the shifted detection of fluorescent molecules, these factors can limit the achievable resolution of a microscopy technique.

Expansion microscopy (ExM) is a recently developed technique that achieves a resolution improvement by physical expansion of an investigated object. Therefore, biological samples such as cultured cells, tissue sections, whole organs or isolated organelles are chemically anchored into a swellable polymer. By absorbing water, this so-called superabsorber increases its own volume and pulls the covalently bound biomolecules isotropically apart. Routinely,

this method achieves a magnification of the sample by about four times its volume. But protocol variants have already been developed that result in higher expansion factors of up to 50-fold.

Since the ExM technique includes in the first instance only the sample treatment for anchoring and magnification of the sample, it can be combined with various standard methods of fluorescence microscopy. In theory, the resolution of the used imaging technique improves linearly with the expansion factor of the ExM treated sample. However, an insufficient label density and the size of the antibodies can here again impair the effective achievable resolution. The combination of ExM with high-resolution fluorescence microscopy methods represents a promising strategy to increase the resolution of light microscopy.

In this thesis, I will present several ExM variants I developed which show the combination of ExM with confocal microscopy, SIM (Structured Illumination Microscopy), STED (STimulated Emission Depletion) and *d*STORM. I optimized existing ExM protocols and developed different expansion strategies, which allow the combination with the respective imaging technique. Thereby, I gained new structural insights of isolated centrioles from the green algae *Chlamydomonas reinhardtii* by combining ExM with STED and confocal microscopy. In another project, I combined 3D-SIM imaging with ExM and investigated the molecular structure of the so-called synaptonemal complex. This structure is formed during meiosis in eukaryotic cells and contributes to the exchange of genetic material between homologous chromosomes.

Especially in combination with *d*STORM, the ExM method showed its high potential to overcome the limitations of modern fluorescence microscopy techniques. In this project, I expanded microtubules in mammalian cells, a polymer of the cytoskeleton as well as isolated centrioles from *C. reinhardtii*. By labelling after expansion of the samples, I was able to significantly reduce the linkage error of the label and achieve an improved label density. In future, these advantages together with the single molecule sensitivity and high resolution obtained by the *d*STORM method could pave the way for achieving molecular resolution in fluorescence microscopy.

Table of contents

Chapter 1

Theoretical Background

Cells form the basic building blocks of living organisms. With a size of about 1 – 100 µm [UCW19], they encompass various biomolecules that range scales of roughly a tenth of a nanometre (10^{-10} m) up to a millimetre (10^{-3} m). Besides water, protein macromolecules make up the largest part of a cell and fulfil a diverse range of functions. The human eye is able to distinguish structures with a distance of ~ 0.15 mm. This makes most cells smaller than some algae or large bacteria invisible to the naked eye. Only the invention of optical magnification aids such as the microscope opened up the possibility to explore cellular components and processes that take place in the molecular size range. The application and further development of microscopy techniques in medical and biological sciences has contributed to the understanding of the composition and structural organization of various macromolecules as well as the interaction of biomolecules in the cellular context. Therefore, microscopy represents a unique tool in the study of basic cellular processes and contributes to the understanding and treatment of a variety of diseases.

As a researcher, one is also aware of the limitations of science and how little we already understand about our world. The curiosity to decipher the undiscovered is what drives science forward. This also led to the invention of new techniques in microscopy which are constantly evolving and are designed to unravel the secrets of our world. As a revolutionary imaging approach, I personally count the development of a recently emerged sample preparation tool called expansion microscopy (ExM) which will be the topic of this thesis. To place this technique in the context of microscopy and to understand its potential as a scientific tool, I will first give a brief overview of the historical development of light microscopy up to the present day. Thereby, I will focus on fluorescence microscopy and the development of so-called ‘super-resolution’ imaging techniques. This will help to understand my main topic, which is the further development of ExM and its combination with different fluorescence

microscopy techniques. In the second part, I will present different variants of ExM that were developed in the last years. Finally, I will present the articles I have published which include the application of optimized ExM protocols on different biological specimens. I will conclude by discussing the advantages and disadvantages of each technique in combination with ExM and the remaining limitations as well as possible future developments.

1.1 Optical Microscopy

The first use of a magnifying system can be traced back at least to the 1st century AD, when *Lucius Annaeus Seneca* mentions globes of water used as magnifiers for reading. It is also described that the emperor *Nero* owned a concave emerald at that time as a vision help to watch gladiator fights [Ila07]. In the centuries that followed, it is difficult to reconstruct who really was the original inventor of the first glass lens. Spectacles were invented around 1280 in Florence and were widely spread until the end of the 16th century. The magnification properties of several combined lenses were obviously soon discovered, and the first compound microscope can be attributed to *Jansen* and his son *Zacharias von Middleburg* (Holland, 1595) [Cro06]. Indispensable in the context of optical science is the pioneering work of the Dutch natural scientist *Antoni van Leeuwenhoek* in the 17th century. He can be seen as the first microbiologist who manufactured powerful lenses able to magnify about 300 times with a resolution down to 1.4 µm. This enabled him to discover organisms and cells that at that time had never been described before. Between 1674 and 1682 the Royal Society published several detailed drawings by Leeuwenhoek of infusoria (1674), bacteria (1676), spermatozoa (1677) and muscle fibres (1682) [For91].

Despite today's technical advances, the resolution of modern microscopes is physically limited by the wave nature of light. In 1873, the physicist *Ernst Abbe* was the first who described the theoretical limit of light microscopy which gives the minimum resolvable distance d in an object by

$$d = \frac{\lambda}{2n\sin\alpha} = \frac{\lambda}{2NA}, \tag{1.1}$$

where λ is the wavelength of the illumination light, n is the diffraction index of the object surrounding medium, α is the half-angle of the diffracted light that can enter the objective, where $n\sin\alpha$ is defined as the numerical aperture NA of the objective [Abb73].

The diffraction of light limits optical microscopy in resolving structural details below $\sim$ 200-300 nm when imaging is performed using visible light. At the end of the 19th century, handcrafted lenses had already reached the maximum possible numerical aperture so that an improvement in resolution seemed only possible by reducing the wavelength of the illumination light. This assumption led *Köhler* and *von Rohr* of *Zeiss* in 1904 to build a microscope which operates in the ultraviolet (UV) range of the light spectrum. Based on their invention, seven years later in 1911 *Otto Heimstaedt* and *Heinrich Lehmann* built the first fluorescence microscope which was used to detect auto-fluorescence in living cells. The design of today's standard fluorescence microscopes, could be realized with the implementation of dichroic mirrors presented in 1967 [Plo67]. This allowed the spectral separation of the illumination and fluorescence light [BRA14].

In the years that followed, further technical advances were made in the design of optical instruments (like detectors and lenses) as well as the development of sophisticated strategies to mark biomolecules. However, it took until the past two decades for fluorescence microscopy to break the diffraction limit of light by the emergence of so-called 'super-resolution' techniques. These methods enable imaging of biomolecules in the nanometric scale beyond the diffraction limit of light. Until then, only Electron Microscopy (EM) offered sub-diffraction imaging by decreasing the wavelength of illumination. This concept was already introduced in 1931 by *Ernst August Friedrich Ruska* and *Max Knoll* who built the first electron microscope. Instead of a beam of light as in optical microscopy, a beam of electrons with wavelengths of 1-2 Å and magnetic lenses are used in an electron microscope. The further development and unprecedented resolving power of this method has undoubtedly made a major contribution to our understanding in cell biology, neuroscience and virology [Mas01]. Still, up to the present day, no light microscopy technique could achieve the resolution obtained by Electron Microscopy.

1.2 Fluorescence Microscopy

Modern fluorescence microscopy combines high contrast imaging together with high labelling specificity and minimal perturbation to biological samples. This allows the study of dynamics of specific biomolecules in living biological specimens. To achieve these unique properties, several technical advances as well as understanding of the fundamentals of fluorescence were necessary, and developed in the 18th and 19th centuries.

1.2.1 The principle of fluorescence

The phenomenon of fluorescence was already described 1852 by the Irish mathematician and physicist *George Gabriel Stokes* [Sto52]. Classified as a version of luminescence, it refers to the ability of a substance to emit light as a result of the absorption of an electromagnetic wavelength. Depending on its atomic and molecular composition, a fluorescent molecule interacts and absorbs light at specific wavelengths, defined as its absorption spectrum. The so-called Jablonski diagram is often used to explain the molecular processes occurring after absorption of a photon. It describes the electronic states and radiative or non-radiative transitions of a photoexcited molecule (Figure 1.1).

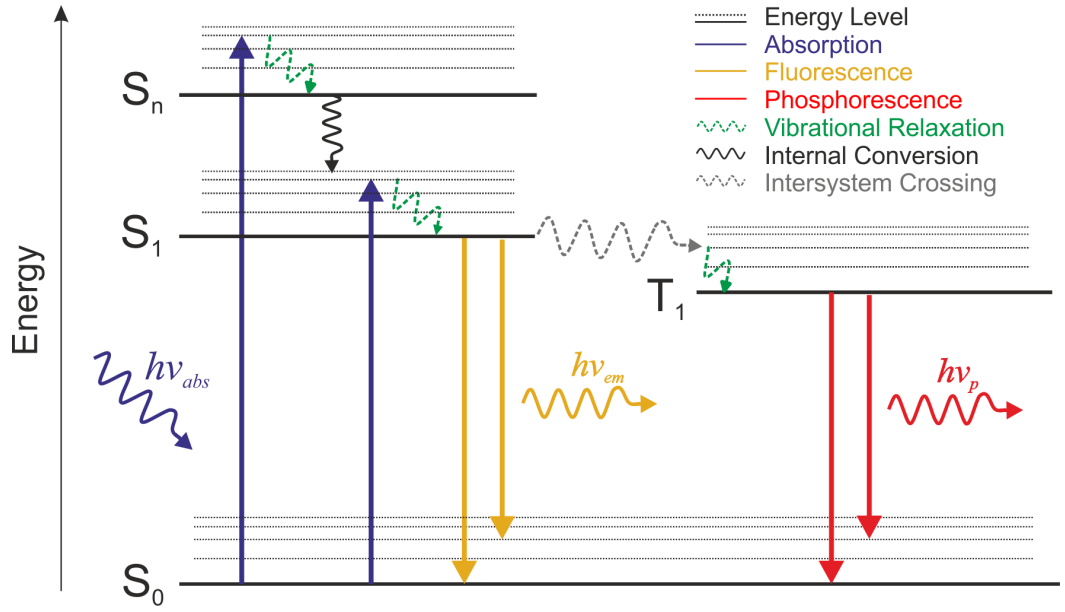

Figure 1.1: Jablonski diagram illustrating the photoexcitation of a molecule. The horizontal black lines indicate the energy levels of the molecule with S_0 as the singlet ground state, S_1 as the first excited singlet state and S_n the n^{th} excited singlet state. Each electronic state includes several vibrational levels shown as black dotted lines with the lowest level represented as bold line. The radiative transitions absorption, fluorescence and phosphorescence include the absorption or emission of a photon with the energy $E = h\nu_{abs}$ (absorbed photon), $h\nu_{em}$ (emitted fluorescence photon) and $h\nu_p$ (emitted phosphorescence photon), respectively. Non-radiative transitions include vibrational relaxation, internal conversion and intersystem crossing.

After absorption of a photon, a molecule is promoted from its singlet ground state S_0 to any vibrational level of a higher excited singlet state (S_1, S_n). This transition takes place at a time scale of 10^{-15} s. From there, a non-radiative transition to a lower vibrational level within the residing electronic state occurs through vibrational relaxation. If a molecule is in

an excited state S_n it can undergo non-radiative internal conversion to a lower electronic state (e.g. from S_2 to S_1), with a subsequent relaxation to its lowest vibrational level. The emission of a photon upon the transition from the excited state S_1 to the ground state is known as fluorescence. It occurs in a timescale of 10^{-9}-10^{-7} s. Whereas phosphorescence describes the emission of a photon upon transition from the triplet state T_1 to S_0. As the excitation to a triplet state involves a quantum-mechanically 'forbidden' spin orientation of the excited electron, the probability of this process is lower than fluorescence and occurs in a longer time range of 10^{-6} to 10 s [Lak10].

Due to the energy loss caused by non-radiative transitions, the emitted light typically exhibits a lower energy than the absorbed light and therefore has a longer wavelength (Figure 1.2a). The presence of this so-called 'Stokes shift' is a prerequisite for fluorescence microscopy and can advantageously be used to spectrally separate the excitation light from the emission light. In biological sciences, fluorescence imaging is often combined with a confocal microscope, also known as Confocal Laser Scanning Microscopy (CLSM). (Figure 1.2b).

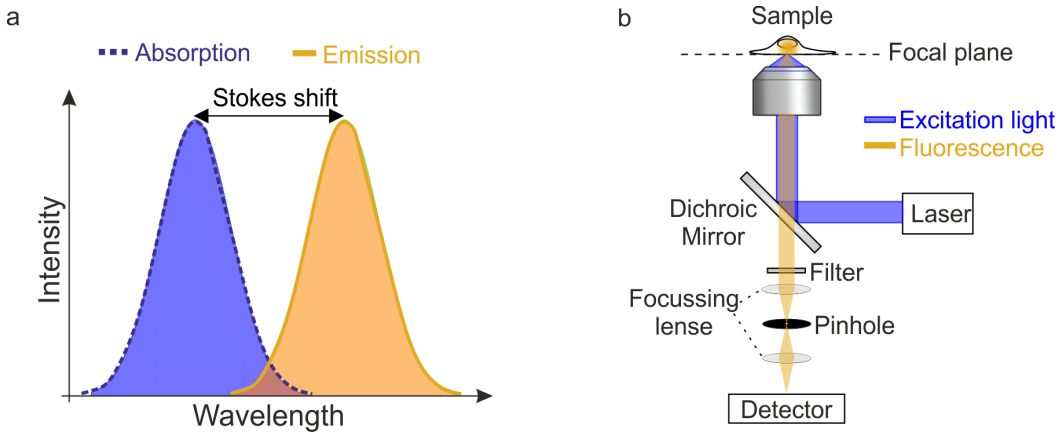

Figure 1.2: Stokes shift and confocal microscopy. a, Stokes shift between absorption and emission spectra. The exemplary spectra illustrate the typical Stokes shift occurring between absorbed and longer wavelength emitted photons which result from non-radiative energy transitions shown in Figure 1.1. **b**, Schematic of a confocal microscope. The illumination light (blue) deriving from a laser is reflected from a dichroic mirror (DCM) and focused by an objective into the fluorescently labelled sample. Excited fluorophores emit fluorescence with Stokes shifted wavelength and are able to pass the dichroic mirror. The light is then spectrally filtered using appropriate emission filters and focused on a pinhole aperture which spatially confines the detected light and only allows fluorescence to pass from the focal plane before it reaches the detector (a photomultiplier tube (PMT)).

The basic idea of a confocal microscope was already developed in the 1950's by Minsky [Min88] and patented in 1961 [Min]. The illumination of the specimen in a confocal micro-

scope is performed by scanning a focused beam of light across the focal plane. In the original setup, the excitation light passes through a pinhole aperture located in a conjugate plane with the focal plane of the objective within the specimen and a second pinhole positioned in front of a detector. These two pinholes conjugated in the same image plane give the name 'confocal' to the technique. Nowadays, the use of lasers as light source generating a Gaussian beam that can be focused to a small spot in the sample makes the implementation of the excitation pinhole obsolete. In contrast to widefield fluorescence microscopy which illuminates the entire sample volume, confocal microscopy eliminates out-of-focus light and enables optical sectioning of thick specimens with improved contrast. Theoretically, the use of an infinitely small pinhole could improve the spatial resolution with a factor of $\sqrt{2}$, but in practice this is not feasible as no photon would be able to reach the detector [CS04].

To further improve the performance of confocal microscopy, related techniques were developed that use computational and/or hardware extensions that combine the advantages of optical sectioning with high signal to noise imaging. Among these are Image Scanning Microscopy techniques like Airy Scan Microscopy [Huf15] or Re-scanning Microscopy [dLDB$^+$17] that in combination with Deconvolution achieve a resolution gain of 1.7-fold.

1.2.2 Fluorescent labels

Cells observed under a bright-field microscope naturally exhibit a low contrast due to their high-water content. The incident light is therefore only weakly scattered, making cells or even structural details very difficult to observe. To circumvent this issue, bright fluorescent molecules can be specifically attached to a cellular target. Several staining techniques evolved that utilize fluorescent markers to enhance contrast in a biological sample.

Chemical staining methods like the silver staining of *Camillo Golgi* enabled scientists to increase the contrast and thereby reveal cellular structures in the µm-scale. *Satiago Ramon y Cajal* used this method at the end of the 19$^{\text{th}}$ century to study the nervous system. His detailed drawings revealed small membranous protrusions, the so-called dendritic spines. Cajal's observations that dendrites and axons end freely led to the neuron doctrine that explains the organization of the brain circuit as a system made up of individual neuron cells [Yus15]. Chemical staining methods like the hematoxylin and eosin staining (HE stain) already introduced in 1876 are still widely used as a standard procedure in diagnostic histopathology [Wit03].

A milestone in labelling strategies in fluorescence microscopy is the discovery of fluorescent proteins (FPs). The first discovered FP, named Green Fluorescent Protein (GFP) was isolated from the jelly fish *Aequorea victoria* in 1962 by *Shimomura et al.* [SJS62]. Recombinant gene expression enables the fusion of FPs to a variety of proteins in other organisms other than the jelly fish. This enables the specific marking of proteins by GFP and its colour-shifted derivates and allows the monitoring of cellular processes in living cells. The use of GFP as a fusion protein was first shown by *Chalfie et al.* in 1994 [CTE+94]. Nowadays, FPs have been engineered that exhibit optimized photophysical properties spanning a large colour palette that can be used in different applications [RCL+17]. The genetic fusion of fluorescent proteins provides very high specificity, but overexpression can lead to significant increase in background signal.

An alternative approach using recombinant protein expression for tagging proteins in living cells represents the genetic fusion of enzymes to a protein of interest. Similar to the labelling approach of FPs, enzymes like the SNAP- or CLIP-tag are attached genetically to a protein. Fluorescently labelled ligands bind to the protein tags and serve as covalently bound fluorescent markers. Enzymatic tags allow the combination of synthetic fluorophores which offer higher photostability and brightness compared to fluorescent proteins. These optimized photophysical properties allow single molecule sensitive fluorescence imaging in living cells [vHS12]. Synthetic fluorophores can also be conjugated to peptides like phalloidin. This toxin is isolated from the mushroom *Amanita phalloides* and can be used to selectively stain F-actin filaments in fixed cells.

Nowadays, a broadly utilized approach is immunofluorescence which uses antibodies to which fluorescent dyes are coupled, for highly specific labelling of antigens in fixed samples. The use of antibodies as fluorescent markers was first described by *Coons et al.* in 1941 [CCJ41]. Together with advances in the synthesis of bright and photo-stable organic dyes, immunofluorescence has become a widely used tool for highly specific, multi target labelling in combination with high signal to noise ratio imaging.

1.2.3 Super-Resolution Fluorescence Microscopy

Super-resolution imaging methods provide spatial resolution that is well below the diffraction limit of light microscopy. Together with the advanced labelling strategies described above, these techniques allow the study of the three-dimensional (3D) architecture of macromolecules and the interactions of biomolecules in living cells, thereby shedding light on

fundamental biological questions.

Farfield super-resolution techniques include PhotoActivated Localization Microscopy (PALM) [BPS+06], Stochastic Optical Reconstruction Microscopy (STORM) [RBZ06], direct Stochastic Optical Reconstruction Microscopy (*d*STORM) [HvS+08], Structured Illumination Microscopy (SIM) [Gus00], STimulated Emission Depletion (STED) [KJD+00], Ground-State-Depletion Imaging (GSDIM) [FBB+08], Super-resolution Optical Fluctuation Imaging (SOFI) [DCI+09] as well as variants and further developments thereof [HGM06] [GPB+20]. Near-field Scanning Optical Microscopy (NSOM) [BLH+86] is arguably the simplest way to avoid the limitations of the far-field capable of imaging beyond the classical Abbe-limit. The detector is typically placed only 1-10 nm apart from the fluorescent emitter. Since this distance is less than the wavelength of light, the technique is not subject to diffraction. However, NSOM is restricted to image surfaces and is not compatible in combination with embedded and expanded biological specimens.

In the following, I will briefly introduce the above-mentioned imaging techniques and the basic principle they rely on to bypass the diffraction limit of light. Although, there exist of course further method variants that achieve sub-diffraction resolution, I will focus on these farfield techniques since they represent the basic strategies of super-resolution microscopy and I realized the combination of SIM, STED and *d*STORM (Figure 1.3) with ExM which I will present in chapter 3.

1.2.4 Structured Illumination Microscopy (SIM)

SIM is a wide-field microscopy technique that achieves a lateral resolution twice as high as conventional diffraction-limited instruments and can be extended to 3D-imaging [Gus00] [GSC+08]. It extracts sub-diffraction information from processing captured images of the sample excited with a patterned illumination (Figure 1.3c). The resolution improvement is based on the formation of Moiré patterns generated from the interference of the usually striped structured illumination with the sub-diffraction details in the sample. SIM imaging is compatible with any fluorophore and provides a volumetric imaging with in a large field-of-view. However, the algorithmic post-processing can be time-consuming and is prone to artifacts that require critical review [DIN+17]. Among other sources of error, image artifacts can arise from too low signal-to-noise ratio, photobleaching during acquisition or refractive index mismatch between the immersion and sample media.

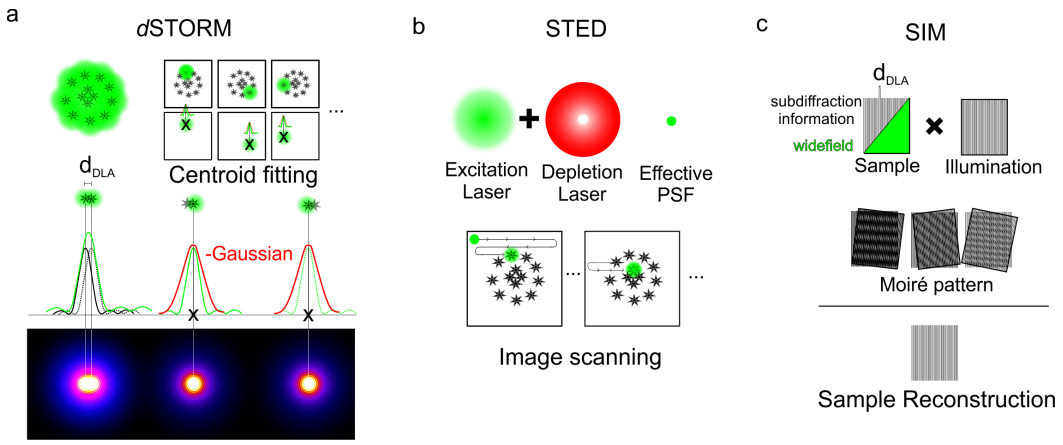

Figure 1.3: Super-resolution microscopy technique. a, *d*STORM. Adjacent fluorescent molecules with a distance d_{DLA} within a diffraction limited area (*DLA*) are resolved by centroid fitting of the point spread function (PSF) of successively photoactivated emitters using a Gaussian function. The coordinates from several molecules are reconstructed in a super-resolved image. **b,** STED. The use of a doughnut shaped depletion laser (red) with ideally zero intensity in the centre spatially restricts fluorescence emitting fluorophores. Molecules within a diffraction limited area can thereby be photoactivated separately by the excitation laser PSF with reduced spot size (effective PSF). The lasers are scanned over the sample to get a super-resolved image. **c,** SIM. The sample imaged with a diffraction-limited widefield microscope (green) contains unresolved sub-diffraction information which is hidden in the details with a distances d_{DLA} within a diffraction limited area (striped pattern). The sample is illuminated with periodic intensity (fine striped illumination grid pattern). Altering rotation angles of the illumination pattern generates Moiré patterns by interfering with sub-diffraction features of the sample. Mathematical reconstruction results in a super-resolved image.

1.2.5 Stimulated Emission Depletion (STED) Microscopy

STED microscopy relies on the spatial restriction of fluorescence within a photoexcited diffraction limited region. In order to reduce the diameter of the fluorescence emitting area, a ring-shaped laser beam with ideally zero-intensity at the centre suppresses spontaneous fluorescence from fluorophores located in the periphery of the excitation laser PSF. In this way, only fluorescence of molecules located in the centre of the depletion laser are detected. The suppression of spontaneous fluorescence relies on the process of stimulated emission depletion. Stimulated emission occurs when an excited fluorophore in a higher electronic state absorbs a depletion photon and returns to the singlet ground state by emitting two photons with wavelengths equivalent to the depletion photon. As the depletion wavelength is significantly different to the fluorescence wavelength, it can be spectrally filtered preventing detection of fluorophores that have undergone stimulated emission depletion. This process reduces the effective PSF of the excitation laser which is scanned over the sample and thereby

allows sub-diffraction limited imaging (Figure 1.3b). STED requires complex microscope configurations and photo-stable fluorophores as the use of high intensity lasers can cause photobleaching or photodamage to the sample. However, advantageous in this method is the fast recording time and no need for image post processing.

1.2.6 Single-molecule localization microscopy (SMLM)

The super-resolution methods PALM, FPALM, STORM and *d*STORM achieve an improvement in resolution by mathematically estimating the position of fluorescent molecules. This approach uses the fact that an image of a single molecule appears blurred by diffraction while its position can be calculated with diffraction unlimited precision [TLW02]. This is performed by determining the centre of an Airy disk pattern which refers to the intensity distribution of an individual fluorescent emitter. In practice, a Gaussian function is fitted to the point spread function (PSF) of an imaged fluorophore.

The detection of fluorescent molecules is performed following a photoconversion process of the fluorophores which converts them from a dark OFF to a light emitting ON state. This allows the sequential activation of a subset of fluorophores so that emitters within a diffraction-limited area are temporally isolated and recorded separately from one another.

*d*STORM uses photoswitchable organic fluorophores which are transferred from a fluorescent ON state to a nonfluorescent OFF state by irradiation with light. In the presence of a reducing agent exposed to an oxygen-depleted environment, a large proportion of the fluorophores reside in a long lasting dark OFF state. (Figure 1.3a) Single molecules get activated stochastically which results in a temporal separation of fluorescence of single molecules. In this way, adjacent fluorophores whose emission patterns overlap and which therefore cannot be detected as separated molecules when imaged with a far-field microscope, now can be resolved as single molecules. The position of the fluorophores can be approximated by fitting a Gaussian function to the emission pattern (the PSF). A super-resolution image can then be reconstructed from the determined molecule coordinates which are normally collected over a series of several thousand images.

PALM/FPALM typically uses photoactivatable or photoconvertible fluorescent proteins like photoactivatable GFP (PA-GFP) expressed as fusion proteins in transfected cells. However, the main difference between *d*STORM and PALM is not the type of fluorophore but their photoconversion process. In practice, PALM activates a portion of non-fluorescent

molecules by irradiation with a high frequency light (e.g. 405 nm laser). These molecules are then exited by lower-frequency light (e.g. 561 nm laser) and recorded on a camera. This process of photoactivation, excitation and subsequent photobleaching is serially repeated and as in *d*STORM the localization of fluorophores is determined by fitting the recorded intensity distribution of single emitters. In contrast to this sequential activation and read out of fluorescence signal, in *d*STORM, fluorophores are activated reversibly in a random manner and the same fluorophores can be imaged multiple times.

A *d*STORM setup can be implemented relative easily in a wide field microscope. However, this method depends on the presence of suitable fluorophores, which require optimal imaging conditions for photoswitching to obtain relatively stable non-fluorescent OFF states. This guarantees that only a subset of molecules is fluorescent at a time and single emitters can be detected temporally separated within a diffraction-limited region. The presence of glutathione in cells even allows *d*STORM imaging in living cells [vHS12].

1.2.7 Super-resolution optical fluctuation imaging (SOFI)

SOFI is a widefield microscopy technique which analyses the temporal fluctuations of fluorescent emitters and theoretically can achieve unlimited resolution gain. However, in practice it was shown that SOFI is able to improve the resolution with a factor of 2-4-fold compared to diffraction-limited imaging [DPB$^+$13]. In comparison with SMLM methods, it obtains lower resolution improvement but it does not require controlled photoswitching or photoactivation of the fluorophores and comes with shorter acquisition times compared to *d*STORM or PALM. The only prerequisite of the utilized fluorophores is that they must exhibit photophysical properties that enable them to transit stochastically and independently of each other between two optically distinguishable states (e.g. ON/OFF state, or distinguishable intensity states). It has been demonstrated that SOFI works with blinking quantum dots (QDs) but also organic dyes or reversibly switchable fluorescent proteins (RSFP) [DCI$^+$09] [DCV$^+$10] [DHV$^+$10] [DMDZ12]. The use of RSFPs as genetically encoded markers that require low excitation powers together with the high imaging speed makes SOFI to a powerful tool in imaging living cells.

1.3 Optical resolution

Optical resolution can be described as the ability of an imaging approach to distinguish details of an imaged object down to a certain level. General resolution criteria were first defined by *Ernst Abbe* [Abb73] and *Lord Rayleigh* [Ray96]. The Rayleigh criterion describes the minimum distance with which two luminescent point sources can be distinguished as two separate objects by an optical system. Whereas Abbe defines the resolution limit by the smallest line distance that still can be detected in an imaged grid.

Under optimal conditions, the theoretically achievable lateral x,y-resolution of super-resolution microscopy techniques is in the range of 100-130 nm using SIM, 20-100 nm using STED and 20-50 nm using PALM/STORM/*d*STORM [SHL10]. However, the performance of an imaging approach in resolving details of a biological structure depends on many factors which can affect the actual achievable resolution of an imaging technique. In the following, I will describe the influence of label density and label size on the achievable spatial resolution. In this context, I will also explain how localization precision and actual resolution are related in SMLM.

1.3.1 Localisation precision and accuracy

The correct interpretation of SMLM data requires knowledge of the accuracy in which a position of a fluorescent molecule relative to ground truth can be determined by centroid fitting. In proteins, the ground truth represents the true molecular position x, y, z of the investigated epitope of a protein or another biomolecule of interest.

In *d*STORM, the same emitter of a label can be recorded several times independently in different frames of the recorded image series. This allows the statistic calculation of the localization precision of this emitter which describes the variance of the estimated positions x_i around its mean value $\bar{x}$. Mathematically, this is given by the formula of the standard deviation σ_x which is defined as the root mean square of the variance:

$$\sigma_x = \sqrt{\frac{1}{n-1}\sum_{i=1}^{n}(x_i - \bar{x})^2}, \tag{1.2}$$

where n is the number of frames in which the molecule was detected, x_i the estimated position in frame i and $\bar{x}$ the average localization.

Several experimental parameters can influence the achievable localization precision including optical pixel size, fluorescent background, detector noise, sample drift, PSF deformation through refractive-index mismatch or orientation effects of the emitter [BAP+16]. The localization precision is often calculated theoretically by describing the emitter profile (or PSF) as photons distributed over a pixel grid with Poisson distributed shot noise. With these assumptions, the PSF can be integrated as 2D Gaussian function with the standard deviation s ($\sim FWHM/2.4$, where $FWHM$ is the full width at half maximum of the function) of the PSF (describing the shot noise). Together with the pixel size, a, of the camera, the signal background, b, and the number of collected photons, N, the localization precision σ_x is given by [TLW02]

$$\sigma_x = \sqrt{\frac{\sigma^2 + a^2/12}{N} + \frac{8\pi\sigma^4 b^2}{a^2 n^2}}. \tag{1.3}$$

Assuming a negligible background, the localization uncertainty can be approximated by $\sigma_x/\sqrt{N}$ where N is the number of detected photons and σ_x is the standard deviation of the corresponding PSF [vHS12]. When collecting more photons, the standard deviation of the PSF becomes arbitrarily small and the localization precision depends largely on the number of collected photons. Typically, *d*STORM achieves a localization precision in the order of 5-20 nm.

However, besides the localization precision, other factors must be considered that contribute to the effective achievable resolution. This refers to the accuracy in which a position of a fluorescent molecule relative to ground truth can be determined. Uncertainties can arise from biased localization algorithms which e.g. assume an isotropic photon emission. As fluorophores often behave as dipoles they exhibit an anisotropic photon emission that can result in intensity peaks shifted from the centre of the molecule and lead to inaccurate localization by biased algorithms [BAP+16]. Another impact on the accuracy of localization is given by the size of the label that is used to mark the biomolecule of interest (discussed in detail in the next chapter). In summary, this means that even if a very high localization precision is achieved by a technique, it is possible that the actual molecule of interest cannot be resolved as different factors affect the accuracy of the localization.

1.3.2 Linkage error and strategies to reduce the label size

The emergence of super-resolution microscopy paved the way for sub-diffraction-resolution imaging but has also pointed out the need for smaller labels as the resolution of these techniques approaches the size of the labels themselves. The label size contributes to a detection of the fluorescent molecules shifted away from the target protein. This distance between the fluorophore and the actual investigated molecule (besides the size of the label) depends on the way in which the label is bound and oriented as well as the location and orientation of the fluorophores on the label. In the worst case, the dislocation of the fluorophore has a distance equal to the size of the marker molecule. This so-called linkage error can lead to highly inaccurate imaging of investigated structures.

In order to reduce the linkage error, immunolabelling with single domain antibodies, known as nanobodies, can be performed. These have a size of $\sim$1.5 nm x 2.5 nm and this significantly reduces the displacement of fluorescent markers compared to commonly used Immunoglobulin G (IgG) antibodies with a size of $\sim$9 nm x 15 nm. So far, only a limited number of nanobodies are available but their small size makes them a promising tool for super-resolution imaging. Nanobodies designed to detect GFP have already been used successfully for nanoscale imaging with a reduced linkage error [RKP$^+$12]. Also super-binding peptides (SBPs) that consist of short linear sequences have been designed which specifically detect linear sequence motifs of ligand binding proteins like neuronal receptors [MHN$^+$17]. These small peptides exhibit high target affinity but require extensive work in analysis and design of the specific sequence.

A further improvement in decreasing fluorophore displacement represents the methodology of genetic code expansion (GCE). Here, a functionalized non-canonical amino acid (ncAA) is incorporated into a protein of interest which then can be targeted by tetrazine-dyes in a click chemistry reaction. This enables the highly specific conjugation of small fluorescent molecules with minimal linkage error. As the specific click chemistry does not interfere with native biological processes it is suitable as a bioorthogonal label for super-resolution imaging in living cells [BKK$^+$19].

1.3.3 Resolution criteria based on the Nyquist Shannon Theorem

Despite the advances in labelling techniques, the reduction of label size and improved properties of fluorescent molecules and their accurate detection, a limiting factor of the spatial resolution is often given by the label density. This relation is described by the Nyquist

Shannon theorem which states that the minimum sampling rate must be twice as high as the desired resolution [Sha49] [SGGB08]. This means that even if individual molecules can be detected with very high accuracy of a few nanometres, structural details in this scale can only be resolved if the labelling density is high enough to fulfil the Nyquist criterion. This can be the case in standard staining methods when labels like antibodies sterically hinder efficient labelling of dense protein complexes [Sau13]. This proves to be one of the biggest limitations for advanced super-resolution techniques that achieve a localization precision of only a few nanometres [GLZ$^+$19] [CHT$^+$20] [BEG$^+$17].

1.4 Expansion Microscopy

Expansion Microscopy (ExM) is a super-resolution technique which physically expands a biological specimen to achieve sub-diffraction-limited imaging. Since its first introduction by *Boyden* and co-workers in 2015 [CTB15], the field of ExM techniques has experienced a rapid increase in protocol variants and applications to different biological samples. This is mainly due to its easy feasibility and low material cost that makes ExM applicable for many biological laboratories. Additionally, it is a tool that promises high-resolution imaging without the need of expensive equipment or expertise in a super-resolution technique. In the following chapter, I will describe the principle and procedure of the ExM method in detail and present the different protocol variants available.

1.4.1 Principle of Expansion Microscopy (ExM)

Optical magnification by spherical lenses is based on increasing the visual angle of incidence of an object. ExM uses a similar approach but increases the angle of the incident light by magnifying the object itself. For this purpose, the ExM procedure embeds a biological specimen in a hydrophilic polymer that physically shifts fluorescent labels used for protein marking or proteins themselves evenly in space to obtain an enlarged view on the sample. This physical expansion causes an increase in resolution through separation or at least an increase in distance between individual fluorescent molecules within a diffraction limited area. This effect on resolution enhancement can be explained by the Rayleigh criterion [Ray96] (Figure 1.4).

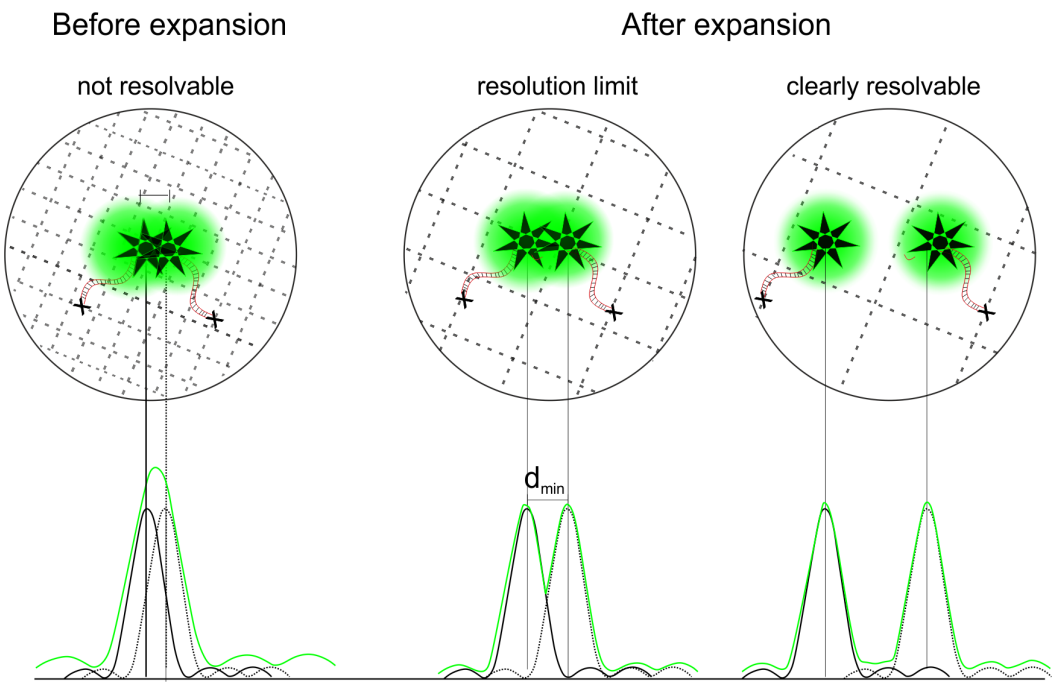

Figure 1.4: Resolution enhancement by physical specimen expansion. The schematic shows two fluorescent molecules attached via a DNA linker to a hydrophilic polymer network (dashed lines). The green curve shows the intensity pattern resulting from the overlay of two Airy disc diffraction patterns (2D) of two luminous point sources that are imaged through a circular aperture like a lens. The central region of each profile (from peak to the first minimum) is defined as an Airy disk. The Rayleigh criterion mathematically describes the minimum distance d_{min} at which the point sources still can be resolved as distinct emitters. This is given by $d_{min}= 0.61\lambda/\mathrm{NA}$ (1.4), where λ is the wavelength of light illuminating the circular aperture and NA the numerical aperture of the microscope. Two overlapping diffraction patterns are just resolvable when the first minimum of one curve is coincident with the maximum of the other curve (resolution limit).

The ExM processing spatially shifts adjacent fluorophores (not resolvable) within a diffraction limited area (Figure 1.4). Depending on the expansion factor, single emitters reach the distance dmin (resolution limit) or get separated further (clearly resolvable). The spatial displacement results in resolving single emitters after expansion even when imaged with the same diffraction limited microscope used for imaging before expansion where the molecules could not be distinguished.

1.4.2 Superabsorbent hydrogels

A key component of Expansion Microscopy is a hydrophilic macromolecule which belongs to the class of so-called superabsorbent polymers (SAPs). It is the driving force during expansion, pulling anchored biomolecules or labels isotropically apart in space. Such hydrogels form a three-dimensional network composed of crosslinked polymer chains. The co-monomers acrylamide (AA) and sodium-acrylate (SA) are polymerized in a free radical polymerization chain reaction and crosslinked using N,N‘-methylenebisacrylamide (Bis-AA) (Figure 1.5).

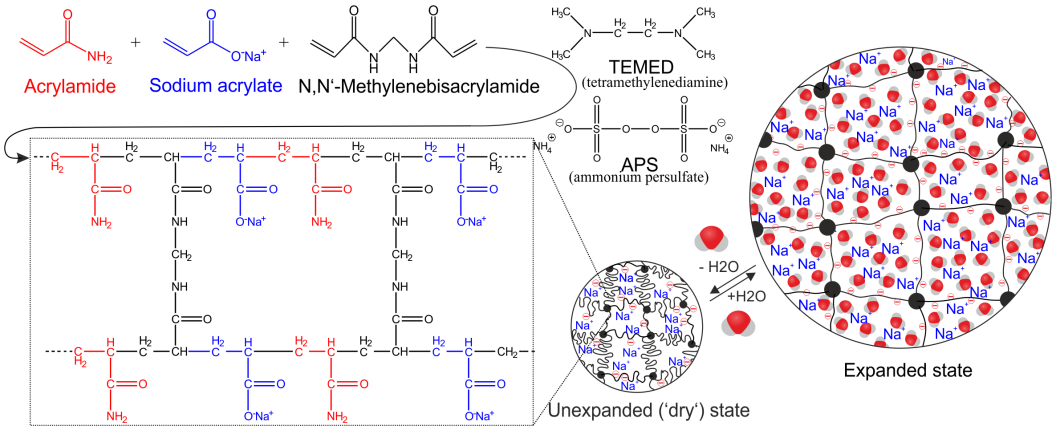

Figure 1.5: Superabsorbent hydrogel. The hydrogel is formed through radical polymerization of the monomers acrylamide (red), sodium acrylate (blue) and the crosslinker molecule N,N’methylenebisacrylamide (black). Ammonium persulfate (APS) serves as radical starter and tetramethylethylendiamine (TEMED) as accelerator of the polymerization reaction. In the unexpanded state the polymer chains (illustrated as black curved line) are packed densely and connected by the crosslinker molecules (represented as black dots). Upon exposure to water, the water molecules get absorbed by the polymer and the polymer chains become stretched but are still held together by the crosslinker molecules (expanded state).

Sodium acrylate exhibits an ionic group that interacts with polar liquids like water. This renders the polyelectrolyte capable of holding a large amount of water. When exposed to water, SAPs are able to absorb and hold a volume of water that can exceed their own mass by over 100 times. In industry, these unique material properties are primarily used for hygiene products like baby diapers or sanitary napkins. But the potential of water absorption makes SAPs suitable for a wide variety of applications in other fields, including agriculture, biomedicine and pharmacy, e.g. as soil conditioner, scaffold in tissue engineering, as wound

dressing, for drug delivery or to remove body fluids during surgery [ZMODK10].

In dry conditions, the acrylic based polymer chains are in a densely packed and coiled conformation. The ionic side groups of the polymer backbone give the polymer a salty character. In contact with pure water or an aqueous solution, the absorption of the solvent molecules is driven by an osmotic process. Carboxylic side groups and sodium ions get solvated upon water uptake. As a result, the negatively charged side groups are exposed and repel each other. This leads to an extension of the elastic polymer chains and an expansion of the hydrogel structure. Only the crosslinking molecules prevent a complete dissolving of the polymer chains. The hydrogel network structure can be adjusted on the molecular level by varying the concentration of the crosslinker. The cross-link density determines the network's mesh size and thereby the maximum water absorption capacity. The swelling degree of the hydrogel is sensitive to the pH and ionic strength of the surrounding medium.

1.4.3 Workflow of the original ExM protocol

The first version of ExM (called 'original' ExM protocol in the following) performs immunostaining before expansion using primary antibodies for antigen binding and DNA-modified secondary antibodies, followed by gelation of the sample, homogenization of the sample-hydrogel hybrid and expansion in water (Figure 1.6).

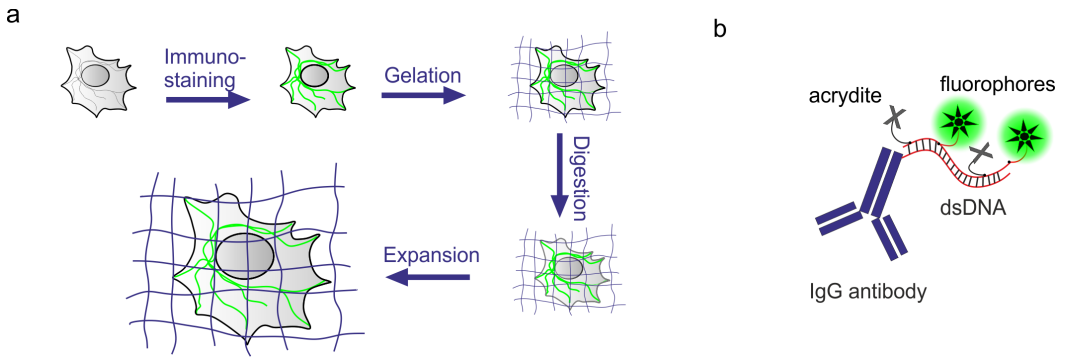

Figure 1.6: Original ExM protocol. a, Schematic workflow of ExM. The biological sample is immunostained, embedded in a superabsorbent hydrogel, mechanically homogenized by enzymatic digestion and expanded by washing in water. **b,** Trifunctional label. A chemically modified ssDNA is coupled to an IgG antibody. Two complementary DNA oligos are then hybridized to the ssDNA and each carries a fluorophore for imaging and an acrydite modification which allows covalent incorporation into the swellable hydrogel during gel formation.

As secondary antibodies, custom-made oligo-antibody conjugates are required that provide a chemical linker group for incorporation in the polyacrylamide gel as well as a fluorescent dye modification for imaging (Figure 1.6b). Oligonucleotides are short DNA molecules that can be used to attach different internal or 5' and 3' modifications compatible for different ExM strategies. The original ExM protocol, utilized a 42 basepair (bp) long single stranded amino DNA oligo which is coupled to an IgG antibody and two complementary 21 bp long ssDNA strands each containing a 3'-acrydite and a 5'-fluorophore modification. After immunostaining with primary antibody and secondary oligo-antibody, the complementary sequences are hybridized to the oligo-antibody conjugate. Specimens can then be incubated with acrylic co-monomers and crosslinker molecules of the hydrogel. During radical co-polymerization, hydrogel components together with the 3'-acrydite moiety of the DNA strand form a covalently connected polymer network.

To ensure an isotropic expansion of the attached DNA molecules, a homogenization step of the sample-hydrogel conjugate is performed after gelation. Protein-protein interactions otherwise might hinder an even displacement of the labels. Thus, proteins are broken down by enzymatic digestion using Proteinase K as a broad-spectrum serine protease. As a result, the fluorophore bearing dsDNA can be pulled apart isotropically by the polymer chains while maintaining the native organization of the labelled proteins. The hydrogel composition of the original ExM protocol achieves a $\sim$4.5-fold expansion factor. This enabled *Boyden* and his co-workers to perform confocal imaging of expanded cultured cells and mouse brain tissues with $\sim$70 nm lateral resolution [CTB15]. Besides the improvement of resolution, the ExM treatment also reduces effects of light scattering by clearing the sample and thereby improves the signal-to-noise ratio. This allows volumetric imaging in thick tissues with improved image quality.

1.4.4 ExM variants and applications

Since ExM is accessible to many laboratories working in different biological fields, a range of protocols have been developed in recent years for different samples and in combination with different fluorescence microscopy techniques. Thereby, impressive results could be obtained by the magnified visualization of various biomolecules including proteins [CTB15] [TCP$^+$16] [CCY$^+$17] [KSP$^+$16], RNA [CWC$^+$16] [AGS$^+$20] in fixed mammalian cells and tissues. Among others, as reviewed by *Wassie et al.* [WZB19] and described in the *Methods in Cell Biology volume 161* [PV21], optimized ExM approaches exist for different organisms including protocols for expansion and imaging of human tissue for clinical diagnosis [ZBI$^+$17]

[BFC+20], pathogens like *Chlamydia trachomatis* [KGSR19], Zebrafish [FOF+17], imaging of a whole *Drosophila melanogaster* larvae [HRP+19], the expansion of *Caenorhabditis elegans* [YBW+20] or plant tissue [KN19]. With the mentioned protocols, the expanded samples are mostly imaged using confocal microscopes. But there have been also attempts to combine ExM with other imaging modalities like SIM [CYW+17] [HAC+17] [KGG+20], STED [GMB+18] [LCL+18], PALM [TCP+16], STORM [TBY+16] [XTY+19], SOFI [LCL+18], and Lattice Light Sheet Microscopy (LLSM) [GAU+19].

From the methodological point of view, the protocols mainly differ in the type and time of labelling, the chemical composition of the hydrogel and the method of homogenization of the hydrogel-sample conjugate required for an isotropic expansion. In this section, I will describe variants of the original ExM protocol which result in the simplification of the original protocol, the preservation of the protein content of the sample, and the optimization of hydrogel chemistry.

1.4.5 Protein retaining ExM protocols

The original ExM protocol required custom-made functionalized antibody-DNA conjugates as fluorescent labels that are linked into the hydrogel (Figure 1.6b). The use of the DNA labels made it unnecessary to maintain the protein content of the expanded sample and enabled free expansion of the labels after protein destruction. On the other hand, the loss of proteins also limits the procedure to pre-expansion labelling which may entail several drawbacks. Firstly, pre-expansion labelling contributes to an increased label inaccuracy compared to post-expansion labelling due to a higher linkage error caused by the impact of the label size. Additionally, in the case of multi-target labelling, it also requires the design of several custom-made DNA-antibody conjugates which can become costly and time-consuming.

These limitations led several laboratories to the development of expansion protocols able to preserve the protein content of a sample yet still allow isotropic expansion of it. Methods that cross-link proteins directly into the hydrogel provide the possibility to label epitopes after expansion, an approach which reduces the linkage error. Furthermore, post-expansion labelling eliminates the need for fluorophores that survive the radical polymerization step of the hydrogel. With pre-expansion labelling protocols, fluorophores often get chemically attacked by radicals during gel formation which leads to a reduction or in the worst case, a complete loss of fluorescence signal after the ExM treatment.

Protein-retention expansion microscopy (proExM)

ProExM [TCP+16] was designed by the laboratory of *Edward Boyden* in order to anchor and preserve protein labels like fluorescent proteins, conventional fluorescently labelled antibodies and streptavidin that were introduced pre-expansion. For this purpose, the proExM protocol makes use of a commercially available succinimidyl ester of (6-((acryloyl)amino)hexanoic acid (acryloyl-X,SE; abbreviated AcX). Active esters like succinimidyl esters (SE) are amine-reactive groups that form stable carboxamide bonds with primary amino groups. Practically all proteins contain primary amino groups either situated as α-amino group in the N-terminus of the polypeptide chain or present as ε-amino group of lysine residue. Using amine reactive molecules allows the functionalization of proteins with acrylamide monomers and the covalent conjugation into the hydrogel network during polymerization. The proExM workflow includes the AcX treatment of the specimen followed by gelation, strong Proteinase K digestion and expansion of the sample (Figure 1.7a).

The treatment enables the magnified imaging of FPs, commercially available antibodies and enzymatic tags which persist following the expansion procedure. In their publication, they also describe the possibility of immunolabelling of native endogenous proteins or FPs which are anchored to the hydrogel and stained by antibodies after expansion. For this purpose, they present different strategies to homogenize the sample-hydrogel conjugate including heat and chemical induced denaturation as well as mild digestion by the endoproteinase Lys-C which specifically cleaves the C-terminal of lysine residues. However, they point out that their findings suggest the need of the strong Proteinase K digestion as performed in the original ExM protocol to ensure an isotropic expansion.

Magnified analysis of the proteome (MAP)

MAP [KSP+16] is an expansion protocol which incorporates proteins of fixed cells or tissues into a superabsorbent hydrogel and is designed to stain proteins in the expanded state using fluorescently labelled antibodies. According to the developer of the protocol, the key to the MAP protocol is to prevent intra- and interprotein crosslinking during hydrogel-sample conjugation. Adapted from the tissue clearing approach CLARITY [CWK+13], acrylic monomers in high concentration are incubated together with formaldehyde (FA) before thermally triggered polymerization of the gel. During this step, FA acts as crosslinker between amide groups on proteins and the acrylic monomers. In a first step, FA reacts to amides and leaves reactive methylols that can react to adjacent amine or amide groups within the

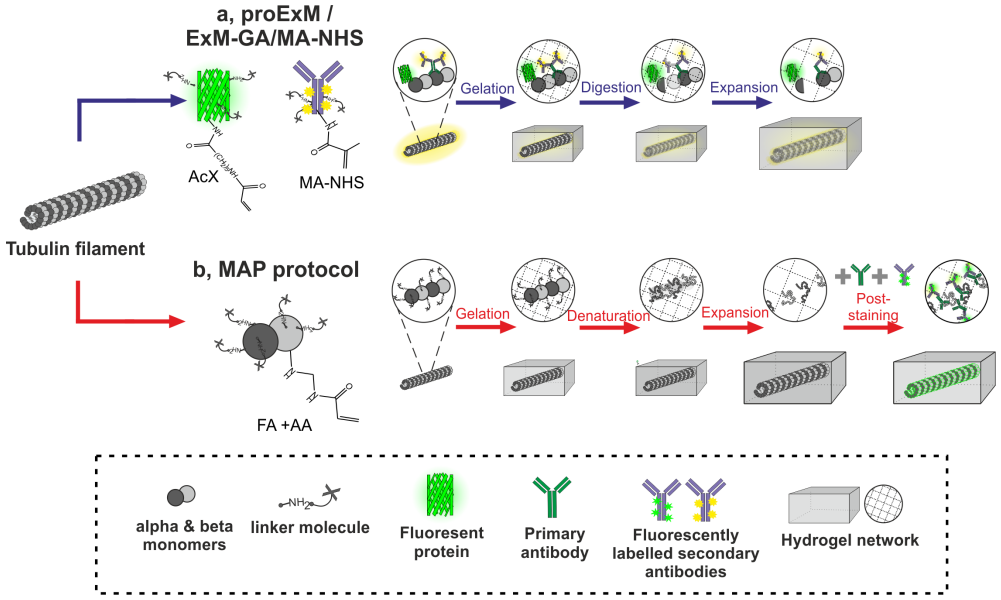

Figure 1.7: Workflow of protein retaining ExM protocols. a, proExM / ExM-GA/MA-NHS. The biological sample (tubulin filament) is either immunolabelled with primary and fluorescently tagged secondary antibodies or marked by the expression of genetically encoded FPs pre-expansion. In the next step linker molecules are attached to the respective label. In the case of proExM, AcX reacts to FPs or fluorescently labelled antibodies. In the case of the ExM-GA/MA-NHS protocol either MA-NHS (methacrylic acid N-hydroxysuccinimidyl ester) or glutaraldehyde (GA) are used as amine reactive compounds that form stable bonds between proteins and the hydrogel during gelation. The samples are then homogenized using Proteinase K digestion and expanded in water. **b,** MAP protocol. Before gelation, samples are incubated in a buffer containing formaldehyde (FA) and acrylamide monomers (AA). In this way, AA monomers become attached to the proteins and can be incorporated into the hydrogel network. Subsequently, the sample is homogenized by heat and chemical induced denaturation and expanded in water. Finally, primary and secondary fluorescently labelled antibodies are added to the expanded sample.

same or neighbouring proteins. This intra- or interprotein conjugation by the formation of methylene bridges is quenched by the presence of the high concentration of acrylic monomers (Figure 1.7b). In this way, proteins are coated with hydrogel monomers which subsequently can be cross-linked into the polymer during hydrogel formation.

MAP provides optimized expansion protocols for hydrogel embedding of tissues and whole organs (General MAP protocol) as well as a variant for expanding cultured cells (Cell-MAP). Both include a heat and chemical induced denaturation step after hydrogel embedding of the sample. This step ensures the free dissociation of proteins without a hindered expansion through coherent proteins. As a consequence of the denaturation step,

the proteins are present as linear polypeptide chains cross-linked in the hydrogel. Since antibodies often require only the linear amino acid sequence to recognize epitopes, they can be added for protein marking, post-expansion. Nevertheless, each antibody has to be tested for recognition of epitopes after the MAP treatment. *Ku et al.* [KSP$^+$16] could demonstrate positive recognition of epitopes by 100 from 122 tested antibodies ($\sim$82% positive).

ExM using conventional antibodies

Another simplification of the original ExM protocol by the preservation of fluorescently labelled antibodies introduced pre-expansion was demonstrated by *Chozinski et al.* [CHO$^+$16]. They crosslinked conventionally immunostained samples into the hydrogel by treating them with glutaraldehyde (GA) before expansion or the amine-reactive MA-NHS (methacrylic acid N-hydroxy succinimidyl ester) (Figure 1.7a). The approach will be called ExM-GA or ExM-MA-NHS protocol in the following depending on the linker used.

1.4.6 Hydrogel variants yielding higher expansion factors

At first glance, the resolution improvement achieved by the ExM method is mainly determined by the maximum achievable expansion factor of the hydrogel. Due to this, efforts have been made to optimize the water absorbency and mechanical properties of hydrogels yielding higher swelling degrees and stability of the expanded polymer. In this context, several factors are decisive in contributing to artifact free imaging of the expanded sample without distortions of the native structure introduced by the ExM treatment.

One important role in the development and optimization of hydrogels for ExM is the stability of the expanded gels. A certain stiffness of the hydrogel must be guaranteed so that gels are stable and do not break during sample handling. The mechanical properties and swelling capacity of hydrogels are mainly determined by the crosslinker molecule density. Weakly cross-linked gels result in larger pore sizes and achieve higher expansion factors, but also become more fragile and tend to break more easily. In contrast, increasing the crosslinker density results in more stiff hydrogels but also lowers the achievable swelling capacity. A compromise must therefore be made between the stability and the swelling capacity of the hydrogel. The original ExM protocol was designed with a crosslinker concentration that resulted in a $\sim$4.5-fold expansion factor. Higher expansion factors could be shown by decreasing the Bis-acrylamide concentration, but the gels are not suitable for ExM as they

became more fragile.

Truckenbrodt et al. [TMC+18] developed an expansion protocol called X10 expansion microscopy which achieves a 10-fold gel expansion factor using N,N-dimethylacrylamide (DMAA) and SA as co-monomers. DMAA based hydrogels provide high mechanical stability which allows the handling and imaging of the specimen after 10-fold expansion. In the presence of potassium persulfate (KPS) as radical starter, DMAA is able to undergo self-crosslinking and can be polymerized with SA as co-monomer in a free-radical polymerization. DMAA based hydrogels exhibit unique mechanical properties. Swelling ratios of up to ∼3000 (mass of swollen gel / mass of dry gel) were reported yet still provided robust hydrogels due to the homogenous distribution of cross-links [CBS+14]. X10 ExM so far achieves an ∼1000-fold increase in volume.

An alternative strategy which results in higher expansion factors of up to 50-fold, is iterative expansion microscopy (iExM) developed by the *Boyden laboratory* [CCY+17]. With this technique, samples are routinely magnified ∼20-fold by expanding the sample twice in series ∼4.5-fold using two swellable hydrogels with different crosslinker molecules. As in the original ExM protocol, the procedure embeds the sample that was immunolabelled with primary and specially designed secondary IgG-oligonucleotide conjugate antibodies. In contrast to the original protocol, the first hydrogel is synthesized with N,N‘-(1,2-dihydroxyethylene) bis-acrylamide (DHEBA) as crosslinker molecule which can be cleaved at high pH. To stabilize the first gel, an uncharged polyacrylamide gel (re-embedding gel) is synthesized within the polymer network which is also synthesized with the cleavable DHEBA crosslinker. This allows the introduction of another DNA-label that is hybridized to the DNA label anchored to the first polymer. A second hydrogel containing the regular bis-acrylamide crosslinker molecule is then polymerized within the first gel which remains held in the expanded state by the re-embedding gel. This allows the covalent insertion of the acrydite moiety of the second DNA label into the second hydrogel. Using a NaOH containing buffer with high pH cleaves the DHEBA crosslinker and thereby dissolves the first hydrogel and the re-embedding gel.

Finally, the second hydrogel which is not pH sensitive can be expanded. In this way, the positions of the labels become shifted apart another ∼4.5-fold in space. In summary, the molecular information of the immunolabelled proteins in the unexpanded state first get encoded and imprinted in the first hydrogel at the position of the anchored DNA label. Then, this positional information is expanded 4.5-fold and transferred in the expanded state to the second hydrogel which again is expanded 4.5-fold. So far, iExM achieves the highest

possible expansion factor of all ExM variants but requires custom-made DNA labels and additional protocol steps which can be very time consuming. Although expansion factors of up to 53-fold could be shown, the positional error introduced by the size of the antibodies and DNA labels increases in a linear fashion with the expansion factors and limits the effective resolution.

Another aspect to consider when gels are designed for higher expansion factors is the dilution of the fluorescence signal. The volumetric dilution of fluorescent molecules ($\sim$90-fold with a $\sim$4.5-fold expansion and $\sim$1000 fold with a $\sim$10-fold expansion) decreases the sample brightness in the imaged optical section and thereby can reduce image quality. DNA or locked nucleic acid (LNA) probes can be used for signal amplification but also increase the positional error caused by the label [CCY$^+$17].

1.4.7 Non-radical hydrogel polymerization (tetra-gel ExM)

To ensure an isotropic expansion at the nanometric scale, biomolecules must be cross-linked homogenously into the hydrogel. This can only be achieved if the pore size of the hydrogel network is in the size range of the investigated molecules and the polymer is distributed uniformly throughout the specimen. Consequently, although an increase in pore size leads to a higher expansion factor, above a certain mesh size it can also lead to an inhomogeneous expansion of the specimen and a reduction of the effective resolution. In this context, structural heterogeneity of the polymer network might cause distortions of the native specimen introduced by an inhomogeneous linking. Acrylic based hydrogels synthesized by free-radical polymerization often exhibit spatial inhomogeneity caused by unequal distribution of monomer and crosslinker molecule densities as well as topological defects of the formed polymer chains.

An alternative hydrogel chemistry is non-radical terminal linking of tetrahedral shaped monomers which form highly homogenous gel structures which could potentially reduce the distortions introduced by the hydrogels developed thus far for ExM [GYG$^+$19]. The so called tetra-gel (TG) is formed by click-chemistry based linking of polyacrylate and polyethyleneglycol (PEG) monomers. Proteins can be crosslinked in the TG by covalently adding an azide group to primary amines on the proteins which can then react with the gel monomers in a click reaction. With this gel variant, an expansion factor of $\sim$3.0-3.5-fold could be shown. Even higher expansion factors are possible when using modified monomers which exhibit a cleavable moiety that can be used to perform iExM.

Chapter 2

List of puplications

This thesis is based on the following publications:

M1 Gambarotto, D.*, Zwettler, F.U.*, Le Guennec, M., Schmidt-Cernohorska, M., Fortun, D., Borgers, S., Heine, J., Schloetel, J.-G., Reuss, M., Unser, M., Boyden, E.S., Sauer, M., Hamel, V., Guichard, P. (**2019**) Imaging cellular ultrastructures using expansion microscopy (U-ExM). *Nature Methods* **16**, 71–74.
**authors contributed equally*

M2 Zwettler, F.U.*, Spindler, M.-C.*, Reinhard, S., Klein, T., Kurz, A., Benavente, R., Sauer, M. (**2020**). Tracking down the molecular architecture of the synaptonemal complex by expansion microscopy. *Nature Communications* **11**, 3222.
**authors contributed equally*

M3 Zwettler, F.U., Reinhard, S., Gambarotto, D., Bell, T.D.M., Hamel, V., Guichard, P., Sauer, M. (**2020**). Molecular resolution imaging by post-labeling expansion single-molecule localization microscopy (Ex-SMLM). Nature Communications **11**, 3388.

M4 Zwettler, F.U.*, Reinhard, S.*, Sauer, M. (**2020**). Ex-*d*STORM and automated quantitative image analysis of expanded filamentous structures. *Elsevier, Methods in Cell Biology. (**In Press**, available online 10 June 2020, https://doi.org/10.1016/bs.mcb.2020.05.004)*
**authors contributed equally*

Further publications

M5 Rozario A. M., Zwettler F. U., Duwé S., Hargeaves R. B., Brice A., Dedecker P., Sauer M., Moseley G. W., Whelan D. R., Bell T. D. M. (**2020**) 'Live and Large': Super-Resolution Optical Fluctuation Imaging (SOFI) and Expansion Microscopy (ExM) of Microtubule Remodelling by Rabies Virus P Protein. *Australian Journal of Chemistry* **73**, 686-692.

Chapter 3

Results and Discussion

In this section, I will give a comprehensive overview of the different ExM approaches I developed for the combination of ExM with confocal microscopy, SIM, STED and *d*STORM. I will present and discuss the results obtained and published in the manuscripts M1-4 listed in chapter 2 as well as unpublished data related to them. This includes the magnified visualisation of isolated centrioles, microtubules, clathrin-coated pits (CCPs), mitochondria and the synaptonemal complex. The methods and reagents used are described in detail in the respective online methods of the publications M1-M3 and illustrated in the methodological paper M4 providing a step-by-step protocol for the ExM procedure.

3.1 Imaging cellular ultrastructures using expansion microscopy (U-ExM)

(This chapter represents the work of manuscript M1.)

The cellular world contains numerous molecular components involved in controlling and maintaining homeostasis and functioning of the cell. As specialized macromolecular complexes in the size range of tens to hundreds of nanometres, organelles are involved in essential cellular processes. For this purpose, they exhibit a specific structure and 3D architecture related to their function. Available imaging technologies permit the study of these cellular units at different scales. Super-resolution fluorescence microscopy can successfully visualize and quantify the organization of proteins in macromolecular complexes with a size beyond the optical diffraction limit [SL17] [SHJ17] [SH17]. But so far, these techniques are still limited in resolution due to the linkage error introduced by the size of conventionally used

IgG-antibodies and inefficient labelling densities which do not meet the Nyquist criterion. As structural details of cellular organelles often lie in the nanometric range, so far only electron microscopy has been capable of visualizing these features.

The aim of this work was the development of an ExM protocol which in combination with fluorescence imaging is able to reveal ultrastructural details of organelles beyond the resolution achieved by super-resolution microscopy (SRM). We called the approach ultrastructure expansion microscopy (U-ExM) since it allows the study of preserved ultrastructures of macromolecules in vitro and in cells. As a reference structure, we studied centrioles isolated from the green algae *Chlamydomonas reinhardtii*. Electron microscopy studies could already reveal precise dimensions and structural features of this barrel-shaped organelle that has a length of ∼500 nm and a diameter of ∼250 nm [WO14] (Figure 3.1).

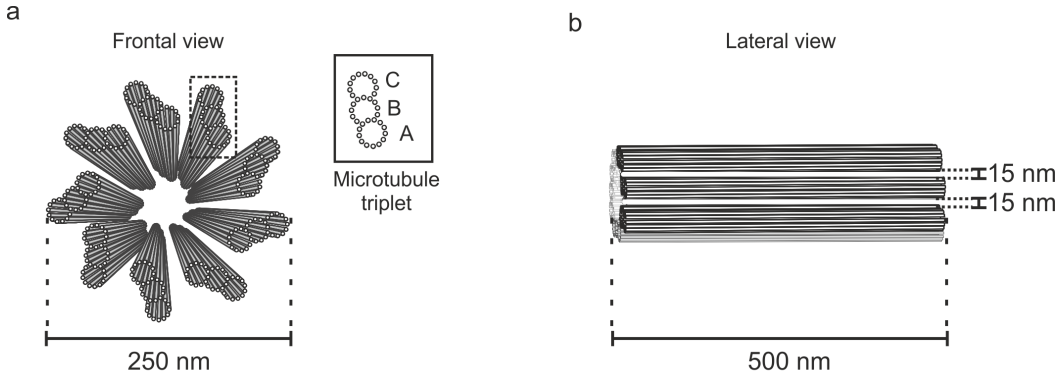

Figure 3.1: Model structure of centrioles. a, Schematic of a centriole in frontal view showing the cylindrical arrangement of 9 microtubule triplets with a diameter of ∼250 nm. The microtubule triplets each consist of a complete microtubule containing 13 α- and β-tubulin protofilaments, called A-tubule and two assembled B- and C-tubules consisting of 10 protofilaments each. **b,** Schematic of a centriole in lateral view with a length of ∼500 nm with 15 nm distance between neighbouring microtubule triplets. (*Material adapted from M3*)

As a part of the centrosome, centrioles are responsible for the assembly of the mitotic spindle during cell division [Bor12]. Among other roles, they are also involved in cell motility and signalling forming cilia in cells and organizing microtubules in the cytoplasm [CWR15]. In quiescent cells, two adjacent centrioles are arranged orthogonally to each other. Centrioles duplicate during the cell cycle whereby the more mature centriole is referred to as mother and the newly assembled centriole is called procentriole [HS10]. In algae, they serve as basal-

body which initiates the formation of the flagellar apparatus [PGD00]. Centrioles exhibit an evolutionary conserved structural organization of 9 microtubule-triplets which are arranged at a 120-degree angle to each other. Cryo- electron tomography of purified basal bodies of *Chlamydomonas reinhardtii* could reveal their polarity of centrioles in distinguishing three regions in lateral view; the ∼100 nm-long proximal region, the ∼250-nm-long central core region and the ∼150 nm-long distal region as well as the distinction and organization of the A, B and C microtubule triplets [LFMA12] [GHM$^+$13]. The precisely known dimensions of the centriole structure make it a suitable reference structure for the development of an imaging approach that is capable of revealing details in the nanometre size range.

3.1.1 Development of the U-ExM approach

To compare the performance of already existing ExM protocols, we imaged unexpanded centrioles using confocal and *d*STORM imaging. As centrioles mainly consist of tubulin, we immunolabelled isolated centrioles immobilized on round cover glasses with α-tubulin and polyglutamylated tubulin (PolyE). PolyE is a posttranscriptional modification of tubulin monomers which occurs only in the central core region of the centriole [HSH$^+$17]. We performed a two-color experiment, simultaneously labelling α-tubulin and PolyE, which were imaged with a confocal microscope (Figure 3.2a). In the top view of centrioles, we could observe the hollow structure visible as a ring-like signal distribution of PolyE after deconvolution of the images. However, this feature could not be revealed in the α-tubulin channel which showed a displaced and insufficient signal distribution. The overlay of both channels in the lateral view suggests impaired antibody accessibility when co-staining the centriole.

In order to study the molecular architecture of the centrioles with improved resolution, we tested two ExM protocols performing immunostaining either before or after expansion. To provide a facilitated handling of the sample and reproducibility of the expansion experiments, I developed an expansion workflow for cells and isolated organelles like centrioles immobilized on round coverslips. The protocol uses cost-effective materials and is compatible with all ExM variants. Protocols developed until then required either expensive chambers containing a removable lid for gelation or custom-made gelation chambers made e.g. from Teflon or poly(dimethylsiloxane) (PDMS). In addition, not all commercially available imaging chambers are compatible for the synthesis of hydrogels as their material often contain radical catchers which hinder the polymerization reaction. Also, these chambers require a high volume of gel solution which leads to the formation of relatively thick gels that are difficult to image in the expanded state and need to be cut into slices before imaging. In

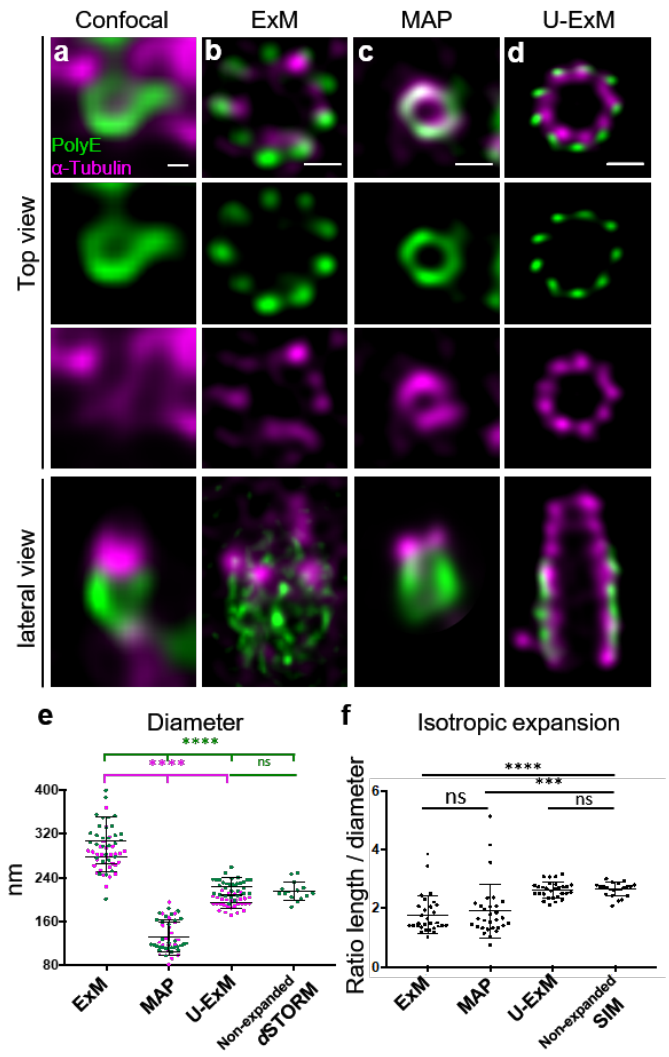

Figure 3.2: Centriole expansion using U-ExM. a-d, Nonexpanded (**a**) and expanded (**b-d**) isolated centrioles stained for PolyE (green, Alexa488) and αtubulin (magenta, Alexa568) imaged by confocal microscopy deconvolved by HyVolution (HyV) post-processing. Centrioles were expanded using ExM-GA (**b**), MAP (c) or U-ExM (d). **e,** Diameter of the centrioles in the different conditions. Green and magenta dots represent PolyE and α-tubulin diameters, respectively. Averages and standard deviation are as follows: PolyE: 308 ± 42 nm, 133 ± 27 nm, 225 ± 15 nm and 216 ± 17 for ExM-GA, MAP, U-ExM and non-expanded *d*STORM respectively. α-tubulin: 279 ± 29 nm, 130 ± 32 nm and 195 ± 12 nm, for ExM-GA, MAP and U-ExM respectively. **f,** Isotropic expansion measured as the ratio between the centriolar length and diameter: ExM-GA =1.8 ± 0.6, MAP=1.9 ± 0.9, U-ExM = 2.6 ± 0.3, Non- expanded SIM=2.6 ± 0.2. Scale bar, 100 nm (a), 450 nm (b-d). (*Material adapted from M1*)

order to vary the thickness of the gels as desired and to allow the use of cover glasses which are standard for seeding and immunostaining of cells, I designed an ExM workflow that performs the gelation of the samples on a parafilm coated surface (Figure 3.3).

Parafilm is a hydrophobic film which is a standard material available in most biological and chemical laboratories. A culture well plastic lid or a similar flat surface can be coated with the film and serves as a gelation platform on ice (Figure 3.3a). Thanks to the hydrophobicity of the film, the gelling solution forms a drop when it is placed on the surface (Figure 3.3b). The cover glass with sample facing down can then be placed on top of the drop which stays under the glass. Thereby, the thickness of the synthesized gel can be adjusted by varying the volume of the gelling solution. After hydrogel formation the hardened gel is still attached to the cover glass and can be easily removed from the film and together with the

glass transferred to another well in which further steps like homogenization and expansion are performed. The optimized expansion workflow described in Figure 3.3 allowed the comparison of existing ExM protocols applied on isolated centrioles.

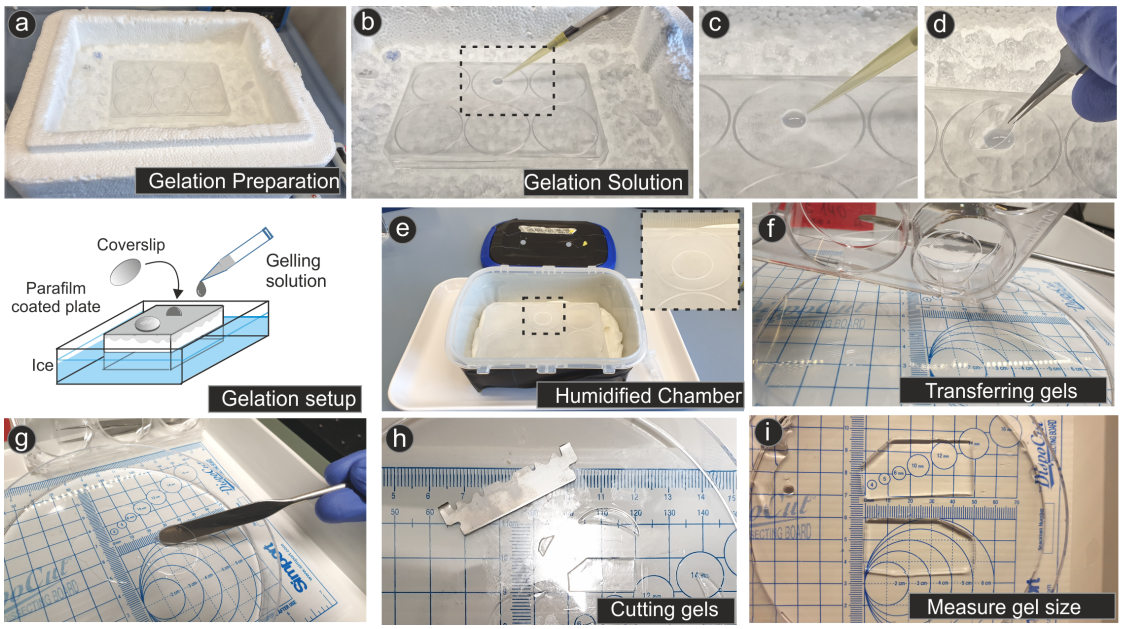

Figure 3.3: ExM workflow steps for cultured cells and isolated organelles. **a,** Preparation of gelation. A culture plate lid covered with parafilm serves as a hydrophobic gelation surface and is put on ice together with the gelling reagents (acrylic monomers, APS and TEMED). **b,** Gelation. Depending on the size of the coverslip a 35-90 µl drop of the Gelling Solution is placed on top of the parafilm coated plate. **c,** Zoom in on the highlighted area in (b). **d,** The coverslip with cells facing down is placed on top of the gelling solution drop. The solution will spread out flat and stay under the coverglass due to the hydrophobic properties of the parafilm. **e,** Humidified chamber. The image shows the humidified chamber used for gelation. The plate with the sample is carefully transferred to the tupperware with wetted tissue at the bottom of the container. The lid of the tupperware is closed and put at 37°C for gelation. **f-g,** Transfer of gels. After homogenization of the hydrogel-sample hybrid (digestion or denaturation), hydrogels are carefully transferred to an appropriate container for expansion in water. **h,** Cutting of gels. Gels are cut in a recognizable shape that clearly identifies the top and bottom of the gel. **i,** Measure gel size. During expansion the gel size can be measured to determine the expansion factor which does not change within several washing steps when the maximum achievable swelling is reached. (*Material adapted from M4*)

To test an ExM protocol which performs immunostaining pre-expansion, we treated samples according the ExM-GA protocol [$CHO^{+}16$] using glutaraldehyde as chemical linker to incorporate fluorescently labelled antibodies directly into the hydrogel. The protocol includes the synthesis of the original ExM hydrogel with a chemical composition that achieves

a ∼4.5-fold expansion factor. As a post-expansion labelling protocol, we performed the MAP-Cell protocol [KSP$^+$16] which first incorporates proteins into the hydrogel and labels epitopes after denaturation and expansion of the sample.

We imaged ExM-GA and MAP expanded centrioles by confocal fluorescence microscopy and determined the average diameters of expanded centrioles in frontal view for each condition (Figure 3.2b-c, e). Expanded lengths given in the following are divided by the expansion factor determined by measuring the hydrogel size before and after expansion for the respective experiment. For ExM-GA treated centrioles an average diameter of 308 ± 42 nm for the PolyE signal and a 279 ± 29 nm for the α-tubulin signal was determined. MAP expanded samples showed an average diameter of 133 ± 27 nm for the PolyE signal and 130 ± 32 nm for the α-tubulin signal. When compared to unexpanded *d*STORM images where a diameter of 216 ± 17 nm was determined for the PolyE signal the results showed a mismatch between the measured diameter and the respective expansion factors for each expansion protocol. The expected diameter of ExM-GA expanded centrioles was too large by a factor of 1.4 and too small for MAP expanded centrioles by a factor of 0.6. This suggests a defect in the macromolecular expansion of centrioles introduced by the respective ExM-GA or MAP treatment or an increased linkage error when using the ExM-GA protocol. This observation was also evident in the investigation of the isotropy performed by comparing the length to diameter ratio for unexpanded SIM to the respective expanded ratios (Figure 3.2f).

We tested and compared the performance of different FA and AA concentrations of the FA/AA protein linking buffer in order to find optimal conditions for an isotropic expansion of the centrioles. By avoiding an initial fixation step and by lowering the concentrations of the MAP-Cell linking buffer for FA from 4% to 0.3–1 % and for AA from 30 % to 0.15–1% resulted in intact centrioles with expected diameters (Figure 3.2d-e). The resulting diameter of 225 ± 15 nm determined from U-ExM expanded centrioles is in good agreement with the unexpanded diameter of 216 ± 17 determined as well as similar length to diameter ratios of ∼2.6, for both unexpanded and expanded centrioles (Figure 3.2f). The diameter and isotropy analysis confirmed the preservation of the near-native conformation of centrioles. Remarkably, U-ExM could clearly reveal the 9-fold symmetry of centrioles in the PolyE and as well in the α-tubulin signal when co-staining the sample. This shows an improved epitope accessibility deriving from additional space created by the protein displacement. Also, the distribution of the PolyE signal could be located at the central region of the organelle (Figure 3.2d).

In comparison with unexpanded *d*STORM where the 9-fold symmetry cannot be clearly resolved, images of U-ExM expanded centrioles acquired with a diffraction-limited confocal microscope appear similar in image quality when taking the 9-fold symmetry as criterium (Figure 3.4a-b). In combination with image post-processing by a deconvolution algorithm, the image quality can be further improved by enhancing the signal-to-noise ratio (SNR). With the reduced noise and enhanced contrast, the 9-fold symmetry becomes clearly visible in U-ExM treated centrioles imaged with confocal microscopy (Figure 3.4c).

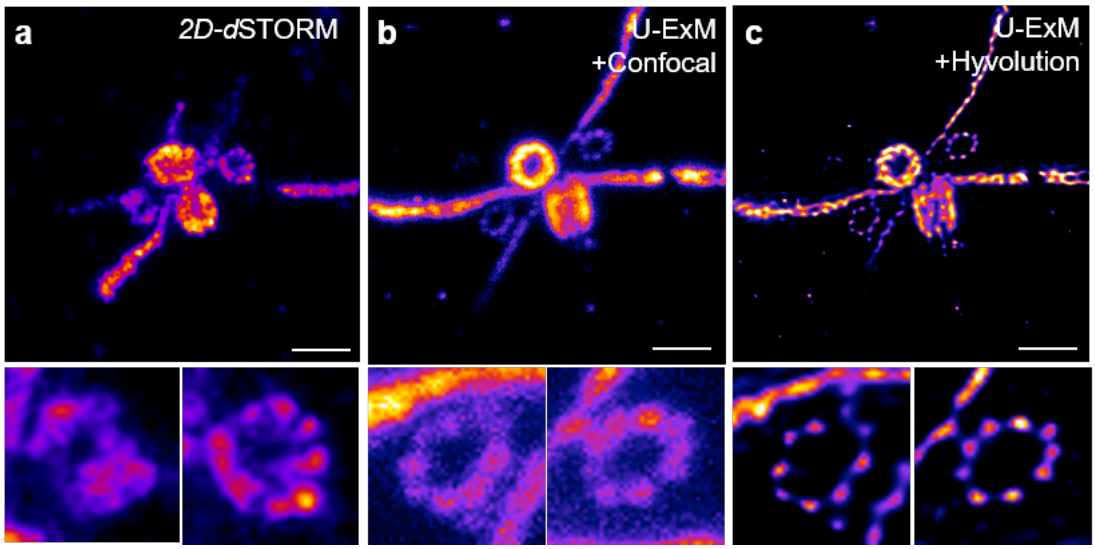

Figure 3.4: U-ExM reaches the *d*STORM precision limits. a, Top, 2D *d*STORM image of an isolated centriole. **b,** Top, confocal image of an U-ExM expanded centriole. (**c**) Top, deconvoluted image of the centriole shown in (**b**) obtained with Hyvolution. Bottom, magnified views (3-fold relative to upper images) of the procentrioles shown in the respective image above. Scalebars, 250 nm (a), 1µm (b,c). (*Material adapted from M1*)

3.1.2 The combination of U-ExM with super-resoltuion imaging

Confocal microscopes are diffraction limited and can reach a lateral resolution of ∼200-300 nm depending on the illumination wavelength. Imaging of expanded hydrogels improves the resolution by a factor equal to the expansion factor of the sample. This enabled the resolution of the 9-fold symmetry by an improved lateral resolution of ∼70 nm with the achieved ∼4-fold expansion factor. The super-resolution technique STED is able to image beyond the classical diffraction limit. In order to further improve the resolution of U-ExM and to study the ultrastructure of centrioles, we combined U-ExM expanded centrioles with STED imaging (Figure 3.5).

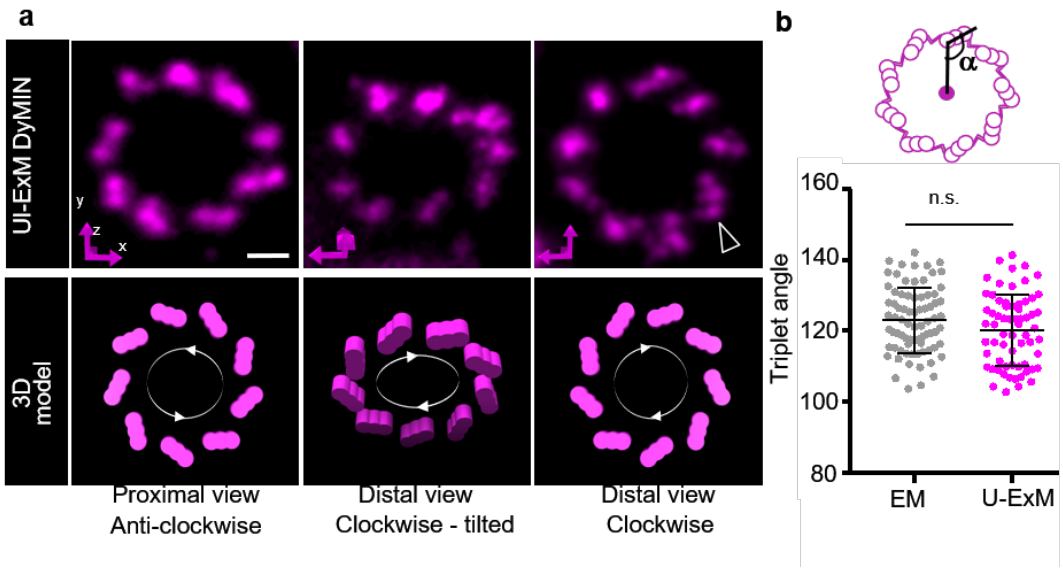

Figure 3.5: U-ExM combined with STED imaging. **a,** Top, representative Dynamic Minimum (DyMIN) STED images of procentrioles stained for α-tubulin and STAR RED conjugated antibodies, highlighting their counter-clockwise or clockwise orientations. Bottom, the interpretation of such orientations in a 3D schematic model. Arrowhead points to individual blades within a microtubule triplet (11 out of 90 procentrioles). **b,** Quantification of the angle between the centre of the centriole and the microtubule triplet, both from electron microscopy (123°±9° (mean±s.e.)) (n=77 triplets) and DyMIN (120°±10° (mean±s.e.)) (n=65 triplets) images. P=0.0912, unpaired two-tailed t-test. Scalebar, 200 nm (a). (*Material adapted from M1*)

STED images of U-ExM treated procentrioles clearly reveal the 9-fold symmetry and additionally resolve the orientation of the microtubule triplets (Figure 3.5). So far, only electron microscopy was able to quantify the average angle of the triplet blades measured from the centre of the centriole to 123°±9° (mean±s.e.). The resolution improvement by the combination of ∼4.2-fold U-ExM expanded centrioles with DyMIN STED allowed the calculation of the preserved angle to 120°±10° (mean±s.e.) (Figure 3.5e). Thus, the orientation of the centrioles could be determined to be clockwise or anti-clockwise depending on the proximal or distal view of the organelle (Figure 3.5a).

3.1.3 Sub-microtubule triplet localization of tubulin glutamylation

Polyglutamylation is a tubulin posttranslational modification that is critical for long-term stability of centriolar microtubules [BKM$^+$98]. So far, the exact position of the modification at the triplets could not be determined. This information could help in understanding how

exactly the polyglutamylation protects the triplets. Therefore, we set out to analyse precisely the signal distribution of the PolyE signal along the microtubule triplet when co-stained for α-tubulin and expanded centrioles using U-ExM in combination with confocal imaging (Figure 3.6a).

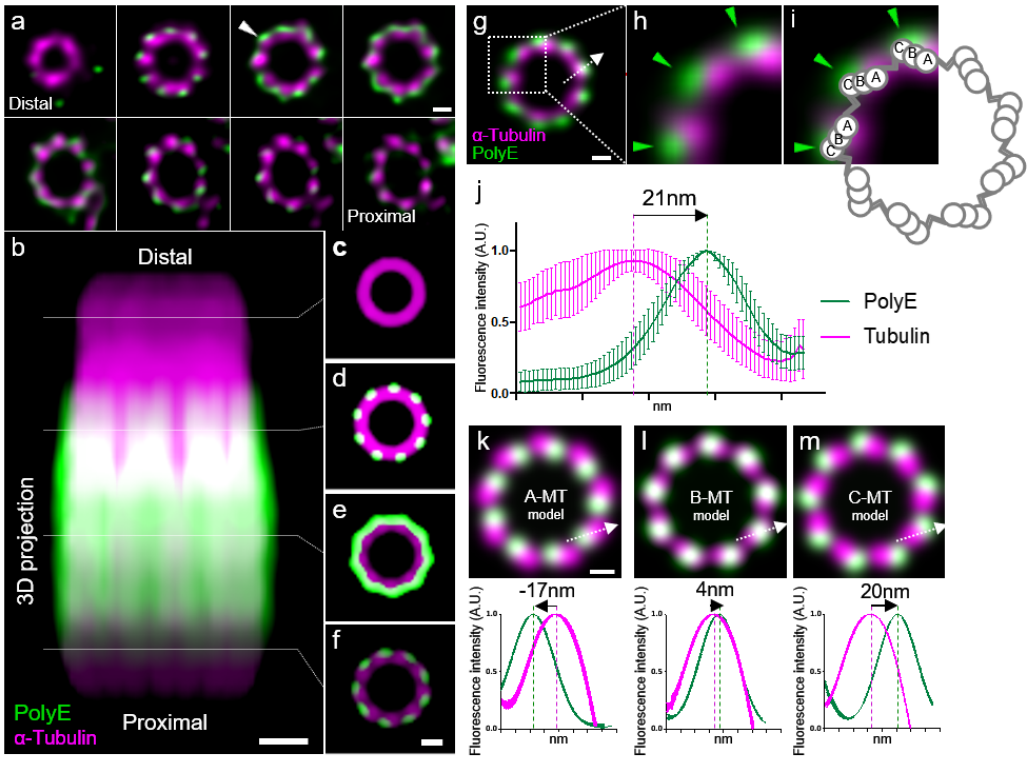

Figure 3.6: Sub-triplet localization of PolyE. a, Z-stack gallery from distal to proximal of an U-ExM expanded mature centriole stained for α-tubulin (magenta) and PolyE (green). Arrowhead points to the PolyE signal. **b**, 3D volume reconstruction of a mature centriole stained for α-tubulin (magenta) and PolyE (green). **c-f,** Sections through the centriole spanning the proximal (c) and the central core (d-f) regions. **g-i,** Image of the distalmost part of the central core of a mature centriole stained for α-tubulin (magenta) and PolyE (green). Green arrowheads highlight the PolyE signal. The white arrow illustrates the cross-section measured in (j). **i,** Schematic representation of microtubule triplets superimposed onto the fluorescent signal shown in (g). **j,** Quantification of the fluorescence shift between the magenta and the green signal of 21 nm (n=61). **k-m,** Model representation of PolyE signal located on specific microtubule blades, A- (k), B- (l) and C- (m) microtubule triplet (MT). Below, the fluorescence peak shift is represented with -17 nm, 4 nm and 20 nm for the A-, B- or C-MT model, respectively. Scale bar, 200 nm (a, b, g), 300 nm (d-f). (*Material adapted from M1*)

In both distal and proximal view of the centrioles, we could observe a localization of the PolyE signal at the outer region of the microtubule triplets. By particle averaging of

14 U-ExM expanded centrioles imaged with confocal microscopy, we could simulate a 3D model that shows the reconstructed volume of a mature *Chlamydomonas* centriole revealing the average protein distribution of α-tubulin and PolyE (Figure 3.6 b-f).

The model confirms that PolyE fully decorates the outer surface of the central core region of mature centrioles. This observation suggests that tubulin polyglutamylation shelters the outer surface of centriolar microtubules thus potentially stabilizing centrioles. At the most distal part of the mature centriole we analysed the exact localization of the PolyE signal (Figure 3.6g). We measured a fluorescence signal shift between the tubulin and PolyE signals with a displacement of the PolyE signal of 21 nm to the outside of the centriole (Figure 3.6j). To assign the modification to the A-, B- or C- microtubule triplet (see Figure 3.6h for a schematic of the triplet classification), we modeled the theoretical position of the α-tubulin fully decorating all three triplets and PolyE only present at one of the microtubule triplets (Figure 3.6 k-m). We therefore scaled cryo-EM data with the U-ExM expansion factor (4.5-fold) and filtered the images with a bandpass filter of 140 nm to simulate the convolution of the PSF of a confocal microscope in combination with deconvolution. The resulting models could be used to calculate a theoretical fluorescence shift of PolyE with -17 nm, 4 nm or 20 nm present at the A, B, or C-triplet, respectively. Our result of a 21 nm fluorescence shift demonstrates that the polyglutamylation at mature centrioles occurs only at the C-triplet.

3.1.4 General applicability of U-ExM

We tested whether U-ExM is applicable with fixed cultured cells and therefore immunostained microtubules and centrioles as well as the membrane-bound organelles mitochondria and clathrin-coated pits (CCPs) in mammalian cells. We found that U-ExM treatment following fixation of cultured cells nicely preserved methanol-fixed microtubules and mitochondria fixed with Paraformaldehyde (PFA) and GA and stained for the outer mitochondrial membrane translocase TOMM20 which surrounds the MitoTracker signal (Figure 3.7).

In a multicolour experiment, we fixed Cos-7 cells using FA and immunostained the cells with primary tubulin and primary CCPs and fluorescently labelled secondary antibodies as well as the DNA intercalator dye Hoechst-33342 to stain the nucleus of the cells (Figure 3.8a-c). By the treatment of U-ExM in combination with re-scanning microscopy, we could clearly resolve the hollow structure of the clathrin coated vesicles (Figure 3.8d-e).

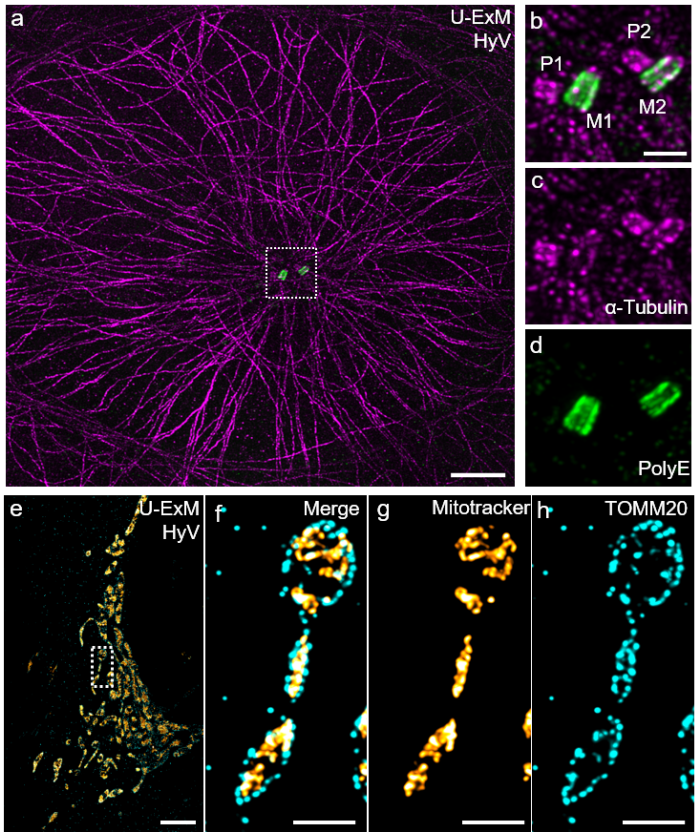

Figure 3.7: U-ExM applied on human cells. a-d, Representative HyVolution (HyV) confocal image of a U2OS cell fixed with methanol, expanded with U-ExM, and stained for α-tubulin (magenta) and PolyE (green). **b–d**, Magnified views of the centriolar pair visible within the dotted square in (a). P, procentriole; M, mature centriole. Representative images from 3 independent experiments. **e–h,** Representative HyVolution confocal images of a U2OS cell fixed with PFA + GA and stained for MitoTracker (orange) and the outer membrane mitochondrial translocase TOMM20 (cyan). The dotted square in (e) outlines the region shown at higher magnification in (f-h). Note that as expected, the TOMM20 signal surrounds the MitoTracker signal. Representative images from 1 experiment. Scalebars, 10 μm (a), 2 μm (b-d), 12 μm (e), 3 μm (f-h). (*Material from M1*)

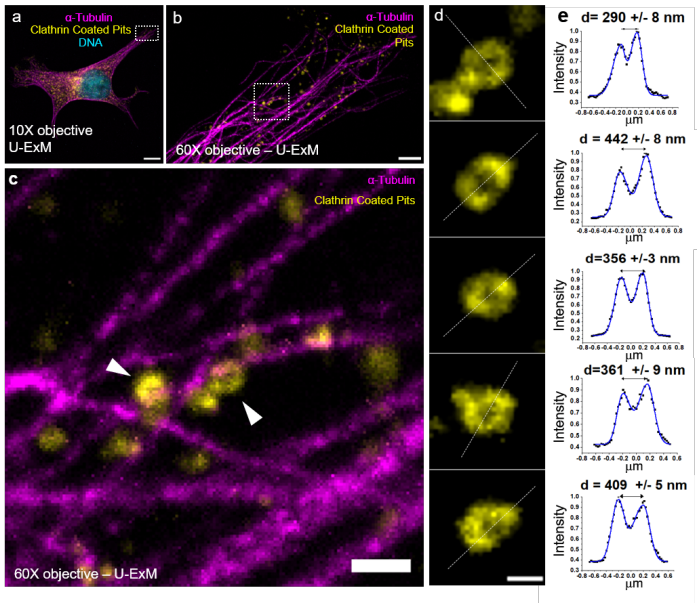

Figure 3.8: Clathrin Coated Pits (CCP) visualized after U-ExM treatment. a, Cos-7 cells staind for tubulin (magenta), CCPs (yellow) and DNA (blue) imaged with a 10X objective. **b,** Same cell as in (**a**) imaged with a 60X objective. **c** Zoom-in on the highlighted region in (**b**) with arrows indicating hollow CCPs. **d,** Gallery of U-ExM CCPs showing the hollow structure of the pits. **e,** Plot profiles along the CCPs along the white dashed lines in (**d**). Double Gaussian fits (blue line) were used to calculate the diameter of the CCPs. Using an expansion factor of 4-fold, the values translate to: 72 nm, 110 nm, 178 nm, 90 nm and 102 nm. Scale bars, 40 μm (a), 4 μm (b), 400 nm (d). (*Material from M1*)

3.1.5 Summary

The optimization of existing ExM protocols resulted in the development of a novel ExM variant, U-ExM, which together with a facilitated workflow is amenable to study ultrastructural details of molecular complexes present in cultured cells as well as in in vitro purified and isolated particles. U-ExM improved the structural integrity compared to other ExM approaches and revealed the 9-fold symmetry of isolated centrioles, both for tubulin and polyglutamylated tubulin. Combined with confocal imaging the sub-triplet localization of polyglutamylated tubulin could be determined to the C-triplet. Moreover, in combination with STED imaging the improved resolution shows the chirality of the microtubule triplets which was so far only accessible by electron microscopy. As U-ExM benefits from improved epitope accessibility, this approach could potentially overcome the limits of super-resolution microscopy techniques by increasing the label density. In addition, fixation of samples often causes artifacts in conventional immunostaining approaches [WB15]. U-ExM combined with isolated organelles does not require a fixation step and thereby can improve the preservation of the native structure of the specimen.

3.2 Tracking down the molecular architecture of the synaptonemal complex by ExM

(This chapter represents the work of manuscript M1.)

The synaptonemal complex (SC) is a multiprotein complex which forms during meiosis and is involved in the segregation of homologous chromosomes. We developed an optimized expansion protocol which in combination with 3D-SIM imaging is able to study the molecular composition of the SCs of a whole chromosome set in a spermatocyte cell with a lateral resolution of 20-30 nm. As an optimized version of the MAP-protocol, we called our approach MAP-SIM which allows multicolour expansion experiments with improved epitope accessibility in big volumes. For the comparison of the performance of different ExM protocols applied on SCs, we developed an image processing software which we used for the unbiased analysis of SC dimensions.

3.2.1 Architecture of the synaptonemal complex

The SC is a multiprotein complex exhibiting an evolutionary conserved ladder-like structure. So far, the molecular composition could mainly be revealed by immunogold EM. Thereby, eight SC proteins were identified in mammals: the proteins SYCP2 and SYCP3 of the lateral elements, SYCP1 of transverse filaments and the proteins SYCE1, SYCE2, SYCE3, TEX12, and SIX6OS1 of the central element [FSAB12] [BFH18] (Figure 3.9). Recently, the molecular three-dimensional organization of the SC could be reconstructed from the analysis of 2D *d*STORM measurements [SHF$^+$15]. In this work, several SC proteins from the lateral and central region of the SC were immunolabelled and visualized with nanometre precision providing insights in the substructure of the helical SC. However, *d*STORM imaging with more than 2 colours can be very challenging and the observed optical section is substantially lower than volumes imaged with 3D-SIM or 3D-Re-scan microscopy.

3.2.2 Development of the MAP-SIM approach

Expansion microscopy is a simple tool that can improve the resolution of an imaging method. But it also confronts the user with some difficulties regarding the handling of the sample and the duration of experiments. In addition, the results obtained must be viewed critically to avoid the presence of artifacts caused by the expansion process.

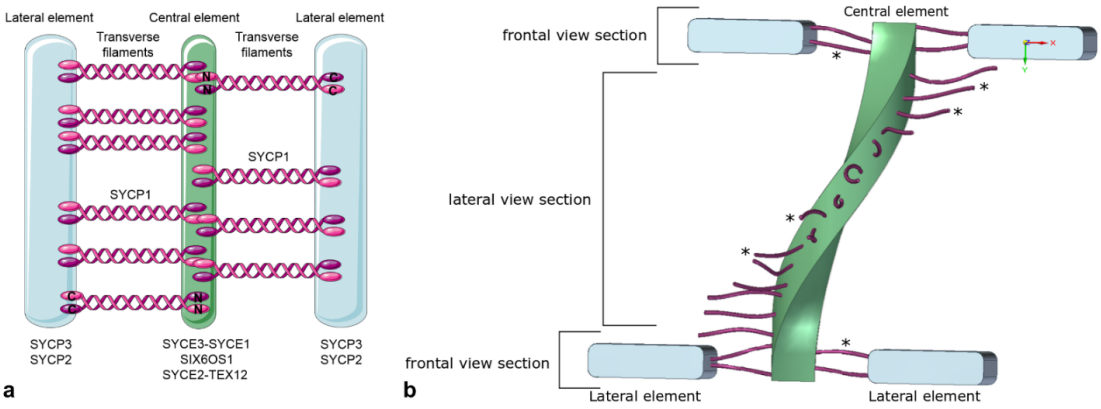

Figure 3.9: The SC structure. a, Schematic representation of the tripartite SC structure of mouse showing the two lateral elements (LEs) consisting of SYCP2 and SYCP3 flanking the central element composed of SYCE1/2/3, Tex12, and SIX6OS1. The transverse filament protein SYCP1 is connecting the lateral element and the central element with the SYCP1 C terminus residing in the lateral and the N terminus in the central element. **b,** Schematic representation of the helical structure of the SC exposing frontal view sections and lateral view sections. Lateral elements (SYCP3, SYCP2) in blue, central element (SYCE3-SYCE1, SIX6OS1, and SYCE2-TEX12) in green, transverse filaments (SYCP1) in purple in accordance with (a). Individual transverse filaments are further marked with asterisks. The lateral elements are not displayed in the lateral view section to expose the central element and transverse filaments. (*Material adapted from M2*)

Compared to conventional imaging of unexpanded samples, it requires additional sample treatment steps when imaging an expanded specimen. This includes the immobilization of the sample to prevent drifting of the hydrogel. Furthermore, there is a reduction of fluorescence signal introduced by the dilution of fluorescent molecules in space, the protease treatment used in some ExM protocols and the exposure to radical starters which chemically attack and destroy fluorophores during gel polymerization. This requires either fluorophores that are stable to these external influences, strategies that introduce fluorophores after expansion or an additional signal amplification. As the hydrogel mainly consists of water, the use of water-immersion objectives is recommended to avoid spherical aberrations induced by a refractive index mismatch between the hydrogel and the immersion medium. When performing multicolour or 3D imaging, the preparation of alignment samples providing a similar aqueous index as the hydrogel is required. To ensure an isotropic expansion, the comparison of pre- and post-expansion images of the same cell has become a standard control in ExM experiments. This requires an imaging strategy to relocate the same cells in the expanded hydrogel.

MAP-SIM workflow

The aim of this project was the development of an expansion and imaging approach that addresses all the above-mentioned issues. As imaging methods, we combined the optimized expansion protocol with 3D-SIM imaging and 3D-Re-scan confocal microscopy. This allowed the analysis of the 3D molecular architecture of SCs in nuclear spreadings of mouse spermatocytes. The spreading of spermatocytes is a widely used technique and is usually performed on 24x60 mm cover slides. In order to perform gelation of the sample on round 18-mm coverslips as described under section 3.1.1, we optimized the cell concentration of the cell suspension and performed the spreading of the SCs directly on 18-mm cover glasses.

Use of round cover glasses facilitated handling of the sample during gelation, homogenization and physical specimen expansion (Figure 3.10).

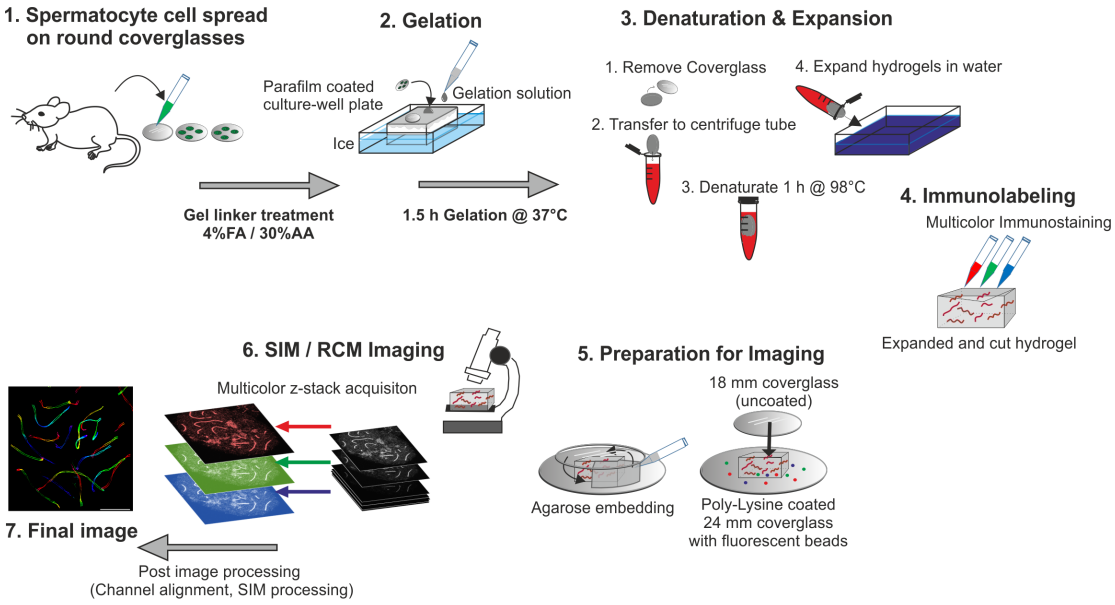

Figure 3.10: Workflow of MAP-SIM expansion of SCs. 1, First, spermatocytes are extracted from mice and then spread on round 18 mm coverslips. **2,** After gel linker treatment, cells are gelated on a parafilm coated culture-well on ice. **3,** Hydrogels are then removed carefully from the cover glass and placed into pre-heated denaturation buffer. After 1 hour of denaturation, gels are placed into water for expansion. **4,** Samples are immunolabelled successively with primary and secondary antibodies. **5,** Immunolabelled gels are then immobilized on Poly-Lysine coated coverslips and additionally embedded with agarose to prevent drift during imaging. **6,** Samples can then be imaged with SIM or another available imaging technique. After image acquisition, SIM post-processing results in the final images (**7**) of SCs. (*Material adapted from M2*)

SIM imaging has no special requirements on the used fluorescent probe which makes it compatible with a wide range of organic fluorophores, FPs and other fluorescent labels. However, SIM requires the acquisition of several images with various illumination patterns, usually 5 phase steps in 3 angles per z-plane. Especially when imaging big volumes, long acquisition times can cause photobleaching which influences the achievable resolution.

Expanded samples already exhibit a reduced brightness due to the fluorescent signal dilution. Therefore, when performing pre-expansion labelling, bright fluorophores which survive the gelation and further expansion steps must be chosen. As fluorescence retention varies between fluorophores [CTB15], multi-colour SIM imaging with pre-expansion labelling methods can be very challenging and can only be performed with an additional post-labelling step [CYW$^+$17]. To perform multicolour imaging and to circumvent fluorescent signal loss, I optimized the post-expansion labelling method MAP-Cell [KSP$^+$16] where fluorophores are introduced after expansion. This included the optimization of the monomer-crosslinker composition of the hydrogel which allows a full transfer of the SC proteins to the hydrogel network and a 4-fold expansion of the sample. As shown in Figure 3.10, the hydrogel-sample hybrid is homogenized by heat and chemically induced denaturation and subsequently expanded in double-deionized water.

Channel alignment

For channel alignment, fluorescent beads are immobilized on the coverslip used for sample imaging and acquired together with the sample. As the sample z-plane is located deeper in the hydrogel, acquisition of fluorescent beads in proximity to the glass surface can cause aberrations in the channel alignment of the sample. Unfortunately, the separate recording of fluorescent beads fixed in the hydrogel away from the cover glass was not possible as the fluorescent dyes of the beads did not survive the radical polymerization sufficiently in all channels. However, by using beads immobilized on the cover glass and surrounded by the hydrogel, a sufficiently good alignment could be obtained.

Immobilization of the hydrogel

Immobilization of expanded hydrogels can be obtained in different ways. When performing SIM imaging in big volumes, we coated the imaging cover glass with poly-lysine and additionally embedded the hydrogel in Agarose. This treatment allowed long-term acquisitions of the sample in the expanded state without drifting of the sample.

3.2.3 Comparison of super-resolution techniques applied on SYCP3

The lateral element of the SC is mainly formed by the SYCP3 protein. The two twisting strands have a distance of ∼220 nm and can clearly be resolved in lateral view by *d*STORM and SIM imaging (Figure 3.11a-b and Figure 3.11d-e)

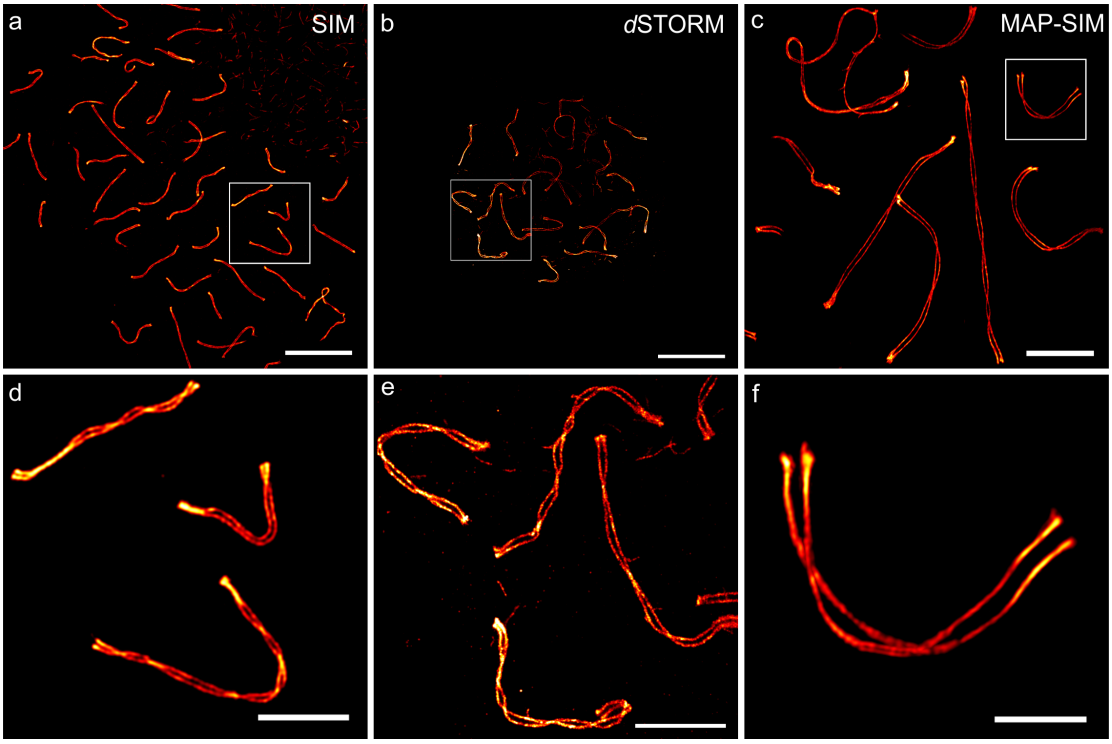

Figure 3.11: Super-resolution imaging of the lateral element protein SYCP3. a, SIM image of unexpanded SYCP3 labelled with Alexa Fluor 568. **b,** *d*STORM image of unexpanded SYCP3 labelled with Alexa Fluor 647. **c,** Expanded MAP-SIM SYCP3 signal (maximum intensity projection) labelled with SeTau647. **d-f,** Magnified views of boxed regions in (a-c), respectively. The images indicate that MAP-SIM provides a similar spatial resolution as *d*STORM of 20-30 nm in the imaging plane. Scale bars, 10 μm (a-c), 3 μm (d–f). (*Material adapted from M2*)

Applying the MAP-SIM protocol on spermatocyte spreads allowed the visualization of the lateral element protein SYCP3 with similar resolution of *d*STORM images (Figure 3.11c,f). The protocol provides an improved epitope accessibility by the expansion process induced protein displacement when performing immunostaining after expansion. Additionally, post-expansion labelling reduces the linkage error introduced by the antibodies with the factor of expansion. Thereby, the linkage error of ∼18 nm [WRO78] induced by primary and secondary IgG antibodies in unexpanded samples should in theory reduce to ∼5 nm when expanding the sample ∼4-times.

3.2.4 3D-multicolor imaging MAP-SIM and image analysis

The MAP-SIM imaging workflow including the immobilization of the hydrogel and channel alignment allowed the study of the SC proteins SYCP3, SYCP1 N terminus and SYCE3 in 3D. SIM imaging could be performed in volumes up to ∼15-20 µm and in volumes of ∼30 µm when combined with Re-scanning microscopy in up to three colours. (Figure 3.12).

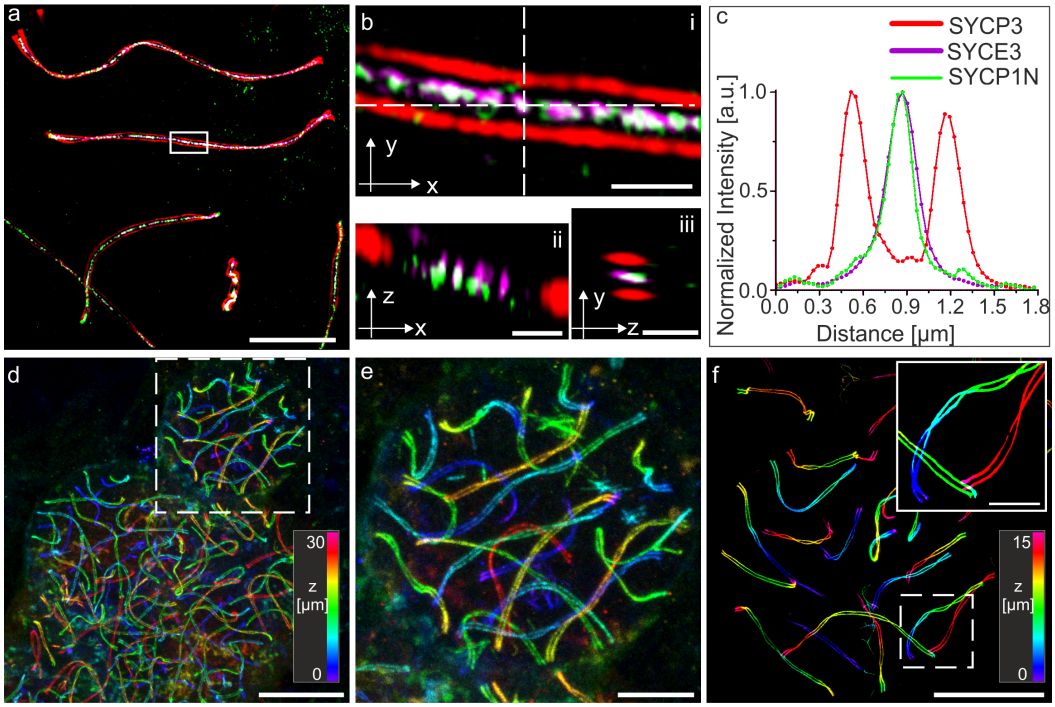

Figure 3.12: 3D-multicolor MAP-SIM of SYCP3, SYCP1 N terminus, and SYCE3. **a,** SIM image of post-expansion SeTau647 labelled SYCP3 as a component of the lateral element (red), the transverse filament SYCP1 N terminus labelled with Alexa Fluor 488 (green), and SYCE3 of the central element labelled with Alexa Fluor 568 (magenta). **b,** Magnified views of white boxed region in (a). **ii,** Orthogonal view of horizontal white dashed line in (**i**). **iii,** Orthogonal view of vertical white dashed line in (**i**). **c,** Transversal intensity profile perpendicular to the orientation of the SC shown in (b). The selected section exhibits a bimodal distribution of the SYCP3 signal separated by 667.0 ± 7.1 nm (SD). The SYCP1 N terminus and SYCE3 signals of the section (b) show monomodal distributions with FWHM of 214.7 ± 6.9 nm (SD) and 258.3 ± 4.8 nm (SD), respectively. **d,** Large field of view (100 x 100 x 30 μm^3) 3D-re-scan confocal microscopy image of several spermatocyte cells. SYCP3 was labelled post-expansion with SeTau647. **e,** Magnified view of boxed region in (d). **f,** 3D-MAP-SIM image of the SCs of an entire set of chromosomes in a spermatocyte visualized by post-expansion labelling of SYCP3 with SeTau647. The inset shows the enlarged view of the boxed region in (**f**). Scale bars, 10 µm (a), 1 µm (b i-iii), 25 µm (d), 10 µm (e), 15 µm (f), 5 µm (f inset). (*Material adapted from M2*)

The expansion protocol allowed the imaging of an entire set of chromosomes in a spermatocyte in combination with SIM (Figure 3.12f) as well as several spermatocyte cells in one field of view by the combination with 3D-re-scan confocal microscopy (Figure 3.12d-e). This enables the study of the protein distribution and composition of several SCs in 3D within the same cell (Figure 3.12a-c). To quantify the SC dimensions, we developed an automated image analysis software 'Line Profiler' which automatically and objectively determines distances between bimodally distributed proteins [ZRS20] [ZSR19] (Figure 3.13).

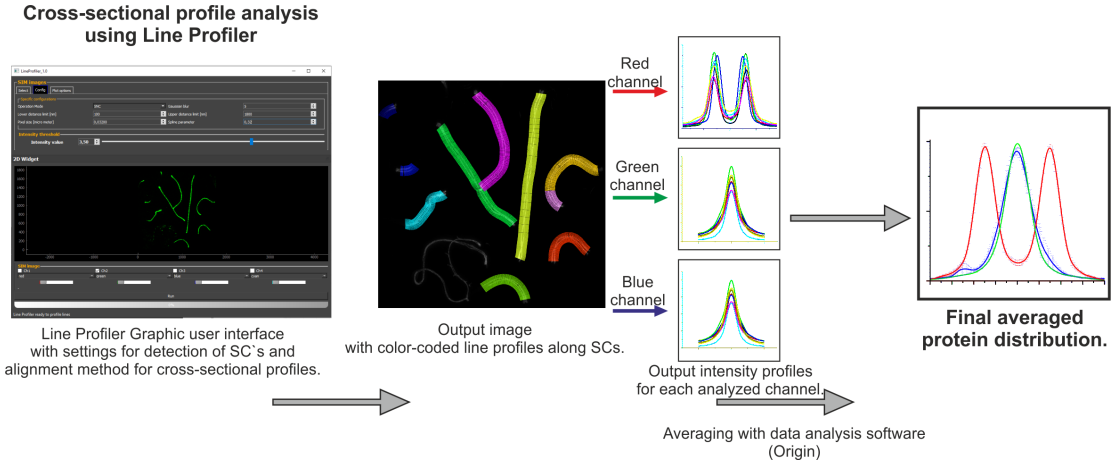

Figure 3.13: Image analysis using LineProfiler. Images are analysed using the automated Line Profiler software enabling analysis of protein distributions in several channels. The screenshot of the graphical user interface (GUI) of the software is shown (left). After loading of SIM images as .tiff or .czi file, image brightness, gaussian blurring and settings for the detection of single SCs can be adjusted. The software detects single SCs and sets cross-sectional profiles pixelwise perpendicular along the course of the SC. The structure detection can be performed either by selecting the channel with a desired fluorescent signal of the central or lateral element. As an output, the software gives averaged intensity profiles of single SCs in all channels as well as corresponding colour coded SCs in a result image and data analysis results like peak-to-peak distances of Gaussian fitting or FWHM of single Gaussian fits. These values can then be used to generate an averaged protein distribution curve of the SC elements. (*Material adapted from M2*)

The software LineProfiler allowed the evaluation of the performance of different ExM variants by comparing distances determined in expanded SIM and pre-expansion *d*STORM images. Remarkably, we could distinguish different labelling errors introduced by pre- and post-expansion immunolabelling. The analysis of the signal distribution of the SYCP1 N terminus and SYCE3 revealed bi- and multimodal protein distributions which suggest a multi-layered organization of the central element (Figure 3.14).

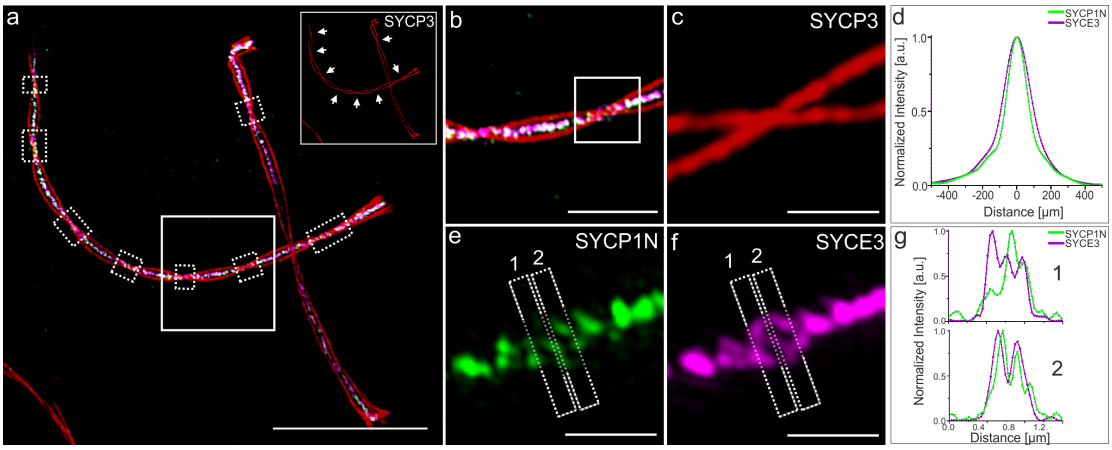

Figure 3.14: MAP-SIM reveals a complex organization of the SC central region. **a,** MAP-SIM image of SYCE3 labelled with Alexa Fluor 568 (magenta), SYCP1N labelled with Alexa Fluor 488 (green) and SYCP3 labelled with SeTau647 (red). Lateral view sections of the SC are visualized as twists in the SYCP3 signal (marked by white dotted boxes and indicated by arrows in the inset of (a) showing only the SYCP3 channel.) **b,** Magnified view of white boxed region in (a). **c, e, f,** Enlarged views of highlighted region in (b) showing the SYCP3 signal in red (c), the SYCP1N signal in green (e) and the SYCE3 signal in magenta (f) with two sites selected for protein distribution analysis (1, 2). **d,** Averaged profile of all cross-sectional intensity profiles along the SYCE3 (magenta) and SYCP1N (green) signals analysed at regions specified in (a) by white dotted boxes showing a monomodal signal distribution of 168.0 $\pm$ 1.1 nm for SYCP1N and 211.43 $\pm$ 0.89 nm (SD) nm for SYCE3 derived from single Gaussian fitting. **g,** Cross-sectional intensity profiles of lateral view sections 1 and 2 of the SC (indicated in e and f) show a multimodal organization of the central element protein SYCE3 (magenta) and the N terminus of SYCP1 (green). Scale bars, 10 μm (a), 3 μm (b), 1 μm (c, e, f). (*Material adapted from M2*)

3.2.5 Morphological features revealed by MAP-SIM

Analysing the SYCP3 signal in murine pachytene spermatocytes expanded with the MAP-SIM approach revealed the occasional splitting of the LE in sub lateral elements (subLEs) (Figure 3.15 a-d) and the doubling of the SYCP3 strands in autosomes (Figure 3.15 e-h). So far, these structural features could not be visualized before by a light microscopy technique.

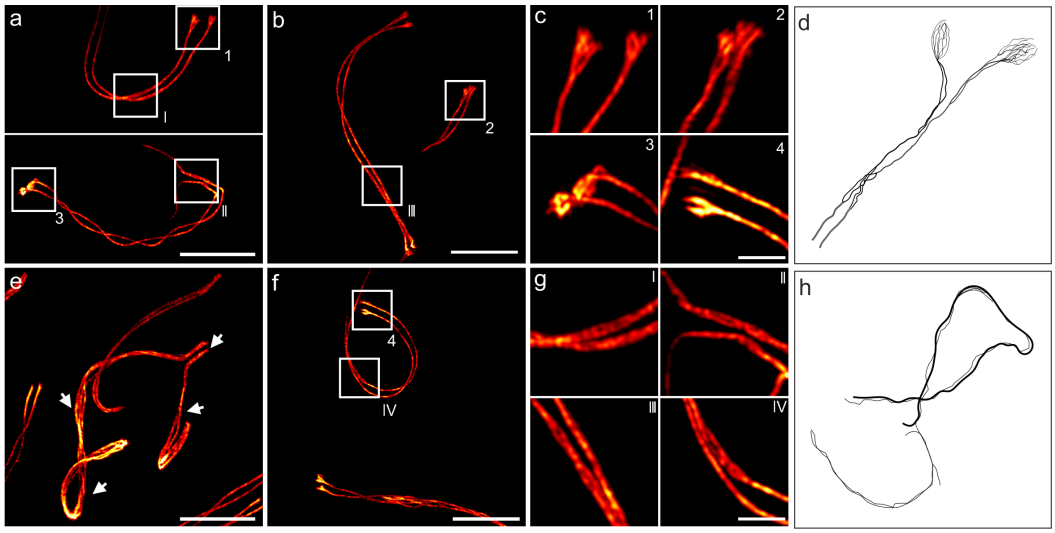

Figure 3.15: Structural details of the SC lateral element revealed by MAP-SIM of SYCP3. a-c,f,g The SYCP3 signal shows occasional bifurcation along the two SC strands (I–IV) and various degrees of fraying at their ends depending on the respective pachytene stage (1–4). **e,** Unpaired regions of the XY pair (arrowheads) also show a strong degree of fraying. **d,h** Schematic representations of early EM reports of two or more sub lateral elements (subLEs) in mammals [DM80] [dGA86] in accordance with the splitting of the SYCP3 signal resolved by MAP-SIM in this study. **d,** Representation of the lateral element strand splitting in two and fraying at its end according to literature [DM80] and [dGA86]. **h,** Fraying of LEs associated with unpaired regions of the XY pair modelled according to literature [dGA86]. Scale bars, 7 μm (a,b), 1.5 μm (c, g), 7 μm (e, f). (*Material adapted from M2*)

3.2.6 Summary

MAP-SIM is an optimized ExM approach which can be used for multicolour super-resolution imaging of multiprotein complexes providing 20-30 nm lateral resolution in high imaging volumes. We could demonstrate the applicability of MAP-SIM by expanding SC proteins and confirming well-studied quantities of structural features of the SC and revealing details of the protein distribution that could so far only be shown by electron microscopy. Improved epitope accessibility of MAP-SIM makes it a promising tool in deciphering further details of the SC architecture in future experiments. The improved labelling efficiency could be used to study dense protein regions of the complex which in unexpanded states of the sample are only poorly or not accessible by immunostaining. Additionally, the approach could be used to study SC protein distribution changes in the SC composition and structure in different meiosis stages with high resolution in multicolour immunolabelling experiments.

3.3 Molecular resolution imaging by Ex-SMLM

(This chapter represents the work of manuscript M3.)

Since ExM is a sample preparation method, it is theoretically compatible with any fluorescence microscopy technique. Combined with SMLM, ExM could potentially reach the resolution of electron microscopy. However, SMLM techniques like *d*STORM require osmotically active imaging buffers for photoswitching of fluorophores. As hydrogels are sensitive to osmotic liquids and hence shrink upon exposure to *d*STORM imaging buffers, the combination of ExM and STORM or *d*STORM is challenging. The goal of this project was the development of an expansion strategy which enables the combination of SMLM with ExM.

3.3.1 Ex-SMLM workflow

I developed an expansion workflow which stabilizes expanded hydrogels by re-embedding in a second uncharged acrylamide gel. Re-embedding is originally used for sequential staining of RNA in the expanded state of the specimens in ExFISH [CWC$^+$16]. Adapting and optimizing this protocol step, enabled *d*STORM imaging in combination with ExM protocols which perform pre-expansion labelling like ExM, ExM-GA/MA-NHS and proExM or post-expansion labelling approaches like MAP and U-ExM. The expansion protocol included the immobilization of the hydrogel on Bind-Silane treated cover glasses [ZRS20]. Casting an acrylic hydrogel on top of Bind-Silane treated glasses, leads to the incorporation of acrylamide monomers bound to the glass surface into the polymer network of the formed gel. In this way, the expanded hydrogel is covalently bound to the glass surface and drifting of the sample is avoided during *d*STORM measurement.

As a reference structure, we immunostained α-tubulin in mammalian cells with primary and secondary fluorophore labelled antibodies. For *d*STORM imaging, usually the carbocyanine dyes Cy5 or Alexa 647 are selected as they outperform other dyes in photoswitching properties. However, these fluorophores get chemically destroyed during gel formation by radical starters like APS as they get attracted by the unconjugated backbone of these molecules. We therefore selected antibodies coupled to the rhodamine dye Alexa Fluor 532 since it is relatively stable to radicals when performing pre-expansion labelling. Cos-7 cells immunolabelled and imaged with *d*STORM pre-expansion using a water objective in epi-illumination mode could reveal the hollow structure of the microtubule filaments visible in the bimodal distribution of cross-sectional profiles (Figure 3.16).

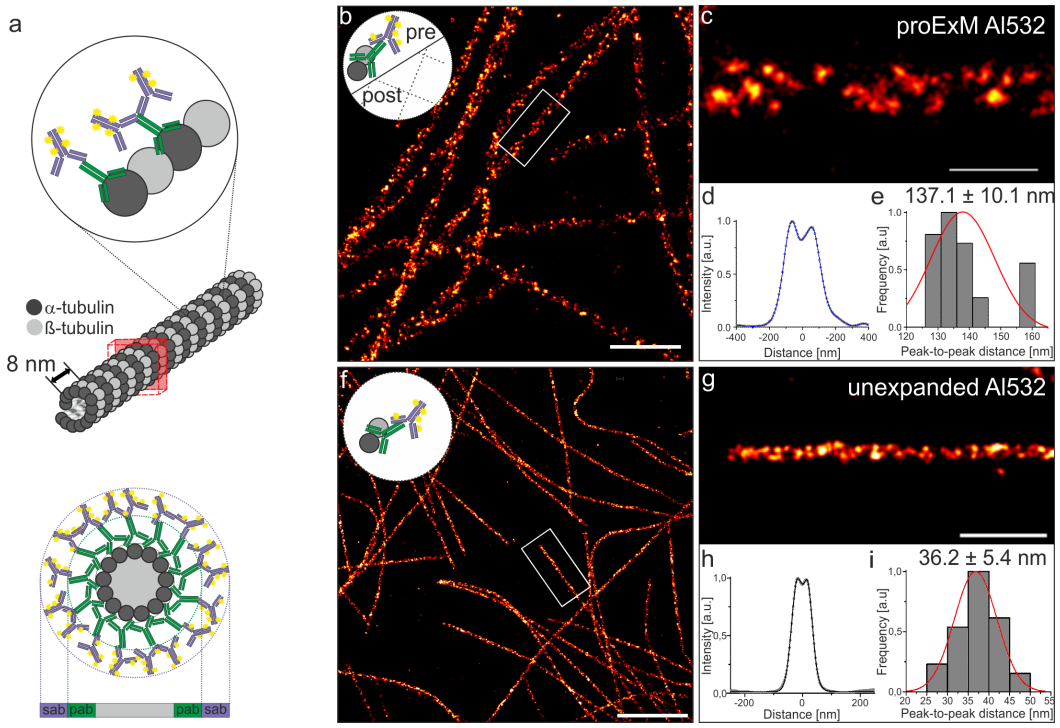

Figure 3.16: Re-embedding enables Ex-*d*STORM. a,, Model of microtubules with an outer diameter of 25 nm stained with conventional primary (pab) and fluorescently labelled secondary IgG antibodies (sab) results in a total diameter of 60 nm with a linkage error (defined by the size of the primary and secondary antibody) of 17.5 nm [WRO78]. **b,** *d*STORM image of pre-labelled proExM expanded and re-embedded Cos-7 cells stained with primary antibodies and secondary Alexa Fluor 532 conjugated antibodies (Al532) for α-tubulin. The small logo in the upper left corner symbolizes that microtubules have been immunolabelled before expansion (pre-labelled). **c,** Zoom in on highlighted region in (b). **d,** Averaged cross-sectional profile of nine microtubule segments with a total length of 29.1 μm measured in two cells from 1 expanded sample. **e,** Histogram of peak-to-peak distances with normalized normal distribution curve (red) determined by bi-Gaussian fitting of the data analysed in (c) with an average distance of 137.1 $\pm$ 10.1 nm (mean$\pm$s.d.). The data were obtained from $n = 9$ microtubule segments in 2 cells from 1 expanded sample. **f,** Unexpanded Cos-7 cells labelled with an anti α-tubulin primary antibody and Alexa Fluor 532 (Al532) conjugated IgG secondary antibodies. The small logo in the upper left cornert microtubules have be symbolizes thaen immunolabelled and not expanded. **g,** Zoom in of the white boxed region in (f). **h,** Average intensity profile of 35 microtubule segments with a total length of 69.9 μm analysed in 12 *d*STORM images. **i,** Histogram of peak-to-peak distances with normalized normal distribution curve (red) determined by bi-Gaussian fitting of cross-sectional profiles of the analysed microtubule segments in (h) with a mean peak-to-peak distance of 36.2 $\pm$ 5.4 nm (mean$\pm$s.d.). The data were obtained from $n = 35$ microtubule segments in 12 cells from 3 independent experiments. Scale bars, 2 μm (b,f), 500 nm (c,g). (*Material adapted from M3*)

The extension of our image analysis software LineProfiler adjusted for the analysis of filamentous structures like microtubules allowed the comparison of unexpanded and expanded *d*STORM images. The software automatically detects microtubule filaments in reconstructed SMLM images and pixelwise sets cross-sectional profiles perpendicular along the course of the filaments. The 2D projection of the cylindrical and hollow microtubule filament results in a bi-modal signal distribution. By fitting a bi-Gaussian curve to the intensity profile, the peak-to-peak-distance of the fit is defined by the distance of the tube wall decorated with fluorescent labels. The typical peak-to-peak distance of unexpanded microtubules labelled with primary and secondary IgG antibodies could be determined to 36.2 $\pm$ 5.4 nm (mean$\pm$sd) using *d*STORM((Figure 3.16)). This corresponds well with EM images of unlabelled and immunolabelled microtubules, where the diameter of tubulin filaments could be determined to 25 nm without antibodies and to 60 nm when decorated with primary and secondary antibodies [WRO78].

3.3.2 Pre-labelling Ex-SMLM

Cos-7 cells were immunostained in the same way as labelling was performed for unexpanded *d*STORM experiments. Subsequently, the samples were expanded according the proExM protocol with re-embedding after expansion in water. The peak-to-peak distance of expanded microtubules increased to an average distance of 137.1 $\pm$ 10.1 nm (mean$\pm$sd). Since the re-embedding step causes a decrease of the expansion factor of $\sim$20 %, this value fits well for simulated peak-to-peak distances of 3.1-fold expanded and pre-expansion labelled microtubule filaments using a cylindrical model (Figure 3.17).

3.3.3 Pre-labelling Ex-SMLM using DNA-labels

With the Ex-SMLM re-embedding approach, we were able to perform and compare different labelling strategies for Ex-SMLM variants including approaches using DNA conjugated IgG antibody labels as used in the original ExM protocol (Figure 3.17j-m) or conventional IgG antibodies used in the ExM-GA method (Figure 3.17b-e). Tubulin filaments expanded according the ExM-GA protocol showed an average peak-to-peak distance of 133.8$\pm$13.2 nm (mean$\pm$sd). As expected, this value is similar to the calculated proExM distance as in both methods IgG antibodies cause the same broadening of the tubule diameter from 25 nm to $\sim$60 nm. In both expansion protocols, the linkage error is increased by a factor equal to the expansion factor of $\sim$3.2-fold.

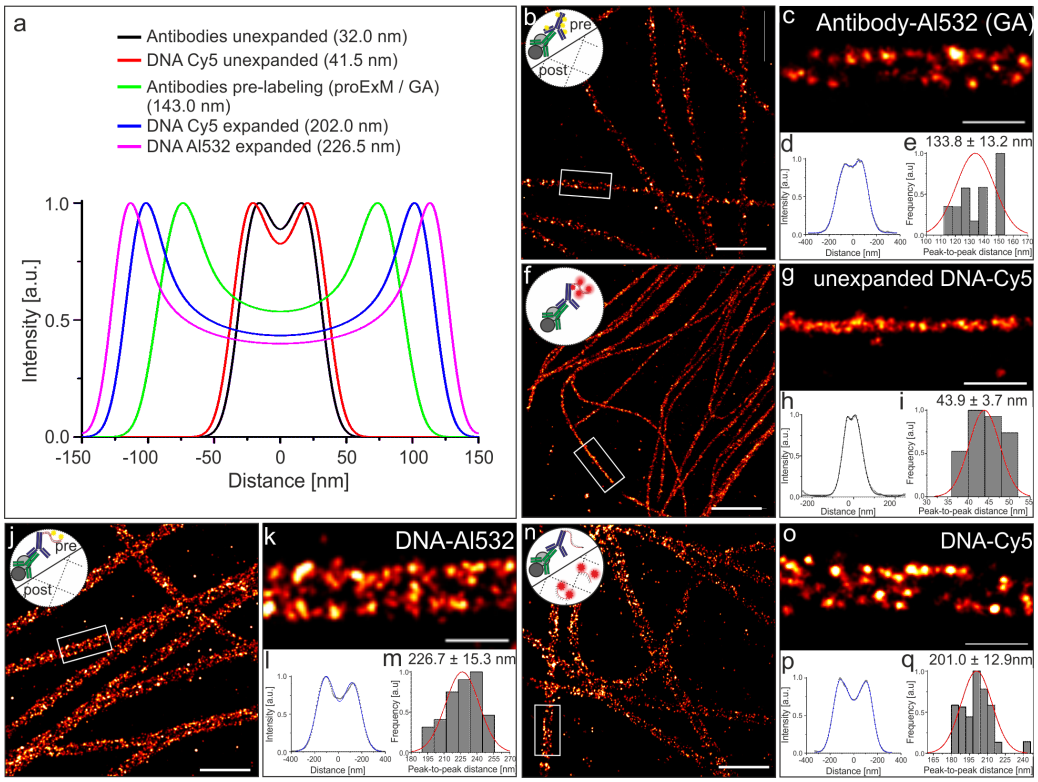

Figure 3.17: Re-embedding enables Ex-*d*STORM. a, Simulated intensity profiles using a cylindrical distribution function to describe unexpanded or 3.2x expanded immunostained microtubules (labelled with IgG antibodies or DNA modified IgG antibodies pre-expansion) and resulting peak-to-peak distances of the cross-sectional profiles. **b,** *d*STORM image of expanded and re-embedded α- and β-tubulin pre-labelled with secondary Alexa Fluor 532 IgG antibodies (Al532) using the MA-NHS/GA method, i.e. antibodies are cross-linked with GA into the hydrogel (Antibody-Al532 (GA)). **c,** Zoom in of white boxed region in (b). **d,** Averaged cross-sectional profile of 8 microtubule segments with a total length of 28.6 μm measured in 4 expanded cells. **e,** Histogram of peak-to-peak distance distribution with normalized normal curve (red) of microtubule segments analysed in (d) with a mean distance of 133.8 $\pm$ 13.2 nm (mean$\pm$sd) **f,** Unexpanded *d*STORM image of ssDNA-Cy5 secondary antibody hybridized with Cy5 bearing oligonucleotides pre-expansion (DNA-Cy5 protocol). **g,** Magnified view of white boxed region in (f). **h,** Average cross-sectional profile of 7 microtubule segments with a length of 8.7 μm in total. **i,** Histogram of peak-to-peak distances with normalized normal distribution curve (red) of the data analysed in (h) with a mean distance of 43.9 $\pm$ 3.7 nm (mean$\pm$sd). **j,** Expanded *d*STORM image of microtubules labelled with α-tubulin and dsDNA (DNA-Al532) conjugated secondary antibodies exhibiting a methacryloyl group to crosslink the DNA with fluorophores pre-expansion into the hydrogel (original ExM trifunctional label concept). **k,** Zoom-in of white boxed region in (j). **l,** Average intensity profile of 26 microtubule segments (118.6 μm in total). **m,** Histogram of peak-to-peak distances with normalized normal distribution curve (red) of the data analysed in (h) showing a mean distance of 226.7 $\pm$ 15.3 nm (mean$\pm$sd). **n,** *d*STORM image of α- and β-tubulin expanded according to the DNA-Cy5 protocol strategy with labels at Cy5-bearing oligonucleotides introduced post-re-embedding. **o,** Zoom in of white boxed region in (n). **p,** Average intensity profile of 15 microtubule segments with a total length of 126 μm from 1 expanded sample. **q,** Histogram of peak-to-peak distances with normalized normal distribution curve (red) determined by fitting the cross-sectional profiles analysed in (p) showing a mean distance of 201.0 $\pm$ 12.9 nm (mean$\pm$sd). Scale bars, 2 μm (b,f,j,n), 500 nm (c,g,k,o). (*Material adapted from M3*)

Additionally, we designed DNA labels which allow immunostaining before gelation but add fluorescent probes after expansion by hybridization of fluorescently modified complementary DNA oligos or the use of Biotin-Streptavidin labelling (Figure 3.18).

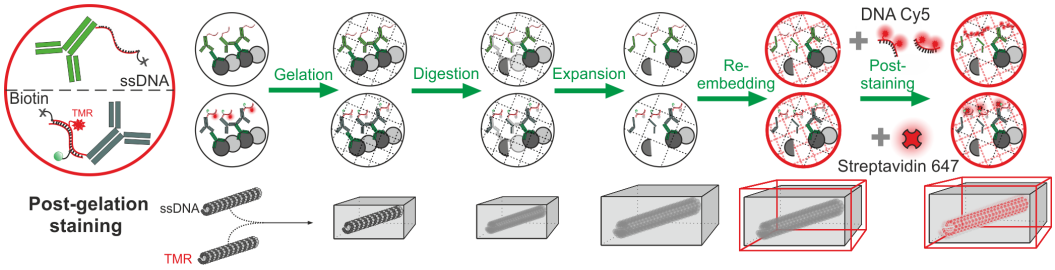

Figure 3.18: Pre-labelling Ex-SMLM with post-expansion fluorophore introduction (post-gelation staining). Schematic workflow of Post-gelation staining Ex-SMLM. Samples are first immunostained with primary and secondary antibodies. As secondary antibodies IgG antibodies with modified DNA are used, either containing a 40 base pair (bp) long ssDNA with an 5'acrydite linker or a dsDNA bearing a tetramethylrhodamine (TMR) fluorophore on one strand and an acrydite linker as wells as a biotin modification on the complementary strand. The samples are then gelated, digested and expanded according to the ExM procedure. After expansion, hydrogels with incorporated DNA labels are re-embedded and post-stained by either hybridization of Cy5 modified DNA oligos or Alexa 647 conjugated Streptavidin which recognizes the biotinylated DNA. (*Material adapted from M3*)

The Biotin-Streptavidin labelling strategy uses a DNA modified IgG antibody with an internal Biotin DNA modification. Streptavidin is a homotetramer protein purified from the bacterium *Streptomyces avidinii* and has a high affinity for biotin. Fluorophore tagged Streptavidin can be used to introduce fluorophores after expanding and re-embedding of the crosslinked biotinylated DNA label. In this way, Alexa Fluor 647 can be used to perform Ex-SMLM on expanded samples. The peak-to-peak distance of the expanded Biotin-Streptavidin-647 label was determined to 145.5 $\pm$ 16.9 nm and is slightly increased compared to expansion protocols which incorporate IgG antibodies directly to the hydrogel. The biotin modification is set at the 6^{th} base pair (bp) away from the amine modification which is used to couple the DNA to the IgG antibody. This could explain the increase in the peak-to-peak distance compared to the values of proExM or ExM-GA expanded samples.

Similar to the Biotin-Streptavidin labelling strategy, the DNA-Cy5 post-gelation staining approach uses a ssDNA which first gets incorporated into the hydrogel network and serves as a template for Cy5 bearing oligos which are hybridized after re-embedding of the expanded samples (Figure 3.17n-q). As immunostaining of the samples is performed before expansion similarly to the original ExM protocol using DNA-Alexa Fluor 532 as label, both methods

can be categorized as pre-expansion Ex-SMLM when combined with re-embedding and *d*STORM. Thereby the linkage error increases with the expansion factor as shown before for samples treated according the proExM and ExM-GA/MA-NHS protocol.

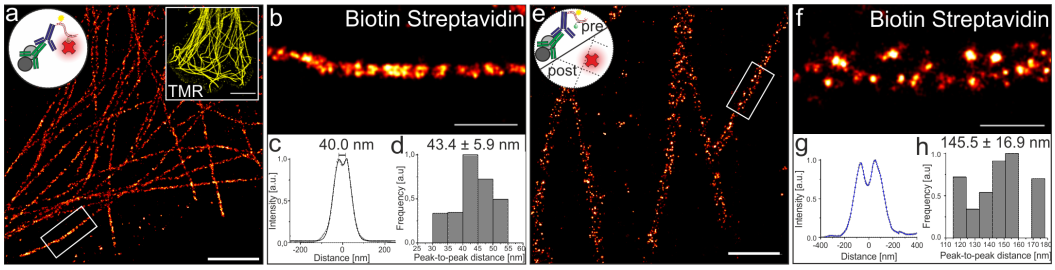

Figure 3.19: Pre-labelling Ex-SMLM with post-expansion fluorophore introduction (post-gelation staining). a, Unexpanded *d*STORM image of Cos-7 cells imunostained with anti β-tubulin antibody and Streptavidin Alexa Fluor 647 bound biotin modified secondary DNA antibodies. The inset shows the pre-expansion fluorescence of the inserted TMR modification of the secondary DNA-antibody conjugate, which can serve as a fluorescence control for imaging pre-expansion when biotin labelling is performed post-re-embedding. **b,** Magnified view of the highlighted region in (a). **c,** Averaged cross-sectional profile of 12 microtubule segments with a total length of 22.5 μm analysed using the software 'Line Profiler'. **d,** Histogram of peak-to-peak distances determined by fitting a bi-gaussian function to the averaged intensity profiles of the microtubule segments in (c) with a mean distance of 43.4 $\pm$ 5.9 nm (mean$\pm$sd). **e,** Expanded *d*STORM image of β-tubulin labelled as in (a) but with biotin binding with Streptavidin Alexa Fluor 647 post-re-embedding. **f,** Zoom-in of white marked box in (e). **g,** Average intensity profile of 15 microtubule segments each with a total length of 47.0 μm. **h** Histogramed peak-to-peak distances of analysed data in (g) with an average distance of 145.5 $\pm$ 16.9 nm. Scale bars, 2 μm (a,e), 10 μm (inset in (a)), 500 nm (b,f). (*Unpublished data*)

Our Lineprofiler results of DNA label ExM methods showed an additional increase of the peak-to-peak distance caused by the size of the 40 bp long DNA strands used in the DNA-Cy5 protocol which resulted in an average peak-to-peak distance of 201.0 $\pm$ 12.9 nm (mean$\pm$sd) as well as in the original ExM protocol using DNA-Alexa Fluor 532 which resulted in an average distance of 226.7 $\pm$ 15.3 nm (mean$\pm$sd). The difference in the calculated distances of the DNA labels can be explained by the coiling of the ssDNA which leads to an incorporation of the label in the hydrogel closer to the microtubule wall. In contrast, the dsDNA is present in a more stretched conformation and thus cross-links further away from the tubulin. Both values fit well with simulated data which consider the length of the DNA (Figure 3.16a). The difference to the shorter peak-to-peak distance of the expanded Biotin-Streptavidin-647 label can be explained by the position of the biotin modification which is set on the 6$^{\text{th}}$ bp on the

DNA strand compared to the furthest away fluorophore modification on the 36th bp and 42th bp for Cy5 or Alexa Fluor 532, respectively.

3.3.4 Post-labelling Ex-SMLM

To increase the label density and brightness of the sample, we performed post-labelling using primary and secondary antibodies on already pre-expansion immunolabelled samples and performed 3D *d*STORM (Figure 3.20).

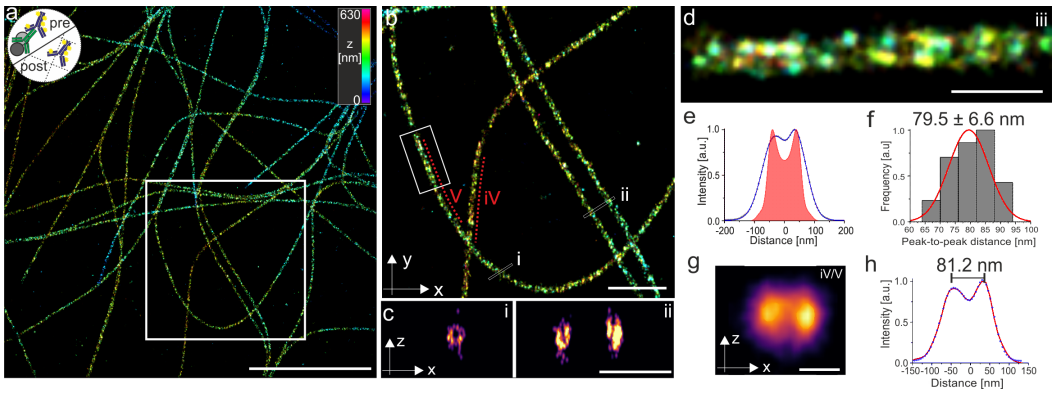

Figure 3.20: 3D post-labelling Ex-*d*STORM. SMLM image of re-embedded and post-expansion labelled microtubules. **a,** 3D *d*STORM image of re-embedded Cos-7 cells expanded according to the Protein-Retention protocol (proExM) pre-labelled with anti α- and β-tubulin antibodies and additionally post-labelled with anti α-tubulin. The secondary antibodies were labelled with Alexa Fluor 532 (proExM Al532). The small logo in the upper left corner symbolizes the labelling method, e.g. pre- and post-immunolabelling with Al532 secondary antibodies. **b,** Magnified view of highlighted region in (a). **c,** xz-side view cross-sections (white lines) (i) and (ii) shown in (b) revealing the hollow structure of microtubules. **d,** Magnified view of highlighted region (white box) in (b). Since post-labelling dominates the signal, the method is termed proExM Al532 (post-labelled). **e,** Averaged cross-sectional profile (blue) of 11 analysed microtubule segments along a total of 28.2 μm filament of one expanded sample. The simulated cross-sectional profile for 3.2x proExM expanded pre- and post-labelled microtubule assuming a pre- to post-labelling ratio of 0.1 is shown in red. **f,** Histogram of peak-to-peak distances with normalized normal curve (red) of fitted profiles analysed in (e) with an average distance of 79.5 $\pm$ 6.6 nm (mean$\pm$sd) analysed along $n = 11$ microtubule segments in 2 cells from 1 expanded sample. **g,** Image projection of the xz-axes averaged along two microtubule filaments (*iv*) and (*v*) shown in (b) (red dotted lines) using the "z projection analysis" of the software Line Profiler. **h,** Cross-sectional profile (blue dots) of the xz-projection shown in (g). Using a bi-Gaussian fit (red) the peak-to-peak distance is determined to 81.2 nm. Scale bars, 10 μm (a), 5 μm (b), 1 μm (c) 500 nm (d), 100 nm (g). (*Material adapted from M3*)

In the xz-view of 3D *d*STORM images of expanded and post-labelled microtubules, we could clearly reveal the hollow structure of the microtubules using a water objective

in epi-illumination (Figure 3.21c). When analysing the average peak-to-peak distance, we observed a substantial shortening of the distance to 79.5±6.6 nm (mean±sd). This can well be explained by a reduced linkage error caused by post-labelling Ex-SMLM using the proExM protocol (Figure 3.21).

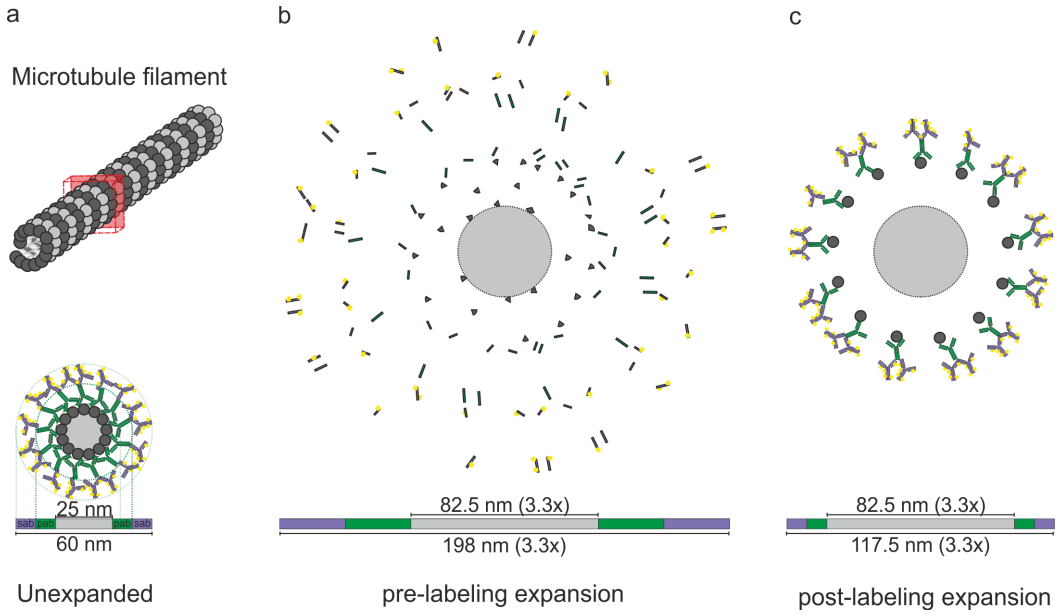

Figure 3.21: Signal dilution in pre- versus post-expansion labelling approaches. a, Model of microtubules with an outer diameter of 25 nm stained with primary and fluorescently labelled secondary IgG antibodies resulting in a total diameter of 60 nm with a linkage error (defined by the size of the primary and secondary antibody) of 17.5 nm (as in Figure 3.16a). **b,** Model of a 3.3-fold expanded microtubule immunolabelled pre-expansion as in (a) which results in an increase of the inner diameter to 82.5 nm and a total diameter of 198 nm. The linkage error increases with the 3.3x expansion to 57.75 nm. **c,** Model of a 3.3-fold expanded microtubule immunolabelled post-expansion with primary and secondary antibodies resulting in a linkage error of 17.5 nm equal to the linkage error in unexpanded labelling (a).

We next applied post-labelling 3D-Ex-SMLM on U-ExM treated isolated centrioles. We therefore immunostained α-tubulin with primary and Alexa 647 fluorophore conjugated secondary Fab fragments (Figure 3.22a-c). The 3D-*d*STORM images of procentrioles and mature centrioles could clearly reveal the 9-fold symmetry of the centrioles (Figure 3.22a-b) in frontal view as shown before in combination of U-ExM and STED imaging in chapter 3.1. In lateral view of the centrioles, we could clearly resolve single microtubule triplets which have a distance of 15 nm (Figure 3.22c). These results demonstrate that post-expansion Ex-SMLM achieves a resolution well below 15 nm. As an alternative strategy to perform Ex-SMLM, we used the spontaneously blinking Si-rhodamine dye HMSiR [UKY$^+$14] for

immunostaining post-expansion.

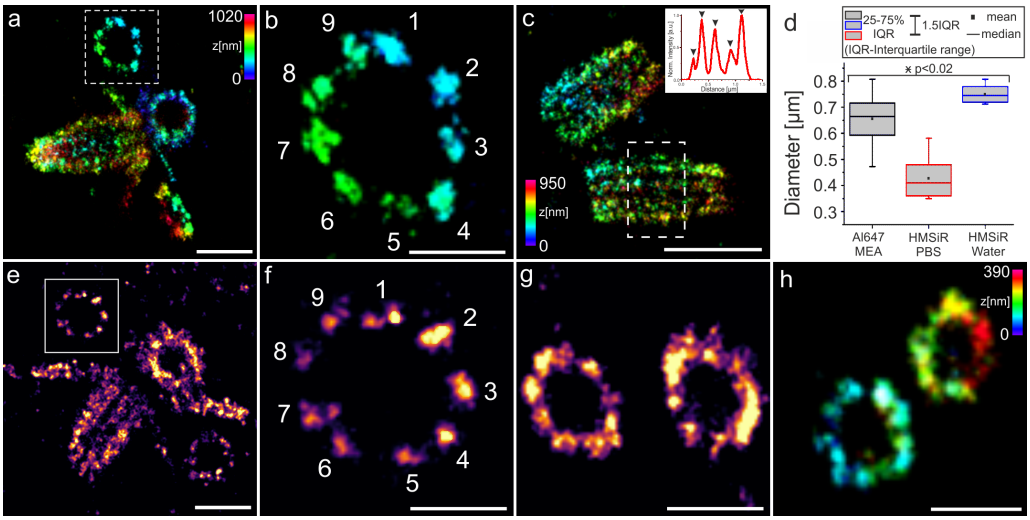

Figure 3.22: Ex-SMLM of U-ExM expanded centrioles a-c, 3D *d*STORM image of U-ExM expanded and re-embedded *Chlamydomonas* centrioles stained post re-embedding for anti α-tubulin with primary and Alexa Fluor 647 (Al647) conjugated secondary antibodies measured in MEA buffer. **b** Zoom-in on highlighted region in (a). **c,** Side view of two mature centrioles with clearly separated triplets. The inset shows the cross-sectional profile along the centriole (white box) showing five distinct peaks of microtubule triplets (marked with arrow heads). **d,** Comparison of the diameters determined from expanded centrioles measured using different protocols (re-embedded and labelled with Al647, and imaged in MEA photoswitching buffer, labelled with HMSiR 647 and imaged in water or in PBS (1x) buffer (pH 7.4)). Mean values are 657 $\pm$ 90 nm (mean$\pm$sd) for Al647 in MEA buffer ($n = 12$ centrioles), 428$\pm$74 nm (mean$\pm$sd) for HMSiR 647 in PBS ($n = 7$ centrioles), and 750$\pm$34 nm (mean$\pm$sd) for HMSiR 647 in water ($n = 8$ centrioles). Divided by unexpanded diameters of α-tubulin labelled centrioles, expansion factors translates into $\sim$3.4x, $\sim$2.2x, and $\sim$3.9x for expanded centrioles labelled with Al647 in MEA buffer, HMSiR in PBS (1x), and HMSiR 647 in water, respectively. Statistical significance was assessed by one-way ANOVA: $p < 0.02$ ($F = 3.80$). **e–g,** 2D *d*STORM image of U-ExM expanded centrioles labelled with HMSiR 647 imaged in water (e–f) or PBS(1x) (g). **f,** Zoom-in on highlighted region in (e). **h,** 3D *d*STORM image of unexpanded isolated centrioles immunostained with antibodies against glutamylated tubulin and Al647 conjugated secondary antibodies. Scale bars, 1 μm (a,e), 500 nm (b,f,g), 1.5 μm (c), 250 nm (h). (*Material adapted from M3*)

We performed *d*STORM in water with a $\sim$4-fold expansion factor and in PBS with optimized pH achieving an expansion factor of $\sim$2-fold. The resulting *d*STORM images acquired in PBS gave similar results as unexpanded *d*STORM images (compare Figure 3.22g and Figure 3.22h). In water, again the 9-fold symmetry in frontal view and single triplets in lateral view could be clearly resolved (Figure 3.22e-f).The analysis of z-galleries of expanded

centrioles re-embedded and post-labelled with Alexa Fluor 647 shows ring-like sub-structures within the microtubule triplets. In some triplets three distinct areas could be distinguished which could correspond to the A, B and C microtubule triplets resolved by post-Ex-SMLM (Figure 3.23).

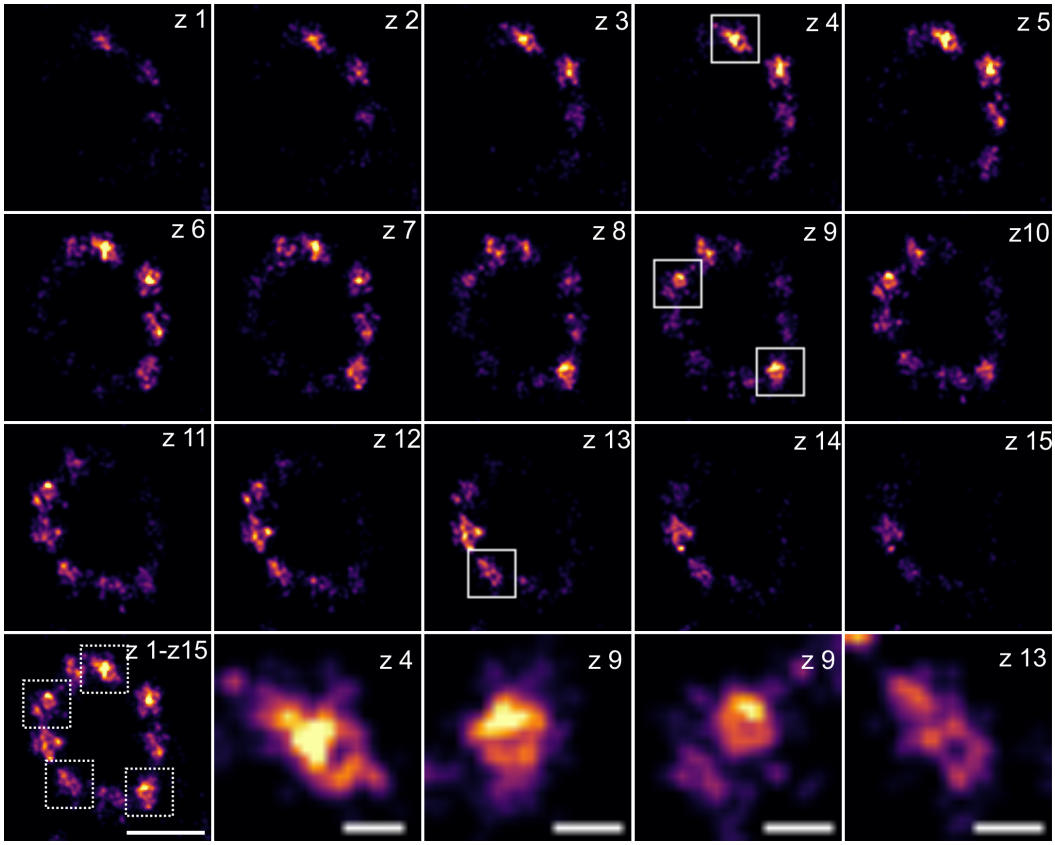

Figure 3.23: Resolving sub-structures of centriole microtubule triplets. Post-labelling 3D Ex-*d*STORM images of expanded centriole displayed in 2D. Single z slices z1-z15 of an image stack with 30 nm z-steps are shown as well as the maximum intensity projection of all z-slices (z1-z15). Highlighted regions (white boxes) are shown in the lowest panel. The ring-like structures in centriole triplets shown in z4, z9 and z13 indicate hollow microtubules. Similar results could be observed in $n = 6$ procentrioles imaged in 2 independent expansion experiments. Scale bars, 500 nm (z1-z15), 100 nm (zoom-in of z4, z9, z13). (*Material adapted from M3*)

3.3.5 Summary

We successfully demonstrated the combination of SMLM with ExM using different protocol strategies. Re-embedding represents a solution to circumvent the shrinking of the hydrogel upon exposure to photoswitching buffers. This allows performing *d*STORM on expanded samples with so far unmatched resolution using different ExM labelling strategies. We could demonstrate reduction of the linkage error when performing post-labelling Ex-SMLM which could reveal the hollow structure of microtubules in 3D measurements. The improved labelling efficiency caused by the smaller linkage error and improved epitope accessibility gives post-labelling Ex-SMLM a big advantage compared to pre-expansion Ex-SMLM approaches and conventional super-resolution imaging techniques. In addition, we showed that the use of spontaneously blinking fluorophores enables Ex-SMLM in water without the need of re-embedding the sample. We applied the Ex-SMLM protocols to isolated centrioles and performed 3D *d*STORM in which we could resolve ring-like sub-structures of centrioles demonstrating the resolution of individual microtubule triplets.

Chapter 4

Conclusion and Outlook

Expansion Microscopy is a sample preparation tool which allows imaging with nanoscale precision using conventional diffraction-limited microscopes. The resolution improvement is achieved by the physical expansion of specimens. This method can be combined with any fluorescence microscopy technique that works with fixed specimens and does not need an interaction between optical instruments in close contact to the sample as in the case of near-field microscopy. For biologists, the combination of ExM and confocal imaging adds a super-resolution technique to their toolbox without the need of expertise in a super-resolution imaging technique or expensive microscopic setups.

Furthermore, the combination of ExM with a super-resolution microscopy technique represents a powerful tool to decipher the structure and function of biomolecules and macromolecular cellular components with so far unattained resolution. However, the development of a reliable expansion procedure can be very challenging since the use of a hydrogel and the physical expansion requires new strategies in sample handling and makes the procedure prone to image artifacts. By careful optimization of existing ExM approaches, it is possible to develop expansion strategies which achieve an isotropic expansion that maintains the native state of the biological sample and allows combination with modern imaging techniques like SIM, *d*STORM or STED. In this way, ExM can address issues that conventional super-resolution techniques are still confronted with, namely labelling efficiency and fixation artifacts.

ExM technology has constantly been developed in recent years in terms of improved hydrogel compositions that yield higher expansion factors and improved network homogeneity as well as labelling strategies to enhance the fluorescent signal. Due to the increase of the linkage error of the label with the expansion factor, smaller labels than the conventionally

used antibodies or post-expansion labelling strategies that are compatible with the ExM treatment will be necessary in future. There would otherwise be no improvement in the effective resolution when the displacement of detected molecules by physical expansion exceeds a certain order of magnitude since this will likely be greater than the precision of the imaging technique being used.

Labels reducing the linkage error

In future ExM studies, an acrydite linker introduced directly to proteins by click chemistry before or after expansion could represent a strategy which completely avoids the use of antibodies and substantially reduces the linkage error. This could enable true molecular resolution imaging when combining click chemistry with Ex-SMLM. However, clicking after expansion could be challenging as azide, alkene or alkyne groups get chemically attacked by radicals during hydrogel formation. Either clicking before expansion and selecting fluorophores which survive the hydrogel formation, or strategies which protect the clicking site from radicals or polymerization of hydrogels without the use of radicals are required. The compatibility of other small labels like nanobodies or SBPs with post-expansion labelling Ex-SMLM could also be tested.

Improved linkage error and label density by post-expansion labelling

Post-expansion labelling approaches improve epitope accessibility by exposing epitopes sheltered in the center of proteins and create space in dense protein regions where antibodies normally would sterically hinder each other due to their size. These effects and the shrinkage of the linkage error with increased expansion factors could potentially solve limiting factors of improved super-resolution microscopy methods. The Nyquist criterion is often taken to describe the required localization density in SMLM studies to resolve a structure of a given size. It states that the label density requires a $\sim$2-fold greater spatial frequency of molecules compared to the desired resolution. By simulating localization microscopy data, Legant et al. [LSG$^+$16] even suggested that it requires a $\sim$5-fold greater level of labelling density compared to the Nyquist criterion. Post-labelling ExM approaches like the U-ExM, MAP-SIM or Post-labelling Ex-SMLM achieve higher label densities due to improved epitope accessibility and could hence be a way to meet the required number of molecules.

U-ExM

U-ExM combines several advantages compared to other ExM protocols. First, the epitope accessibility and label density are improved by the displacement of proteins during expansion.

In addition, we could demonstrate that the approach preserves the native structure of isolated centrioles better than other ExM variants like the original ExM or MAP protocol. When expanding isolated organelles, a fixation step before gelation is not necessary with the U-ExM approach which can lead to structural defects in conventional imaging approaches. However, in expanding the synaptonemal complex it has been shown that U-ExM could not guarantee an isotropic expansion of the multiprotein complex. We observed structural breaks of U-ExM treated SCs which indicates an insufficient incorporation of the protein content of the SC. This underlines the importance of verifying the expansion isotropy in each ExM experiment. Images of expanded samples must be carefully considered, and protocols may need to be optimized depending on the type of the biological sample.

MAP-SIM

Studying biological complexity requires 3D imaging of several labels in high volumes and with high resolution. The MAP-SIM approach achieves a lateral resolution of $\sim$20-30 nm and brings the advantage of SIM imaging which allows multicolour imaging in greater volumes than SMLM. The MAP-SIM gel composition is optimized to achieve a $\sim$4-fold expansion and allows the complete transfer of the protein content of multi-protein complexes like the synaptonemal complex. With the optimized MAP-SIM approach, we were able to resolve sub-structural features of the lateral element of the SC and study the distribution of several proteins within the SC. The advantage of improved epitope accessibility by MAP-SIM could potentially reveal further sub-structures in dense protein regions of the SC which so far could not be revealed by super-resolution techniques or EM studies. In addition, MAP-SIM is an imaging tool which also can be used to study other organelles or biopolymers in cells or in vitro.

Ex-SMLM

Advanced super-resolution methods including interferometric or patterned illumination single-molecule localization [GLZ$^+$19] [CHT$^+$20] and Minflux [GPB$^+$20] can now localize single emitters with a precision of only a few nanometres. But these techniques are still limited in achieving true molecular resolution as limitations in labelling efficiency and linkage error prevents imaging in the sub-10 nm regime. The development of Ex-SMLM including the stabilization of hydrogels by re-embedding allowed for the first time a direct experimental comparison of the linkage errors for pre- and post-labelling strategies in ExM experiments. Post-immunolabelling Ex-SMLM thereby demonstrated many advantages compared to pre-

immunolabelling Ex-SMLM and conventional SMLM of unexpanded samples especially with regard to labelling efficiency and linkage error.

Ex-SMLM combined with iterative ExM

The combination of swellable hydrogels and uncharged re-embedding gels containing different crosslinker molecules that can be melted upon exposure to e.g. high pH could potentially provide a new expansion and stabilization strategy for expanded hydrogels providing higher expansion factors for Ex-SMLM. This would involve the design of short DNA labels providing linker moieties that can be transferred between the different gels.

A possible workflow could first cross-link proteins into the hydrogel performing the MAP-SIM protocol including AA-FA incubation, MAP-SIM hydrogel formation containing DHEBA as crosslinker instead of BIS-acrylamide, denaturation and $\sim$4.5-fold expansion in water followed by re-embedding in an acrylamide gel again containing DHEBA as crosslinker (e.g. 10% AA, 0.2% DHEBA). Then, post-expansion immunostaining with ssDNA coupled to IgG containing an acrydite DNA modification could be performed. Here, the design of short DNA strands would decrease the positional error introduced by the label. In addition, the acrydite linker modification at the DNA could be positioned in close proximity to the IgG-DNA coupling site. After immunostaining, a second swellable gel could be polymerized containing BIS-acrylamide as crosslinker in which the ssDNA label is anchored. The first gel and re-embedding gel could then be dissolved by incubation in a buffer with high pH and the second gel could be expanded another $\sim$ 4.5-fold. Next a second re-embedding gel could be cast to keep the second gel in the $\sim$20-fold expanded state and fluorophore tagged DNA labels could be hybridized and Ex-SMLM imaging could be performed.

Optionally, similar to triple round expansion experiments performed in iExM [CCY$^+$17], the first MAP-SIM gel and first re-embedding gel could be crosslinked with a disulfide-containing crosslinker N,N'-cystaminebis-acrylamide which can be cleaved with tris(2-carboxyethyl)-phosphine (TCEP) and is resistant to NaOH. The DNA would then be linked into the second gel (with DHEBA as crosslinker) and the first gel and first re-embedding gel could be cleaved. For stabilization of the second gel, a second re-embedding gel with DHEBA as crosslinker could be used. In this state, gels would theoretically be $\sim$20-fold expanded. It would then be possible to strip the dsDNA linker using DNase1 and introduce another DNA strand to the remaining crosslinked DNA which is equipped with an additional linker. A third acrylamide gel with BIS-acrylamide as crosslinker could be polymerized in which the linker is finally anchored. By incubation in NaOH the second re-embedding

gel and second gel would be dissolved. The third gel would then contain the DNA label which could be labelled with a complementary fluorphore bearing DNA oligos after DNase1 treatment. With this alternative, only one gel would remain as the final gel. This could be an advantage compared to the first strategy described above where the refractive index mismatch of two gels could lead to opacity of the gel which might affect image quality.

Ex-SMLM combined with X10 microscopy

Another simpler strategy to increase the expansion factor when performing Ex-SMLM could potentially be achieved by combining the X10 hydrogel with the re-embedding approach. With a $\sim$20% reduction in size of the expanded hydrogel as shown with original ExM hydrogel composition, the expansion factor would still be $\sim$8-fold after re-embedding. The combination of incorporation of the protein content as in MAP or U-ExM protocols followed by expansion in the X10 gel could also be tested with or without re-embedding.

Ex-SMLM as a validation tool

The high resolution and single-molecule sensitivity achieved by Ex-*d*STORM could be used as a tool to validate the nanoscale expansion uniformity of different hydrogels like the original ExM gel, the X10 gel or the recently developed tetra-gel (TG). Therefore, DNA origami nanorulers [RJM$^+$18] [ST18] with precisely known distances of fluorophores could be investigated at the nanometre scale.

LineProfiler

LineProfiler is a tool which could become very valuable to the scientific community using super-resolution microscopy techniques. Manually set cross-sectional profiles along reference structures like microtubules often have been used to claim an achievable structural resolution by a microscopy technique. These results are often user-biased and cannot be used to compare values of other publications. Our software provides an unbiased analysis of peak-to-peak distances set along several entire filamentous structures in an image. This provides comparability of obtained values and can be used to compare different methods including conventional imaging techniques, Ex-SMLM variants or other imaging techniques combined to ExM.

Ex-SMLM combined with murine brain tissue

Together with *Janna Eilts* from the department of biotechnology and biophysics in Würzburg, I expanded the synaptic scaffold proteins Bassoon and Homer in synapses of mouse brain

tissues. We immunostained these proteins pre-expansion with primary and secondary Alexa Fluor 532 conjugated antibodies. After incubation of AcX as a crosslinker molecule we expanded the samples according to the proExM protocol and subsequently re-embedded the samples. First results revealed bar-like structures that are typical for these proteins located along the synapses (Figure 4.1).

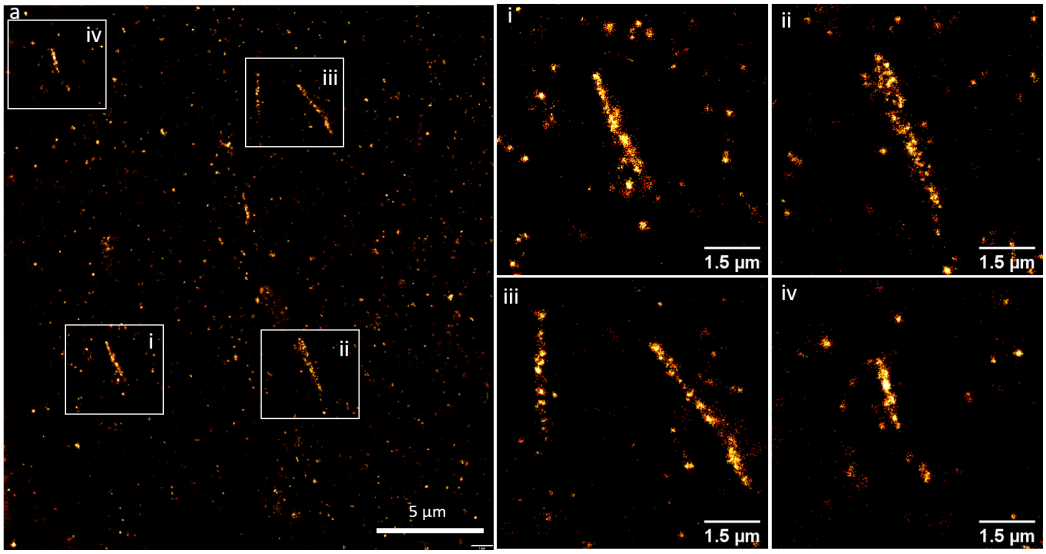

Figure 4.1: Ex-SMLM applied on brain tissue. a, *d*STORM image of Homer and Bassoon immunostained with primary and secondary antibody (stained with Alexa Fluor 532) in mouse brain tissue. **i-iv,** Zoom in on white-boxed regions in (a).

In further experiments, the performance of post-expansion labelling Ex-SMLM on brain tissue could be a versatile tool to investigate synaptic proteins. The improved epitope accessibility and resolution improvement could help to investigate the spatial difference between post- and presynaptic localization of proteins separated by the synaptic cleft within a distance of 15-25 nm [Sau13].

ExM combined with Lattice Light Sheet Microscopy

High-resolution 3D-imaging away from the coverslip and deeper into thick specimen remains challenging for super-resolution techniques as out-of-focus background and premature bleaching of fluorophores limits these techniques. ExM-processed samples mainly consist of water ($> 99\%$) which eliminates scattering of light and allows imaging deep into thick tissue or cells. This makes ExM suitable for fast imaging methods which rely on transparent

samples like light sheet fluorescence microscopy or the advanced version lattice light sheet microscopy. In combination, these technologies provide fast 3D imaging with nanoscale resolution. Gao et al. [GAU+19] demonstrated stunning results when combining ExM and LLSM (ExLLSM) in the visualization of subcellular structures in the brain in a cortex-spanning volume in the mouse and in a brain-wide volume in *Drosophila* at 4-fold expansion. The high speed and nanometric 3D resolution could make ExLLSM a powerful tool for anatomical studies of expanded tissues in pathology.

Bibliography

[Abb73] E. Abbe. Beiträge zur theorie des mikroskops und der mikroskopischen wahrnehmung. *Archiv für Mikroskopische Anatomie*, 9(1):413–468, 1873.

[AGS+20] Shahar Alon, Daniel R. Goodwin, Anubhav Sinha, Asmamaw T. Wassie, Fei Chen, Evan R. Daugharthy, Yosuke Bando, Atsushi Kajita, Andrew G. Xue, Karl Marrett, Robert Prior, Yi Cui, Andrew C. Payne, Chun-Chen Yao, Ho-Jun Suk, Ru Wang, Chih-Chieh Yu, Paul Tillberg, Paul Reginato, Nikita Pak, Songlei Liu, Sukanya Punthambaker, Eswar P. R. Iyer, Richie E. Kohman, Jeremy A. Miller, Ed S. Lein, Ana Lako, Nicole Cullen, Scott Rodig, Karla Helvie, Daniel L. Abravanel, Nikhil Wagle, Bruce E. Johnson, Johanna Klughammer, Michal Slyper, Julia Waldman, Judit Jané-Valbuena, Orit Rozenblatt-Rosen, Aviv Regev, George M. Church, Adam H. Marblestone, and Edward S. Boyden. *Expansion Sequencing: Spatially Precise In Situ Transcriptomics in Intact Biological Systems*. 2020.

[BAP+16] Mikael P. Backlund, Amir Arbabi, Petar N. Petrov, Ehsan Arbabi, Saumya Saurabh, Andrei Faraon, and W. E. Moerner. Removing orientation-induced localization biases in single-molecule microscopy using a broadband metasurface mask. *Nature photonics*, 10:459–462, 2016.

[BEG+17] Francisco Balzarotti, Yvan Eilers, Klaus C. Gwosch, Arvid H. Gynnå, Volker Westphal, Fernando D. Stefani, Johan Elf, and Stefan W. Hell. Nanometer resolution imaging and tracking of fluorescent molecules with minimal photon fluxes. *Science (New York, N.Y.)*, 355(6325):606–612, 2017.

[BFC+20] Octavian Bucur, Feifei Fu, Mike Calderon, Geetha H. Mylvaganam, Ngoc L. Ly, Jimmy Day, Simon Watkin, Bruce D. Walker, Edward S. Boyden, and Yongxin Zhao. Nanoscale imaging of clinical specimens using conventional and rapid-expansion pathology. *Nature protocols*, 15(5):1649–1672, 2020.

[BFH18] Ewelina Bolcun-Filas and Mary Ann Handel. Meiosis: the chromosomal foundation of reproduction. *Biology of reproduction*, 99(1):112–126, 2018.

[BKK+19] Gerti Beliu, Andreas J. Kurz, Alexander C. Kuhlemann, Lisa Behringer-Pliess, Mara Meub, Natalia Wolf, Jürgen Seibel, Zhen-Dan Shi, Martin Schnermann, Jonathan B. Grimm, Luke D. Lavis, Sören Doose, and Markus Sauer. Bioorthogonal labeling with tetrazine-dyes for super-resolution microscopy. *Communications biology*, 2:261, 2019.

[BKM+98] Y. Bobinnec, A. Khodjakov, L. M. Mir, C. L. Rieder, B. Eddé, and M. Bornens. Centriole disassembly in vivo and its effect on centrosome structure and function in vertebrate cells. *The Journal of cell biology*, 143(6):1575–1589, 1998.

[BLH+86] E. Betzig, A. Lewis, A. Harootunian, M. Isaacson, and E. Kratschmer. Near field scanning optical microscopy (nsom). *Biophysical journal*, 49(1):269–279, 1986.

[Bor12] Michel Bornens. The centrosome in cells and organisms. *Science (New York, N.Y.)*, 335(6067):422–426, 2012.

[BPS+06] Eric Betzig, George H. Patterson, Rachid Sougrat, O. Wolf Lindwasser, Scott Olenych, Juan S. Bonifacino, Michael W. Davidson, Jennifer Lippincott-Schwartz, and Harald F. Hess. Imaging intracellular fluorescent proteins at nanometer resolution. *Science (New York, N.Y.)*, 313(5793):1642–1645, 2006.

[BRA14] S. BRADBURY, editor. *The Evolution of the Microscope*. Elsevier Science, Burlington, 2014.

[CBS+14] Bani H. Cipriano, Stephen J. Banik, Renu Sharma, Dominic Rumore, Wonseok Hwang, Robert M. Briber, and Srinivasa R. Raghavan. Superabsorbent hydrogels that are robust and highly stretchable. *Macromolecules*, 47(13):4445–4452, 2014.

[CCJ41] A. H. Coons, H. J. Creech, and R. N. Jones. Immunological properties of an antibody containing a fluorescent group. *Experimental Biology and Medicine*, 47(2):200–202, 1941.

[CCY+17] Jae-Byum Chang, Fei Chen, Young-Gyu Yoon, Erica E. Jung, Hazen Babcock, Jeong Seuk Kang, Shoh Asano, Ho-Jun Suk, Nikita Pak, Paul W. Tillberg, Asmamaw T. Wassie, Dawen Cai, and Edward S. Boyden. Iterative expansion microscopy. *Nature methods*, 14(6):593–599, 2017.

[CHO+16] Tyler J. Chozinski, Aaron R. Halpern, Haruhisa Okawa, Hyeon-Jin Kim, Grant J. Tremel, Rachel O. L. Wong, and Joshua C. Vaughan. Expansion microscopy with conventional antibodies and fluorescent proteins. *Nature methods*, 13(6):485–488, 2016.

[CHT+20] Jelmer Cnossen, Taylor Hinsdale, Rasmus Ø. Thorsen, Marijn Siemons, Florian Schueder, Ralf Jungmann, Carlas S. Smith, Bernd Rieger, and Sjoerd Stallinga. Localization microscopy at doubled precision with patterned illumination. *Nature Methods*, 17(1):59–63, 2020.

[Cro06] William J. Croft. *Under the microscope: A brief history of microscopy*, volume v. 5 of *Series in popular science*. World Scientific, Hackensack, NJ, 2006.

[CS04] Guy Cox and Colin J. R. Sheppard. Practical limits of resolution in confocal and non-linear microscopy. *Microscopy research and technique*, 63(1):18–22, 2004.

[CTB15] Fei Chen, Paul W. Tillberg, and Edward S. Boyden. Optical imaging. expansion microscopy. *Science (New York, N.Y.)*, 347(6221):543–548, 2015.

[CTE+94] M. Chalfie, Y. Tu, G. Euskirchen, W. W. Ward, and D. C. Prasher. Green fluorescent protein as a marker for gene expression. *Science (New York, N.Y.)*, 263(5148):802–805, 1994.

[CWC+16] Fei Chen, Asmamaw T. Wassie, Allison J. Cote, Anubhav Sinha, Shahar Alon, Shoh Asano, Evan R. Daugharthy, Jae-Byum Chang, Adam Marblestone, George M. Church, Arjun Raj, and Edward S. Boyden. Nanoscale imaging of rna with expansion microscopy. *Nature methods*, 13(8):679–684, 2016.

[CWK+13] Kwanghun Chung, Jenelle Wallace, Sung-Yon Kim, Sandhiya Kalyanasundaram, Aaron S. Andalman, Thomas J. Davidson, Julie J. Mirzabekov, Kelly A. Zalocusky, Joanna Mattis, Aleksandra K. Denisin, Sally Pak, Hannah Bernstein, Charu Ramakrishnan, Logan Grosenick, Viviana Gradinaru, and Karl Deisseroth. Structural and molecular interrogation of intact biological systems. *Nature*, 497(7449):332–337, 2013.

[CWR15] Paul T. Conduit, Alan Wainman, and Jordan W. Raff. Centrosome function and assembly in animal cells. *Nature reviews. Molecular cell biology*, 16(10):611–624, 2015.

[CYW+17] Cori K. Cahoon, Zulin Yu, Yongfu Wang, Fengli Guo, Jay R. Unruh, Brian D. Slaughter, and R. Scott Hawley. Superresolution expansion microscopy reveals the three-dimensional organization of the drosophila synaptonemal complex. *Proceedings of the National Academy of Sciences of the United States of America*, 114(33):E6857–E6866, 2017.

[DCI+09] T. Dertinger, R. Colyer, G. Iyer, S. Weiss, and J. Enderlein. Fast, background-free, 3d super-resolution optical fluctuation imaging (sofi). *Proceedings of the National Academy of Sciences of the United States of America*, 106(52):22287–22292, 2009.

[DCV+10] Thomas Dertinger, Ryan Colyer, Robert Vogel, Jörg Enderlein, and Shimon Weiss. Achieving increased resolution and more pixels with superresolution optical fluctuation imaging (sofi). *Optics express*, 18(18):18875–18885, 2010.

[dGA86] J. del Mazo and L. Gil-Alberdi. Multistranded organization of the lateral elements of the synaptonemal complex in the rat and mouse. *Cytogenetics and cell genetics*, 41(4):219–224, 1986.

[DHV+10] Thomas Dertinger, Mike Heilemann, Robert Vogel, Markus Sauer, and Shimon Weiss. Superresolution optical fluctuation imaging with organic dyes. *Angewandte Chemie (International ed. in English)*, 49(49):9441–9443, 2010.

[DIN+17] Justin Demmerle, Cassandravictoria Innocent, Alison J. North, Graeme Ball, Marcel Müller, Ezequiel Miron, Atsushi Matsuda, Ian M. Dobbie, Yolanda Markaki, and Lothar Schermelleh. Strategic and practical guidelines for successful structured illumination microscopy. *Nature protocols*, 12:988 EP –, 2017.

[dLDB+17] G. M. R. de Luca, E. Desclos, R. M. P. Breedijk, L. Dolz-Edo, G. J. Smits, L. Nahidiazar, P. Bielefeld, L. Picavet, C. P. Fitzsimons, R. Hoebe, and E. M. M. Manders. Configurations of the re-scan confocal microscope (rcm) for biomedical applications. *Journal of microscopy*, 266(2):166–177, 2017.

[DM80] M. E. Dresser and M. J. Moses. Synaptonemal complex karyotyping in spermatocytes of the chinese hamster (cricetulus griseus). iv. light and electron microscopy of synapsis and nucleolar development by silver staining. *Chromosoma*, 76(1):1–22, 1980.

[DMDZ12] Peter Dedecker, Gary C. H. Mo, Thomas Dertinger, and Jin Zhang. Widely accessible method for superresolution fluorescence imaging of living systems. *Proceedings of the National Academy of Sciences of the United States of America*, 109(27):10909–10914, 2012.

[DPB+13] Thomas Dertinger, Alessia Pallaoro, Gary Braun, Sonny Ly, Ted A. Laurence, and Shimon Weiss. Advances in superresolution optical fluctuation imaging (sofi). *Quarterly reviews of biophysics*, 46(2):210–221, 2013.

[FBB+08] Jonas Fölling, Mariano Bossi, Hannes Bock, Rebecca Medda, Christian A. Wurm, Birka Hein, Stefan Jakobs, Christian Eggeling, and Stefan W. Hell. Fluorescence nanoscopy by ground-state depletion and single-molecule return. *Nature Methods*, 5(11):943–945, 2008.

[FOF+17] Limor Freifeld, Iris Odstrcil, Dominique Förster, Alyson Ramirez, James A. Gagnon, Owen Randlett, Emma K. Costa, Shoh Asano, Orhan T. Celiker, Ruixuan Gao, Daniel A. Martin-Alarcon, Paul Reginato, Cortni Dick, Linlin Chen, David Schoppik, Florian Engert, Herwig Baier, and Edward S. Boyden. Expansion microscopy of zebrafish for neuroscience and developmental biology studies. *Proceedings of the National Academy of Sciences of the United States of America*, 114(50):E10799–E10808, 2017.

[For91] Brian J. Ford. *The Leeuwenhoek legacy*. Biopress, Bristol, 1991.

[FSAB12] Johanna Fraune, Sabine Schramm, Manfred Alsheimer, and Ricardo Benavente. The mammalian synaptonemal complex: protein components, assembly and role in meiotic recombination. *Experimental cell research*, 318(12):1340–1346, 2012.

[GAU+19] Ruixuan Gao, Shoh M. Asano, Srigokul Upadhyayula, Igor Pisarev, Daniel E. Milkie, Tsung-Li Liu, Ved Singh, Austin Graves, Grace H. Huynh, Yongxin Zhao, John Bogovic, Jennifer Colonell, Carolyn M. Ott, Christopher Zugates, Susan Tappan, Alfredo Rodriguez, Kishore R. Mosaliganti, Shu-Hsien Sheu, H. Amalia Pasolli, Song Pang, C. Shan Xu, Sean G. Megason, Harald Hess, Jennifer Lippincott-Schwartz, Adam Hantman, Gerald M. Rubin, Tom Kirchhausen, Stephan Saalfeld, Yoshinori Aso, Edward S. Boyden, and Eric Betzig. Cortical column and whole-brain imaging with molecular contrast and nanoscale resolution. *Science (New York, N.Y.)*, 363(6424), 2019.

[GHM+13] Paul Guichard, Virginie Hachet, Norbert Majubu, Aitana Neves, Davide Demurtas, Natacha Olieric, Isabelle Fluckiger, Akinori Yamada, Kumiko

Kihara, Yuichiro Nishida, Shigeharu Moriya, Michel O. Steinmetz, Yuichi Hongoh, and Pierre Gönczy. Native architecture of the centriole proximal region reveals features underlying its 9-fold radial symmetry. *Current biology : CB*, 23(17):1620–1628, 2013.

[GLZ+19] Lusheng Gu, Yuanyuan Li, Shuwen Zhang, Yanhong Xue, Weixing Li, Dong Li, Tao Xu, and Wei Ji. Molecular resolution imaging by repetitive optical selective exposure. *Nature Methods*, 16(11):1114–1118, 2019.

[GMB+18] Mengfei Gao, Riccardo Maraspini, Oliver Beutel, Amin Zehtabian, Britta Eickholt, Alf Honigmann, and Helge Ewers. Expansion stimulated emission depletion microscopy (exsted). *ACS nano*, 12(5):4178–4185, 2018.

[GPB+20] Klaus C. Gwosch, Jasmin K. Pape, Francisco Balzarotti, Philipp Hoess, Jan Ellenberg, Jonas Ries, and Stefan W. Hell. Minflux nanoscopy delivers 3d multicolor nanometer resolution in cells. *Nature methods*, 17(2):217–224, 2020.

[GSC+08] Mats G. L. Gustafsson, Lin Shao, Peter M. Carlton, C. J. Rachel Wang, Inna N. Golubovskaya, W. Zacheus Cande, David A. Agard, and John W. Sedat. Three-dimensional resolution doubling in wide-field fluorescence microscopy by structured illumination. *Biophysical journal*, 94(12):4957–4970, 2008.

[Gus00] M. G. Gustafsson. Surpassing the lateral resolution limit by a factor of two using structured illumination microscopy. *Journal of microscopy*, 198(Pt 2):82–87, 2000.

[GYG+19] Ruixuan Gao, Chih-Chieh Yu, Linyi Gao, Kiryl D. Piatkevich, Rachael L. Neve, Srigokul Upadhyayula, and Edward S. Boyden. *A highly homogeneous expansion microscopy polymer composed of tetrahedron-like monomers*, volume 15. 2019.

[HAC+17] Aaron R. Halpern, Germain C. M. Alas, Tyler J. Chozinski, Alexander R. Paredez, and Joshua C. Vaughan. Hybrid structured illumination expansion microscopy reveals microbial cytoskeleton organization. *ACS nano*, 11(12):12677–12686, 2017.

[HGM06] Samuel T. Hess, Thanu P. K. Girirajan, and Michael D. Mason. Ultra-high resolution imaging by fluorescence photoactivation localization microscopy. *Biophysical journal*, 91(11):4258–4272, 2006.

[HRP+19] David Hörl, Fabio Rojas Rusak, Friedrich Preusser, Paul Tillberg, Nadine Randel, Raghav K. Chhetri, Albert Cardona, Philipp J. Keller, Hartmann Harz, Heinrich Leonhardt, Mathias Treier, and Stephan Preibisch. Bigstitcher: reconstructing high-resolution image datasets of cleared and expanded samples. *Nature Methods*, 16(9):870–874, 2019.

[HS10] E. Hatch and T. Stearns. The life cycle of centrioles. *Cold Spring Harbor symposia on quantitative biology*, 75:425–431, 2010.

[HSH+17] Virginie Hamel, Emmanuelle Steib, Romain Hamelin, Florence Armand, Susanne Borgers, Isabelle Flückiger, Coralie Busso, Natacha Olieric, Carlos Oscar S. Sorzano, Michel O. Steinmetz, Paul Guichard, and Pierre Gönczy. Identification of chlamydomonas central core centriolar proteins reveals a role for human wdr90 in ciliogenesis. *Current biology : CB*, 27(16):2486–2498.e6, 2017.

[Huf15] Joseph Huff. The airyscan detector from zeiss: confocal imaging with improved signal-to-noise ratio and super-resolution. *Nature Methods*, 12(12):i–ii, 2015.

[HvS+08] Mike Heilemann, Sebastian van de Linde, Mark Schüttpelz, Robert Kasper, Britta Seefeldt, Anindita Mukherjee, Philip Tinnefeld, and Markus Sauer. Subdiffraction-resolution fluorescence imaging with conventional fluorescent probes. *Angewandte Chemie (International ed. in English)*, 47(33):6172–6176, 2008.

[Ila07] Vincent Ilardi. *Renaissance vision from spectacles to telescopes*, volume 259 of *Memoirs of the American Philosophical Society held at Philadelphia for promoting useful knowledge*. American Philosophical Soc, Philadelphia, Pa., 2007.

[KGG+20] Tobias C. Kunz, Ralph Götz, Shiqiang Gao, Markus Sauer, and Vera Kozjak-Pavlovic. Using expansion microscopy to visualize and characterize the morphology of mitochondrial cristae. *Frontiers in Cell and Developmental Biology*, 8, 2020.

[KGSR19] Tobias C. Kunz, Ralph Götz, Markus Sauer, and Thomas Rudel. Detection of chlamydia developmental forms and secreted effectors by expansion microscopy. *Frontiers in cellular and infection microbiology*, 9:276, 2019.

[KJD+00] T. A. Klar, S. Jakobs, M. Dyba, A. Egner, and S. W. Hell. Fluorescence microscopy with diffraction resolution barrier broken by stimulated emission. *Proceedings of the National Academy of Sciences of the United States of America*, 97(15):8206–8210, 2000.

[KN19] Ping Kao and Michael Nodine. *Transcriptional Activation of Arabidopsis Zygotes Is Required for Their Initial Division*, volume 43. 2019.

[KSP+16] Taeyun Ku, Justin Swaney, Jeong-Yoon Park, Alexandre Albanese, Evan Murray, Jae Hun Cho, Young-Gyun Park, Vamsi Mangena, Jiapei Chen, and Kwanghun Chung. Multiplexed and scalable super-resolution imaging of three-dimensional protein localization in size-adjustable tissues. *Nature biotechnology*, 34(9):973–981, 2016.

[Lak10] Joseph R. Lakowicz. *Principles of fluorescence spectroscopy*. Springer, New York, NY, third edition, corrected at 4. printing edition, 2010.

[LCL+18] Rongqin Li, Xuanze Chen, Zixi Lin, Yao Wang, and Yujie Sun. Expansion enhanced nanoscopy. *Nanoscale*, 2018.

[LFMA12] Sam Li, Jose-Jesus Fernandez, Wallace F. Marshall, and David A. Agard. Three-dimensional structure of basal body triplet revealed by electron cryotomography. *The EMBO journal*, 31(3):552–562, 2012.

[LSG+16] Wesley R. Legant, Lin Shao, Jonathan B. Grimm, Timothy A. Brown, Daniel E. Milkie, Brian B. Avants, Luke D. Lavis, and Eric Betzig. High-density three-dimensional localization microscopy across large volumes. *Nature Methods*, 13(4):359–365, 2016.

[Mas01] Barry R. Masters. History of the electron microscope in cell biology. In *Encyclopedia of Life Sciences*. John Wiley & Sons, Ltd, Chichester, UK, 2001.

[MHN+17] Hans Michael Maric, Torben Johann Hausrat, Franziska Neubert, Nils Ole Dalby, Sören Doose, Markus Sauer, Matthias Kneussel, and Kristian Strømgaard. Gephyrin-binding peptides visualize postsynaptic sites and modulate neurotransmission. *Nature chemical biology*, 13(2):153–160, 2017.

[Min] M. Minsky. Microscopy apparatus. patent us3013467 a (1961).

[Min88] M. Minsky. Memoir on inventing the confocal scanning microscope. *Scanning*, 10(4):128–138, 1988.

[PGD00] Andrea M. Preble, Thomas M. Giddings, and Susan K. Dutcher. Basal bodies and centrioles: Their function and structure. In Gerald Schatten and Robert E. Palazzo, editors, *The centrosome in cell replication and early development*, volume 49 of *Current Topics in Developmental Biology*, pages 207–233. Academic Press, San Diego, 2000.

[Plo67] J. S. Ploem. The use of a vertical illuminator with interchangeable dichroic mirrors for fluorescence microscopy with incidental light. *Zeitschrift fur wissenschaftliche Mikroskopie und mikroskopische Technik*, 68(3):129–142, 1967.

[PV21] Paul Guichard and Virginie Hamel, editors. *EXPANSION MICROSCOPY FOR CELL BIOLOGY*. ELSEVIER ACADEMIC PRESS, [S.l.], 2021.

[Ray96] Rayleigh. Xv. on the theory of optical images, with special reference to the microscope. *The London, Edinburgh, and Dublin Philosophical Magazine and Journal of Science*, 42(255):167–195, 1896.

[RBZ06] Michael J. Rust, Mark Bates, and Xiaowei Zhuang. Stochastic optical reconstruction microscopy (storm) provides sub-diffraction-limit image resolution. *Nature methods*, 3(10):793–795, 2006.

[RCL+17] Erik A. Rodriguez, Robert E. Campbell, John Y. Lin, Michael Z. Lin, Atsushi Miyawaki, Amy E. Palmer, Xiaokun Shu, Jin Zhang, and Roger Y. Tsien. The growing and glowing toolbox of fluorescent and photoactive proteins. *Trends in biochemical sciences*, 42(2):111–129, 2017.

[RJM+18] Mario Raab, Ija Jusuk, Julia Molle, Egbert Buhr, Bernd Bodermann, Detlef Bergmann, Harald Bosse, and Philip Tinnefeld. Using dna origami nanorulers as traceable distance measurement standards and nanoscopic benchmark structures. *Scientific reports*, 8(1):1780, 2018.

[RKP+12] Jonas Ries, Charlotte Kaplan, Evgenia Platonova, Hadi Eghlidi, and Helge Ewers. A simple, versatile method for gfp-based super-resolution microscopy via nanobodies. *Nature methods*, 9(6):582–584, 2012.

[Sau13] Markus Sauer. Localization microscopy coming of age: from concepts to biological impact. *Journal of cell science*, 126(Pt 16):3505–3513, 2013.

[SGGB08] Hari Shroff, Catherine G. Galbraith, James A. Galbraith, and Eric Betzig. Live-cell photoactivated localization microscopy of nanoscale adhesion dynamics. *Nature methods*, 5(5):417–423, 2008.

[SH17] Markus Sauer and Mike Heilemann. Single-molecule localization microscopy in eukaryotes. *Chemical reviews*, 117(11):7478–7509, 2017.

[Sha49] C. E. Shannon. Communication in the presence of noise. *Proceedings of the IRE*, 37(1):10–21, 1949.

[SHF+15] Katharina Schücker, Thorge Holm, Christian Franke, Markus Sauer, and Ricardo Benavente. Elucidation of synaptonemal complex organization by super-resolution imaging with isotropic resolution. *Proceedings of the National Academy of Sciences of the United States of America*, 112(7):2029–2033, 2015.

[SHJ17] Steffen J. Sahl, Stefan W. Hell, and Stefan Jakobs. Fluorescence nanoscopy in cell biology. *Nature reviews. Molecular cell biology*, 18(11):685–701, 2017.

[SHL10] Lothar Schermelleh, Rainer Heintzmann, and Heinrich Leonhardt. A guide to super-resolution fluorescence microscopy. *The Journal of cell biology*, 190(2):165–175, 2010.

[SJS62] O. SHIMOMURA, F. H. JOHNSON, and Y. SAIGA. Extraction, purification and properties of aequorin, a bioluminescent protein from the luminous hydromedusan, aequorea. *Journal of cellular and comparative physiology*, 59:223–239, 1962.

[SL17] Sviatlana Shashkova and Mark C. Leake. Single-molecule fluorescence microscopy review: shedding new light on old problems. *Bioscience Reports*, 37(4), 2017.

[ST18] Max B. Scheible and Philip Tinnefeld. *Quantifying Expansion Microscopy with DNA Origami Expansion Nanorulers*. 2018.

[Sto52] George Gabriel Stokes. *On the Change of Refrangibility of Light: G. G. Stokes*. (London), (1852).

[TBY+16] Zhisong Tong, Paolo Beuzer, Qing Ye, Josh Axelrod, Zhenmin Hong, and Hu Cang. *Ex-STORM: Expansion Single Molecule Super-resolution Microscopy*. 2016.

[TCP+16] Paul W. Tillberg, Fei Chen, Kiryl D. Piatkevich, Yongxin Zhao, Chih-Chieh Jay Yu, Brian P. English, Linyi Gao, Anthony Martorell, Ho-Jun Suk, Fumiaki Yoshida, Ellen M. DeGennaro, Douglas H. Roossien, Guanyu Gong, Uthpala Seneviratne, Steven R. Tannenbaum, Robert Desimone, Dawen Cai, and Edward S. Boyden. Protein-retention expansion microscopy of cells and tissues labeled using standard fluorescent proteins and antibodies. *Nature biotechnology*, 34(9):987–992, 2016.

[TLW02] Russell E. Thompson, Daniel R. Larson, and Watt W. Webb. Precise nanometer localization analysis for individual fluorescent probes. *Biophysical journal*, 82(5):2775–2783, 2002.

[TMC+18] Sven Truckenbrodt, Manuel Maidorn, Dagmar Crzan, Hanna Wildhagen, Selda Kabatas, and Silvio O. Rizzoli. X10 expansion microscopy enables 25-nm resolution on conventional microscopes. *EMBO reports*, 19(9), 2018.

[UCW19] Lisa A. Urry, Michael L. Cain, and Steven A. Wasserman. *Campbell Biologie*. Pearson Studium. 11., aktualisierte auflage edition, 2019.

[UKY+14] Shin-Nosuke Uno, Mako Kamiya, Toshitada Yoshihara, Ko Sugawara, Kohki Okabe, Mehmet C. Tarhan, Hiroyuki Fujita, Takashi Funatsu, Yasushi Okada, Seiji Tobita, and Yasuteru Urano. A spontaneously blinking fluorophore based on intramolecular spirocyclization for live-cell super-resolution imaging. *Nature chemistry*, 6(8):681–689, 2014.

[vHS12] Sebastian van de Linde, Mike Heilemann, and Markus Sauer. Live-cell super-resolution imaging with synthetic fluorophores. *Annual review of physical chemistry*, 63:519–540, 2012.

[WB15] Donna R. Whelan and Toby D. M. Bell. Image artifacts in single molecule localization microscopy: why optimization of sample preparation protocols matters. *Scientific reports*, 5:7924, 2015.

[Wit03] D. Wittekind. Traditional staining for routine diagnostic pathology including the role of tannic acid. 1. value and limitations of the hematoxylin-eosin stain. *Biotechnic & histochemistry : official publication of the Biological Stain Commission*, 78(5):261–270, 2003.

[WO14] Mark Winey and Eileen O'Toole. Centriole structure. *Philosophical Transactions of the Royal Society B: Biological Sciences*, 369(1650), 2014.

[WRO78] K. Weber, P. C. Rathke, and M. Osborn. Cytoplasmic microtubular images in glutaraldehyde-fixed tissue culture cells by electron microscopy and by immunofluorescence microscopy. *Proceedings of the National Academy of Sciences of the United States of America*, 75(4):1820–1824, 1978.

[WZB19] Asmamaw T. Wassie, Yongxin Zhao, and Edward S. Boyden. Expansion microscopy: principles and uses in biological research. *Nature methods*, 16(1):33–41, 2019.

[XTY+19] Huizhong Xu, Zhisong Tong, Qing Ye, Tengqian Sun, Zhenmin Hong, Lunfeng Zhang, Alexandra Bortnick, Sunglim Cho, Paolo Beuzer, Joshua Axelrod, Qiongzheng Hu, Melissa Wang, Sylvia M. Evans, Cornelis Murre, Li-Fan Lu, Sha Sun, Kevin D. Corbett, and Hu Cang. Molecular organization of mammalian meiotic chromosome axis revealed by expansion storm microscopy. *Proceedings of the National Academy of Sciences of the United States of America*, 116(37):18423–18428, 2019.

[YBW+20] Chih-Chieh Jay Yu, Nicholas C. Barry, Asmamaw T. Wassie, Anubhav Sinha, Abhishek Bhattacharya, Shoh Asano, Chi Zhang, Fei Chen, Oliver Hobert, Miriam B. Goodman, Gal Haspel, and Edward S. Boyden. Expansion microscopy of c. elegans. *eLife*, 9, 2020.

[Yus15] Rafael Yuste. The discovery of dendritic spines by cajal. *Frontiers in neuroanatomy*, 9:18, 2015.

[ZBI+17] Yongxin Zhao, Octavian Bucur, Humayun Irshad, Fei Chen, Astrid Weins, Andreea L. Stancu, Eun-Young Oh, Marcello DiStasio, Vanda Torous, Benjamin Glass, Isaac E. Stillman, Stuart J. Schnitt, Andrew H. Beck, and Edward S. Boyden. Nanoscale imaging of clinical specimens using pathology-optimized expansion microscopy. *Nature biotechnology*, 35(8):757–764, 2017.

[ZMODK10] M. J. Zohuriaan-Mehr, H. Omidian, S. Doroudiani, and K. Kabiri. Advances in non-hygienic applications of superabsorbent hydrogel materials. *Journal of Materials Science*, 45(21):5711–5735, 2010.

[ZRS20] Fabian U. Zwettler, Sebastian Reinhard, and Markus Sauer. Ex-dstorm and automated quantitative image analysis of expanded filamentous structures. Methods in Cell Biology. Elsevier, 2020.

[ZSR19] Fabian U. Zwettler, Marie-Christin Spindler, and Sebastian Reinhard. Synaptonemal complex line profiler. 2019.

Acronyms and Abbreviations

λ	Wavelength
Å	Ångström
AA	Acrylamide
AcX	Acryloyl-X,SE (6-((acryloyl)amino)hexanoic acid)
APS	Ammonium persulfate
BisAA	N, N‘-methylenebisacrylamide
CCP	Clathrin-coated pit
CE	Central element
CLSM	Confocal laser scanning microscopy
DHEBA	N,N’-(1,2-dihydroxyethylene) bis-acrylamide
DNA	deoxyribonucleic acid
dsDNA	Double-stranded deoxyribonucleic acid
FA	Formaldehyde
FP	Fluorescent protein
FWHM	Full width half maximum
GA	Glutaraldehyde
GCE	Genetic code expansion
GFP	Green fluorescent protein
GSDIM	Ground-state-depletion imaging
GUI	Graphical user interface
HE	Hematoxylin and eosin
EM	Electron Microscopy
ExM	Expansion Microscop
iExM	Iterative expansion microscopy
IgG	Immunoglobuline G
KPS	Potassium persulfate
LLSM	Lattice Light Sheet Microscopy
LNA	Locked nucleic acid

Lys	Lysine
LE	Lateral element
MA-NHS	Methacrylic acid N-hydroxysuccinimidyl ester
MAP	Magnified analysis of the proteome
NA	Numerical aperture
NaOH	Sodium hydroxide
ncAA	Non-canonical amino acids
NSOM	Near-field scanning optical microscopy
PEG	Polyethyleneglycol
PALM	Photo activated localization microscopy
PDMS	Poly(dimethylsiloxane)
PFA	Paraformaldehyde
PMT	Photomultiplier tube
PolyE	Polyglutamylation
PSF	Point spread function
QD	Quantum dot
proExM	Protein retention expansion microscopy
RSFP	Reversibly switchable fluorescent proteins
SAP	Superabsorbent polymers
SBP	Super-binding peptides
SA	Sodium acrylate
SC	Synaptonemal complex
SD	Standard deviation
SE	Succinimidyl esters
SEM	Standard error of the mean
SIM	Structured illumination microscopy
SMLM	Single-molecule localization microscopy
SNR	Signal-to-noise ratio
SRM	Super-resolution microscopy
SOFI	Super-resolution optical fluctuation imaging
ssDNA	single-stranded deoxyribonucleic acid
STORM	Stochastic optical reconstruction microscopy
TCEP	Tris(2-carboxyethyl)phosphine
TEMED	Tetramethylethylenediamine
TG	Tetragel
TMR	Tetramethylrhodamine

U-ExM	Utrastructure expansion microscopy
UV	Ultraviolet

Acknowledgements

I wish to thank various people for their contribution to this project who accompanied and supported me both professionally and privately during the development of this work.

First of all, I would like to express my deep gratitude to Markus Sauer, my research supervisor, for his enthusiastic encouragement, useful feedback, creative hour-long meetings, and for the creation of a family atmosphere and the scientific freedom in his department, which is so valuable in research and the development of own ideas. Thank you, Markus, for your constant support and the possibilities you offered me, as the many scientific journeys to international conferences and group seminars that have enriched me personally.

In this context I would like to thank Toby Bell, who gave me the great opportunity to work as a guest researcher at his lab for several months at Monash University in Melbourne. Thank you, Toby, for your scientific support, the interesting insights of virus infection ways, for lending Ashley Rozario (who took a lot of work off my hands in the lab), for the English lessons and the great moments of fun and friendship. The visit to Down Under and our scientific cooperation was an unforgettable time.

Special thanks also to Sören Doose, for helping in analysing and understanding my data. Thank you Sören, for always having an open ear and advise for me.

I would also like to thank all of my collaboration partners with whom I could realize this work in different successful projects. I would like to thank Ricardo Benavente and Marie-Christin Spindler for the cooperation in development of the MAP-SIM method. Thank you, Ricardo for your support, patience and advice in the project.

In developing the U-ExM method, I would like to thank Virginie Hamel, Paul Guichard and Davide Gambarotto for a great collaboration. Our scientific exchange has made this

project so successful and I‘m certain it will continue to do so in future projects.

For an excellent working atmosphere, I would like to thank all my colleagues at the Department of Biotechnology and Biophysics. I would like to thank Lisa Behringer-Pließ, Petra Geßner, Albert Gessner, Markus Behringer, Oliver Reichert and Matthias “Willi” Bauer for their valuable technical support in cell culture, mechanical, electrical and computer-related work. Many thanks to our secretary Astrid Thal, who was always a great help to me in bureaucratic matters.

Thanks to Suhaila, Joni, Alex (Icy), Patrick, Domi, Juli, Nora, Tobi Klamp, Christian (Rotbart), Sepp, Sarah (Kolki), Tracy, Simon, Julia, Jan, Mara, Hannes, Uli, Vlad, Lena and Ando for the great time together in the lab, at playing football, table football, at skiing, at sweating together at the Residenz run and watching WM and EM together.

I also had the honour of working in two offices during my doctorate. I first shared my office with Anne, Andrea and Letschi. Thank you for your help in all questions I had at the beginning of my time in the lab. It was always a great time with you. Later, I moved to another office and shared my daily problems with Sina, Felix, Andi and Franzi. Thank you for the great atmosphere, the Friday afternoon music sessions and your support.

Many thanks to Andi and Felix who taught me so many technical things in optics and always supported me in calibrating setups and imaging.

Special thanks also to Sebastian, who developed the LineProfiler software that was a great help for analysing my data. Thank you, Sebastian for always responding to my change requests without questions. I really enjoyed our lunch cooking sessions together with Domi.

Especially, I would like to thank Gerti and Andi for their friendship and never-ending support in the lab and the experiences we share together which go beyond science. The stories I can tell with you will give me pleasure for a long time and I will look back on our time together at the department.

Last but not least, I want to thank my family, especially my mother and brother, who always take care of me, support me and try to understand my concerns.

Verena-thank you for your never-ending patience and love. Through your constant support you have made one of the greatest contributions to this work.

Eidesstattliche Erklärung / Affidavit

Eidesstattliche Erklärung

Hiermit erkläre ich an Eides statt, die Dissertation: „Expansionsmikroskopie kombiniert mit hochauflösender Fluoreszenzmikroskopie", eigenständig, d. h. insbesondere selbständig und ohne Hilfe eines kommerziellen Promotionsberaters, angefertigt und keine anderen, als die von mir angegebenen Quellen und Hilfsmittel verwendet zu haben. Ich erkläre außerdem, dass die Dissertation weder in gleicher noch in ähnlicher Form bereits in einem anderen Prüfungsverfahren vorgelegen hat. Weiterhin erkläre ich, dass bei allen Abbildungen und Texten bei denen die Verwertungsrechte (Copyright) nicht bei mir liegen, diese von den Rechtsinhabern eingeholt wurden und die Textstellen bzw. Abbildungen entsprechend den rechtlichen Vorgaben gekennzeichnet sind sowie bei Abbildungen, die dem Internet entnommen wurden, der entsprechende Hypertextlink angegeben wurde.

Affidavit

I hereby declare that my thesis entitled: „Expansion Microscopy combined with Super-Resolution Fluorescence Microscopy" is the result of my own work. I did not receive any help or support from commercial consultants. All sources and/or materials applied are listed and specified in the thesis. Furthermore, I verify that the thesis has not been submitted as part of another examination process neither in identical nor in similar form. Besides, I declare that if I do not hold the copyright for figures and paragraphs, I obtained it from the rights holder and that paragraphs and figures have been marked according to law or for figures taken from the internet the hyperlink has been added accordingly.

Würzburg, Monday 7th September, 2020

.....
Fabian Zwettler